U.PORTO

FEUP FACULDADE DE ENGENHARIA
UNIVERSIDADE DO PORTO

Development of Electromagnetic Pulse Crimping (EMPC) Process for Electrical Cables

Projeto para a empresa YAZAKI Saltano em colaboração com o INEGI

Joana Margarida Gonçalves da Cruz Canelas

Relatório do Projeto Final / Dissertação do MIEM

Orientador no INEGI: Engª. Inês Vieira Oliveira

Orientador na FEUP: Professora Doutora Ana Rosanete Reis

Mestrado Integrado em Engenharia Mecânica

Faculdade de Engenharia da Universidade do Porto

Departamento de Engenharia Mecânica

Fevereiro de 2015

"When everyone else is losing their heads, it is important to keep yours."

Marie Antoinette.

À Irmã, Mãe, Pai e Avó.

AGRADECIMENTOS

À Professora Doutora **Ana Reis**, orientadora deste trabalho, gostaria de agradecer pela oportunidade de trabalhar nesta área científica e pela sua energia e vitalidade.

À Eng.ª **Inês Oliveira**, orientadora deste trabalho, estarei eternamente grata. Obrigada por iluminares o caminho a seguir durante este percurso.

À Doutora Marta Oliveira, agradeço por toda a disponibilidade e apoio.

Ao **INEGI** – Instituto de Engenharia Mecânica e Gestão Industrial, quero agradecer a disponibilidade de meios concedidos durante a realização deste trabalho, e a todos os elementos da equipa do **CETECOP** – Unidade das Tecnologias de Conformação Plástica, que com o seu trabalho contribuíram para esta dissertação.

Expresso ainda a minha sincera gratidão a toda a equipa da **YAZAKI Saltano Europe**, pelo apoio e disponibilidade essenciais à realização deste trabalho, em particular ao Eng.º Tiago Valente e à Eng.ª Raquel Laranjeira.

Ao **Diogo** e ao **Ricardo**, obrigada pelo companheirismo, apoio e boa disposição.

À **Bárbara**, pela amiga que foste durante todo o meu percurso. Obrigada!

À **Tânia**, agradeço pela amizade e pela capacidade de me ouvir.

Agradeço ainda a todos os meus amigos, que direta ou indiretamente contribuíram para a realização deste meu trabalho.

À minha família, quero agradecer do fundo do meu coração por todas as oportunidades que proporcionaram. Em especial à **Esmeraldina**, **Dulcídia**, **Carlos**, **Catarina**, **Rui**, **Margarida**, **Rita** e **Zé**. Este trabalho e percurso só foi possível graças a vocês!

ABSTRACT

Electromagnetic Pulse Crimping Technology (EMPC) is a high-speed forming process that uses magnetic forces to deform and join parts. EMPC is from the lineage of the Electromagnetic Pulse Technology, and they are characterized by the non-existing contact between the workpiece and the tool. The deformation of the workpiece is a result of the Lorentz forces. These are due to a fast discharge of an intense transient current through a coil, which will induce an opposite transient magnetic field in the workpiece, resulting in the repulsive interaction between the coil and the workpiece. Although EMP is a technology known for a few decades, a current renewed interest is taken on its industrial application, mainly promoted by the advantages inherent to high velocity impact.

The mechanical crimping is one of the most applied methods to joining dissimilar materials. In the field of the electrical applications, this process is of paramount relevance, being widely used to join terminals to the electrical wires, enabling an electrical connection. This connection is achieved by exposing a part of the wire strands and placing them inside the terminal; afterwards the terminal is compressed onto the wire strands using a crimping tool. The tooling systems are key for a proper compression and to guarantee the required electrical and mechanical properties. For each wire size and connector type, it is required to have a specially designed die. The present dissertation intends to promote the industrialization of the EMPC process. Besides the demonstration of the applicability of EMPC to the crimp of YAZAKI Saltano Europe (YSE) products, it is intended to develop a customized tool, capable to joint components of a wide range of diameters, minimizing the number of tooling systems. For such purpose three case studies, provided by YSE, are analysed. Firstly, the feasibility of the process was investigated and exploratory tests were conducted, including the evaluation of the joint strength. Concerning the development of the tool itself, a design solution is presented and is supported by numerical simulation results. Following, the tool was manufactured and tested with a preliminary DoE. This allowed the validation of the developed tool. Reliable joints were attained, creating an initial input regarding the crimpability window.

RESUMO

Electromagnetic Pulse Crimping Technology (EMPC) é uma tecnologia de deformação de elevada velocidade na qual são utilizadas forças magnéticas para deformar e ligar diferentes peças. EMPC pertence à família dos processos de *Electromagnetic Pulse Technology* (EMPT), que são caracterizados pela inexistência de contacto entre a peça a deformar e a ferramenta. A deformação da peça é resultado das forças de *Lorentz*. Estas são devidas à rápida descarga de uma intensa corrente transiente através da bobine, que por sua vez vai induzir um campo magnético transiente oposto na peça, resultado na interação repulsiva entre a bobine e a peça. Embora EMPT seja uma tecnologia conhecida já há algumas décadas, há uma vontade em aplicá-la à indústria, fomentada essencialmente pelas vantagens próprias ao impacto a alta velocidade.

A cravação mecânica é um dos métodos mais aplicados na ligação de materiais dissimilares. No campo das aplicações elétricas, este processo tem especial relevância, sendo um método bastante aplicado para ligar terminais a cabos elétricos, promovendo a conexão elétrica entre ambos. Esta ligação é obtida expondo uma parte dos fios do cabo e inserindo-os dentro do terminal; posteriormente o terminal é comprimido contra o cabo utilizando uma ferramenta própria à cravação. Os componentes da ferramenta de cravação são fundamentais para garantir uma correta cravação e para assegurar que os requisitos elétricos e mecânicos são cumpridos. Isto requer que, para cada tamanho de cabo e tipo de terminal seja necessário uma ferramenta específica. A presente dissertação pretende promover a industrialização do processo de EMPC. Para além da demonstração da aplicabilidade do EMPC à cravação dos produtos da YAZAKI Saltano Europe (YSE), é pretendido desenvolver uma ferramenta customizada capaz de juntar componentes com uma vasta gama de diâmetros, minimizando assim o número de ferramentas necessárias. Para tal, foram analisados três casos de estudo fornecidos pela YSE. Inicialmente, a viabilidade do processo foi investigada e foram realizados testes exploratórios, que incluíram a avaliação da resistência da ligação. Relativamente ao desenvolvimento da ferramenta, uma solução de design é apresentada e validada pelos resultados da simulação numérica. No seguimento, a ferramenta projetada foi produzida e testada com um DoE preliminar, que permitiu a sua validação. Cravações bem sucedidas foram conseguidas levando a um input inicial dos parâmetros dos processo.

Keywords: Electromagnetic pulse crimping; Electrical cables; Numerical simulation; Process development; Coil development.

Palavras-chave: Cravação Electromagnética; Cabos elétricos; Simulação numérica; Desenvolvimento do process; Desenvolvimento da bobine.

CONTENTS

LIST OF FIGURES

LIST OF TABLES

LIST OF SYMBOLS

Symbol	Description	Units
A	Area	m^2
A_0	Initial area	m^2
A_c	Cross section area	m^2
A_i	Internal area	m^2
B	Magnetic field intensity	T
C	Capacitance of the capacitor bank	F
D	Electric flux density	V.m
E	Magnetic field intensity	N/C
E_0	Charging energy	J
F	Electromagnetic force density – Lorentz Force	N
f	Current frequency	Hz
F	Force	N
H	Magnetic flux	T/m^2
H_{diff}	Magnetic field diffused through the workpiece wall	A/m
H_{gap}	Magnetic field in the gap between coil and workpiece	A/m
I_0	Maximum intensity of discharge current	A
I_1	Discharge current	A
I_2	Eddy current	A
J	Electrical current density	A/m^2
L	Final length	m
L_0	Initial length	m
L_1	Coil inductance	H
L_2	Workpiece inductance	H
l_c	Coil length	m
L_c	Connecting wires inductance	H
L_i	Circuit inductance	H
L_T	Total inductance of the circuit	H
N	Number of turns of the coil	
P	Electromagnetic pressure	N/m^2
R_1	Coil resistance	Ω
R_2	Workpiece resistance	Ω
R_c	Connecting wires resistance	Ω
R_i	Circuit resistance	Ω
R_T	Total circuit resistance	Ω
U	Energy density of a magnetic field	J/m^3
V_0	Charging voltage	V
δ	Skin depth	m

ε	True strain	m
ε_{eng}	Engineering strain	m
κ	Electrical conductivity	S/m
μ	Absolute electrical Permeability of the conductor	H/m
μ_0	Absolute electrical Permeability of the free space	H/m
μ_r	Relative electrical Permeability of the conductor	H/m
ρ	Electrical resistivity of the material	Ω.m
σ	True stress	N/m^2
σ_{eng}	Engineering stress	N/m^2
τ	Damping coefficient	s
ω	Angular frequency of the discharge current	Rad/s

1 INTRODUCTION

The **Instituto de Ciência e Inovação em Engenharia Mecânica e Engenharia Industrial** (INEGI) is an interface Institution between University and Industry, oriented to the activities of Research and Development, Innovation and Technology Transfer. INEGI aims to contribute to the increase of the competitiveness of the national industry, in the fields of engineering design, materials, production technology, energy and environment and industrial management and to be recognized as a National reference [**1**]. In line with this strategy, INEGI has recently dedicated efforts towards the development of ElectroMagnetic Pulse Technologies (EMPT). In particular, to promote the transfer and implementation of such technology in the industrial fields.

YAZAKI is a supplier of a broad range of products that support automotive electronics, with a focus on wire, wiring harnesses, instrumentation and electronics sub-assemblies. YAZAKI holds a leading position in the worldwide wiring harness market. Furthermore YAZAKI's product line includes fibre optics, display and clock modules, power centres, electronics, combination switches, connectors, terminals and high voltage cables and components [**2**]. **YAZAKI Saltano Europe** (YSE) has an I&D centre in Ovar-Portugal, which is committed in introducing and developing new technologies for the manufacturing of its products.

In relation to the topics described above, the opportunity to apply EMPT for manufacturing of YSE products has emerged and a partnership has been set between the two companies.

1.1 Motivation

Compression connectors are used for reliable and controllable electrical connections. This type of connection must resist to a wide range of electrical and environmental conditions such as current surges, corrosion and vibration, for an extensive variety of applications [**3**]. Compression connectors can be made of copper or aluminium, though copper is preferable for applications whose electrical conductivity has more relevance. Copper terminals, are coated with tin or led in order to provide corrosion resistance [**4**,**5**].

Crimping consists in a method of compressing connectors that allows obtaining mechanical and electrical connection between a terminal and a conductor. Mechanical crimping of the electrical cables to the terminals is achieved by removing a portion of the insulation exposing a part of wire strands, and placing them inside the terminal. Afterwards, the terminal is deformed using a tool designed to force the wires and the terminal inner surface into intimate contact. The design of the tooling system is essential for proper compression of the connector against the electrical wire. Consequently, for each combination wire size and connector, a specific die must be designed [**6**,**7**,**8**]. As a result of the numerous tools and dies needed, there is a particular interest in alternative technics, which can produce joints with characteristics similar to the ones produced by conventional crimping techniques, but reducing significantly the tool assets.

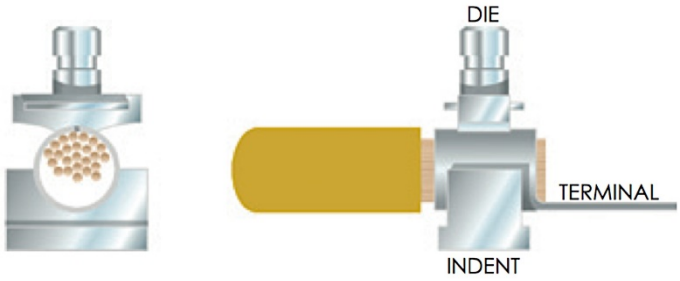

Figure 1: Mechanical crimping [9].

Among different technologies, High Speed Metal Forming (HSMF) processes are being explored as an alternative to conventional metal working methods. High Speed Metal Forming techniques appeared in the late 1800's and were studied during the 1950's and 1960's. They offer certain advantages over conventional metal forming processes that led to their fast development. HSMF is the shaping of materials by transferring energy to them during a short period of time [**10**]. This technology derives its name from the high velocities that the workpiece reaches throughout deformation. During the process, the workpiece is quickly accelerated away from the energy source as it acquires kinetic energy, which is dissipated as plastic work during metal deformation. These techniques are distinguished from each other according to the nature of the force that causes the acceleration of the workpiece, such as explosive forming, electrohydraulic or electromagnetic pulse forming [**10**,**11**,**12**]. While some of the methods were rapidly transferred to the industry, Electromagnetic Pulse Technology (EMPT) was not promoted, due to many technical limitations (lack of high-performance components, proper materials and fast computers). In recent years, there is an improved interest in those technologies since high performance components became available. Additionally, the industry is prone to implement new techniques [**13**]. EMPT can currently be found in four main processes: forming, welding, cutting and crimping; which are briefly described below.

Electromagnetic Pulse Forming is a process, in which a high energy current is discharged through a coil that is surrounding or covering the workpiece. The intense transient currents generate electromagnetic forces between the coil

and the workpiece accelerating the workpiece against the die. Consequently, the workpiece is shaped according to the die contour; using a special die, perforation operations can also be performed. [**14**].

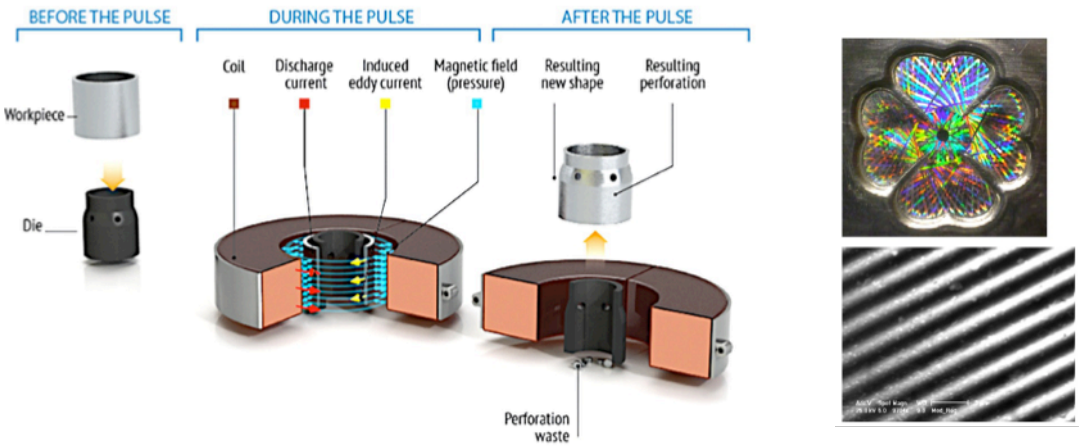

Figure 2: Electromagnetic pulse forming (right - [15]; left – courtesy of the Ohio State University).

Electromagnetic Pulse Welding is a solid state welding process that can be used for welding of dissimilar metals. Electromagnetic pulse welding process is from the lineage of explosive welding technique. Similarly, it consists in accelerating a part using the magnetic pressure induced by the high pulsed current in the coil. High-speed impact between the pieces to be joined can generate welding if appropriate conditions are reached [**16**]. Electromagnetic pulse welding applications have been widely discussed in literature; examples of electromagnetic pulse welding can be found on [**17**,**18**,**19**].

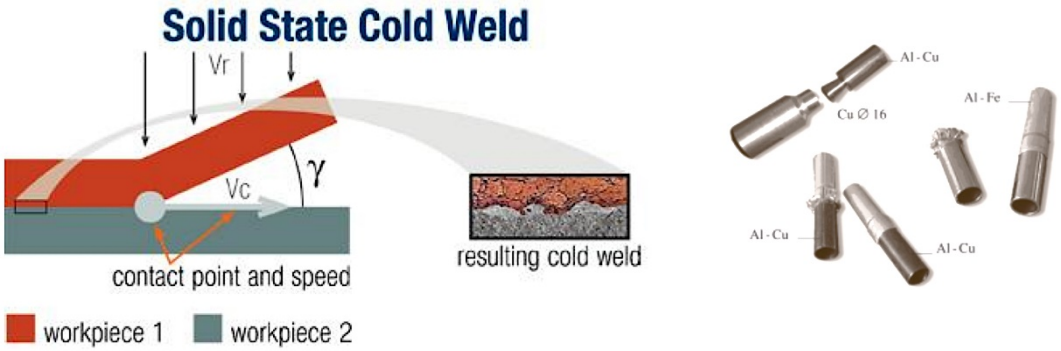

Figure 3: Electromagnetic pulse welding [20,21].

Electromagnetic Pulse Cutting is a process that differs from the conventional cutting processes; in electromagnetic pulse cutting the workpiece is not cropped between two mechanical tools. The current inductor replaces one half of the conventional cutting tool. During the process, parts of the workpiece are accelerated, so that deformation takes place and the separation of the material occurs [**22**].

Figure 4: Electromagnetic pulse cutting (courtesy of the Ohio State University).

Electromagnetic Pulse Crimping, EMPC, is very similar to either magnetic pulse forming of cylindrical tubes and welding, except that the inner part of the assembly replaces the die in the later process and no bonding between the materials is achieved. A high energy current is discharged through a coil surrounding the workpiece; this high current creates magnetic forces between the coil and the workpiece; such forces accelerate the exterior workpiece into the interior one at high speed. The process causes plastic deformation of the exterior workpiece causing a crimp [**14**].

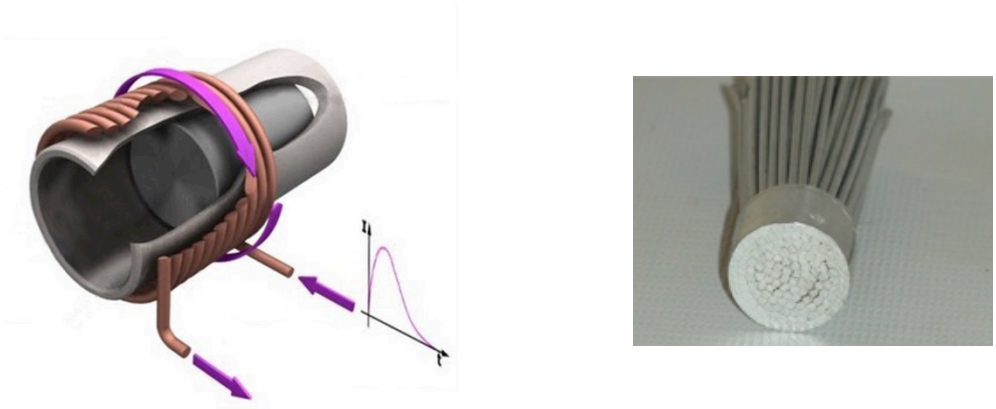

Figure 5: Electromagnetic pulse crimping [23,24].

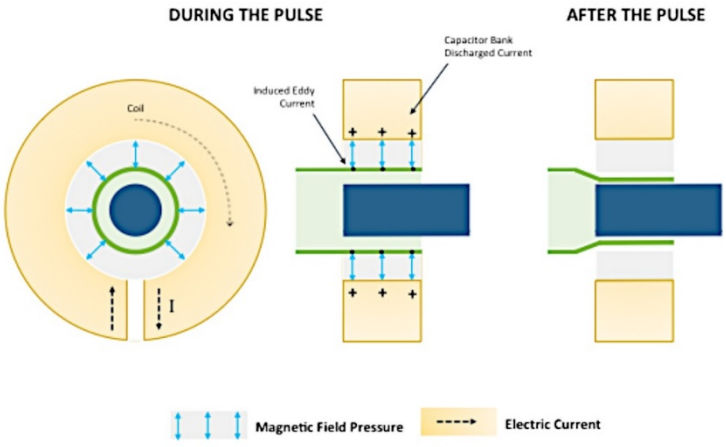

Figure 6: EMPC process: during and after pulse (adapted from [25]).

EMPC presents many advantages that can make it an appropriate alternative to conventional mechanical crimping processes. Besides the ability to compress almost any tubular cross-sections, a more uniform crimp and lower

electrical resistance can be achieved. In addition, the set-up time and flexibility of the process are improved due to the possibility of using the same circuit to join different workpieces [26,27,28]. Due to these advantages several industrial applications of EMPC have been described in literature. Ralph Shäfer [29] presented a study in which three different applications of EMPC are reported: crimping of steel fittings onto rubber hoses, crimping of a steel truck wing holder, and crimping of dissimilar materials for lightweight seat structures of cars and aircraft. Another study presented by Eguia et al [30], in which the production of high strength structural joints with EMPC was reported instead of electromagnetic pulse welding.

This study is focused in verifying the applicability of EMPC for copper cables crimping. Crimping tests will be performed to a variety of terminal-wire combinations provided by YSE. To achieve these goals, firstly the process will be investigated using the numerical simulation of the process. Then, taking into account the computational results, the experimental tests will be performed assessing the joint strength and quality. The experimental tests will be run using a DoE.

1.2 Scope and Layout of the Thesis

Considering the main goals, this dissertation was divided in 5 chapters. Following this introductory one, **Chapter 2** presents the theoretical background of EMPT. This literature review includes the EMP phenomenon description as well as the main components of an EMPT system. Other general aspects, such as the process advantages and potential limitations, crimping applications as well as related patents are also presented. As a final point, regarding the numerical modelling and simulation of EMPT processes, a brief investigation over the common applied approaches is presented.

Chapter 3 deals with the tool development for the EMPC process. The chapter opens with a succinct presentation of the case study and its specifications. Additionally, the applicability of the technology to this individual purpose was investigated with exploratory experiments. These experiments include an evaluation of the joint strength. Regarding the development of the tool itself, the suggested tool design is presented validated by the numerical simulation of the process. This validation has foremost importance since it represents the viability of the design in order to electromagnetic crimp the electrical cables.

Chapter 4 is related to the tool testing and validation. Firstly, a set of tests is presented, in which the strength of the crimped joint with the projected tool is assessed. These initial tests allowed determining the range of energy to be explored in the more extended tests. The crimp connection validation process is next presented using a DoE, adding to the evaluation of the connection's strength metallographic analysis is reported.

Finally, **Chapter 5** presents the main conclusions regarding the topics addressed and work carried out. Additionally, some considerations and suggestions of future work are reported.

2 LITERATURE REVIEW

2.1 Electromagnetic Pulse Technology

Electromagnetic Pulse Technologies (EMPT) are advanced, high-speed manufacturing processes that make use of electromagnetic forces to deform, join or cut parts. These contact free, non-conventional techniques are based on the physical effects described by Maxwell [**31**]. The author explained that a temporarily varying magnetic field induces electrical currents in nearby conductors and additionally exerts forces (Lorentz forces) [**26**,**32**,**33**].

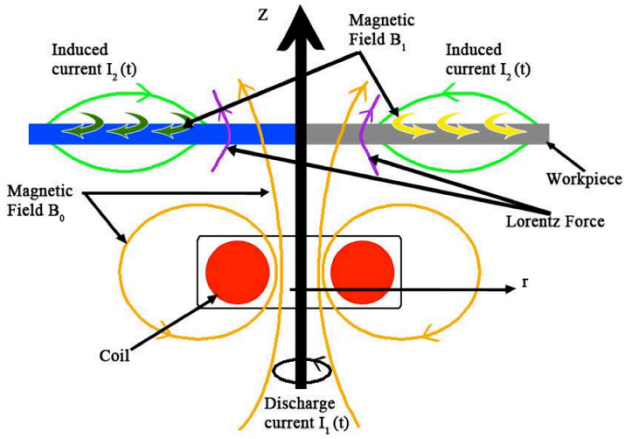

Figure 7: Electromagnetic phenomena representation [12].

In order to create the required magnetic field, a capacitor bank is used to store the energy. The capacitor bank (with a total capacitance C_0) is charged with an initial voltage (V_0), which is rapidly discharged as current $I_1(t)$ that flows through a coil (flat spiral, helical, etc.) using high-speed switches ignitrons. This current creates a transient magnetic field, B_0 that will penetrate into the workpiece, placed in the vicinity of the coil. In addition, B_0 induces Eddy currents $I_2(t)$ in the workpiece, which are responsible for limiting the penetration of the magnetic field B_0 into the workpiece as well as for creating its own induced magnetic field, B_1, in opposite direction of the magnetic field of the coil B_0. The magnetic fields B_0 and B_1 will repulse each other, creating Lorentz body forces F. On the other hand, these electromagnetic forces act as a magnetic pressure into the workpiece surface. Consequently, if this pressure is higher than the yield strength

of the workpiece material, the dynamic plastic deformation of the workpiece takes place [**12**,**27**].

2.2 Principles of the Electromagnetic Pulse Technology

A schematic representation of a typical electromagnetic pulse system is represented in the figure below. As mentioned before, the system consists of a power supply, a bank of capacitors to store the energy, a high current switch, a coil and, in some cases, a fieldshaper.

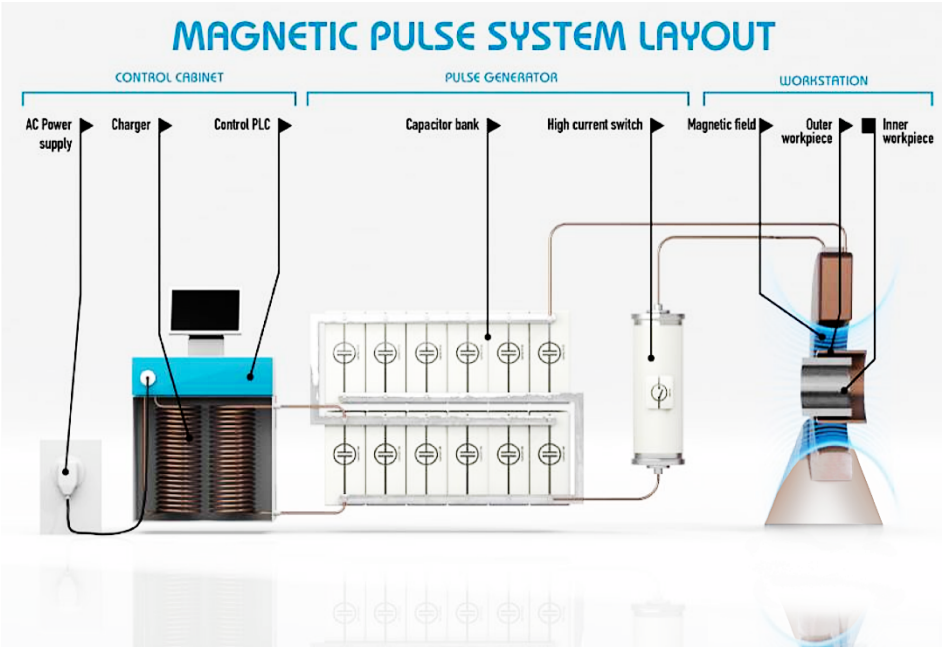

Figure 8: Typical layout of an electromagnetic pulse system [34].

The EMP processes can be described as an electrical RLC circuit, which is represented by a serial circuit consisting of a capacitor C, an inductance L_i and a resistor R_i. The tool coil is represented by its resistance, R_1 and its inductance, L_1, both connected in series to the pulse power generator [**32**,**35**].

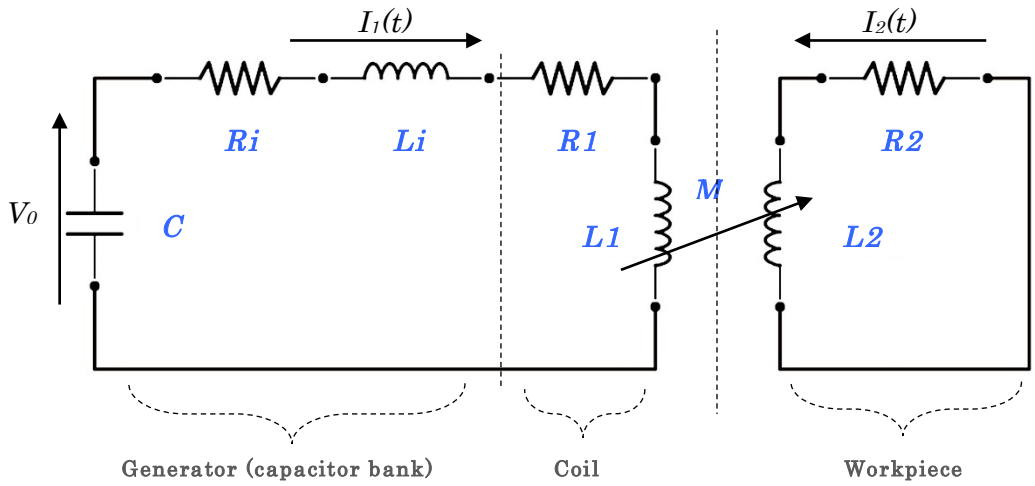

Figure 9: RLC circuit of electromagnetic forming process (adapted from [12,32]).

The current discharge through the capacitor bank into the coil is obtained using the Equations (1) and (2).

$$(L_1 + L_C)\frac{dI_1(t)}{dt} + M\frac{dI_2(t)}{dt} + (R_1 + R_C)I_1(t) + \frac{1}{C}\int I_1(t)dt = 0 \quad (1)$$

$$\frac{d(L_2 I_2)}{dt} + \frac{d(MI_1)}{dt} + R_2 I_2 = 0 \quad (2)$$

where $I_1(t)$ and $I_2(t)$ are the coil current and the Eddy current in the workpiece, respectively; L_1 and R_1 the coil inductance and resistance; L_2 and R_2 the workpiece inductance and resistance; L_c and R_c connecting wire inductance and resistance, and M the total mutual inductance between the coil and the workpiece. Solving this equations will allow to obtain the discharging coil current $I_1(t)$ and the induced Eddy current $I_2(t)$ flowing through the workpiece [**12**,**27**,**36**].

Assuming the capacitor voltage, V_0, and the absence of current at the initial moment, the differential equations can be solved [**32**].

$$I_1 = 0 \quad (3)$$

$$I_2 = 0 \quad (4)$$

$$(L_1 + L_2)\frac{dI_1(t)}{dt} = V_0 \quad (5)$$

In order to compute the values of inductance and the resistance of the coil it is imperative to know its geometry and material. These parameters are of paramount importance since the coil is responsible for the major part of the total inductance of the discharge circuit.

For a simple N-turn solenoid coil, the coil inductance can be calculate by:

$$L = \frac{\mu_0 N^2}{l_c}\left[\frac{A_0}{\left(1 + \frac{A_i}{A_c}\right)}\right] \quad (6)$$

where N is the number of turns, μ_0 the absolute permeability of the material (equal to $4\pi x10^{-7}$ H/m), A_i and A_c are the internal and the cross section area of the wire respectively and l_c is the active length of the coil [**27**].

The resistance, qualifies the tendency of a material to oppose the current flowing through it, and is given by:

$$R = \rho\frac{l_c}{A} \quad (7)$$

where ρ is the resistivity of the material, l_c the length of the coil and A is the active surface area of the section [**27**].

In order to calculate the combined resistance and inductance of the circuit the equations below are necessary.

For elements connected in series:

$$R_t = \sum_{1}^{n} R_i \quad (8)$$

$$L_t = \sum_{1}^{n} L_i \quad (9)$$

For elements connected in parallel:

$$\frac{1}{R_t} = \sum_{1}^{n} \frac{1}{R_i} \quad (10)$$

$$\frac{1}{L_t} = \sum_{1}^{n} \frac{1}{L_i} \quad (11)$$

The total circuit inductance and resistance is the sum of the coil and system inductances and resistances, respectively. It is important to note that the coil inductance has a higher value than the bank and workpiece inductances, this is due to the number of turns that have a significant influence, as seen in Equation (6) [**27**].

The intensity of the discharged current is calculated as shown in Equation (12). Usually the current values are between about 10^4 to 10^6 Ampère.

$$I_1(t) = I_0 e^{-\frac{t}{\tau}} sin\omega t \quad (12)$$

where I_0 is the maximum current intensity, τ the damping factor and ω the current frequency. The discharge of current has an exponential decrease and is characterised by the damping coefficient, given by:

$$\tau = 2\frac{L_T}{R_T} \quad (13)$$

where L_T is the total inductance of the circuit and R_T the total resistance of the circuit. The maximum current intensity is given by:

$$I_0 = V_0 \sqrt{\frac{C}{L_T}} \quad (14)$$

where V_0 is the voltage applied to the circuit and C the total capacitance of the capacitor bank. The angular frequency of the current is calculated using:

$$\omega = \frac{1}{\sqrt{L_T C}} \quad (15)$$

The depth of the region which is affected by the induced current, is given by the skin depth δ, and can be computed using:

$$\delta = \sqrt{\frac{2\rho}{\mu\omega}} \quad (16)$$

with ρ being the electrical resistivity of the workpiece and μ being the absolute magnetic permeability of the conductor [**12**,**27**,**32**].

As referred before, a transient current flowing through a coil will create an intense and transient magnetic field. When a metal workpiece is exposed to this magnetic field, Eddy-currents are induced at its surface. According to Lenz's law, the direction of the currents is such that the magnetic field (induced in the workpiece) opposes the initial magnetic around the coil [**13**]. Figure 10 shows a typical current curve for the discharge (in the coil) and the induced current.

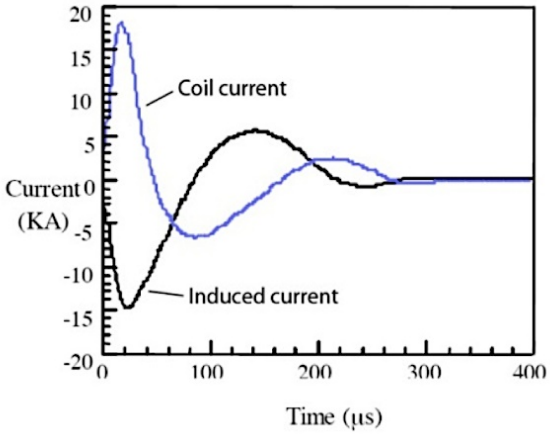

Figure 10: Typical current discharge (in the coil*) and induced current [26].*

The energy density of the magnetic field, which can be calculated using the equation below, produces magnetic pressure acting orthogonally to the magnetic field, causing plastic deformation as soon as the yield strength of the workpiece is exceeded [**13**].

$$U = \frac{1}{2}\mu_0 H^2 \qquad (17)$$

with H being the magnetic flux.

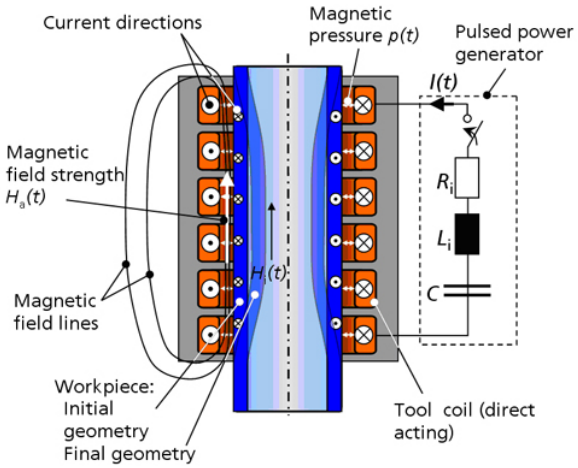

Figure 11: Magnetic pressure acting on tube compression [37].

According to Filip Broekaert [**13**], the magnetic pressure can be calculated as the difference between the energy density in the gap distance, between the coil and the workpiece, and the energy density diffused through the workpiece wall.

$$P(z,t) = \frac{1}{2}\mu_0 \left(H_{gap}^2(z,t) - H_{diff}^2(z,t) \right) \quad (18)$$

where $H_{gap}(z,t)$ is the magnetic field in the gap between coil and workpiece and $H_{diff}(z,t)$ is the magnetic field diffused through the workpiece wall. It is important to refer that the magnetic pressure is a function of the time and the Z-coordinate.

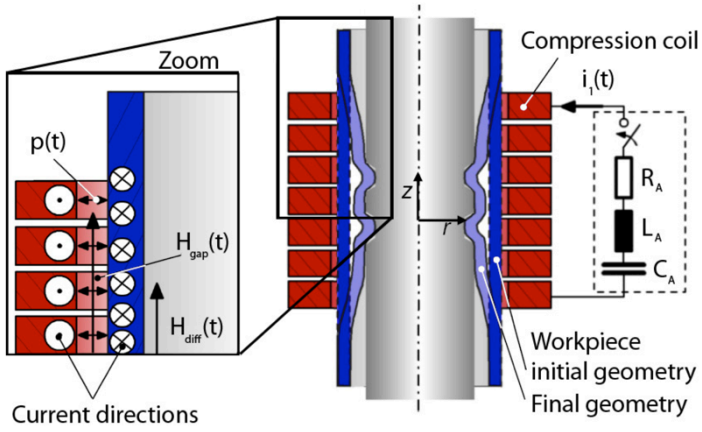

Figure 12: Electromagnetic tube compression. In the zoom section, on the left, the magnetic field in the gap between coil and workpiece and the magnetic field diffused through the workpiece wall are shown [13].

2.3 Physics of the Process

2.3.1 Maxwell's Equations

The Maxwell's first equation is an adaptation of Faraday's law. The experimental work of Michael Faraday revealed that a changing magnetic field which links a wire loop induces a voltage, also called electromotive force, in the loop. This electromotive force is proportional to the rate of change of the magnetic flux through the loop. The Maxwell-Faraday equation states that a time-varying magnetic field is always accompanied by a spatially-varying, non-conservative electric field, and vice-versa [**12**,**31**,**38**].

$$\nabla \times \boldsymbol{E} = -\frac{\partial \boldsymbol{B}}{\partial t} \quad (19)$$

where $\boldsymbol{E}$ is the magnetic field intensity, $\boldsymbol{B}$ is the magnetic flux density, t represents time and the symbol ∇ represents the curl operator.

The second of Maxwell's equation is the Gauss's law for electricity; it gives the most important property of the electric flux density: the electric flux through any closed surface is proportional to the enclosed electric charge. When the charge $\boldsymbol{Q}$, is distributed continuously through a volume, Gauss's law is given by [**12**,**38**,**39**]:

$$\nabla \cdot \boldsymbol{D} = \rho \qquad (20)$$

where $\boldsymbol{D}$ is the electric flux density and ρ is the volume charge density (coulomb per cubic meter).

The Ampère-Maxwell law, Maxwell's third equation, states that an electric current or a changing electric flux through a surface will produce a circulating magnetic field around any path that bounds that surface. This means that Maxwell amended the Ampère law adding that the magnetic fields can be generated by electrical current (original "Ampère's law") as well as by changing electric fields. This modification has higher relevance since it shows that not only does a changing magnetic field induce an electric field but also changing the electric field induces a magnetic field. The differential equation of the third law is given by [**12**,**38**,**39**]:

$$\nabla \times \boldsymbol{H} = \boldsymbol{J} \qquad (21)$$

where $\boldsymbol{H}$ is the electric field intensity and $\boldsymbol{J}$ is the electric current density.

Maxwell's fourth equation is Gauss's law for magnetism, and is related to the magnetic flux properties. Magnetic poles appear in nature as equal and opposite pairs. The sources for a magnetic field are currents or moving charges. For a magnetic dipole, all magnetic flux lines entering a closed surface must also leave it. Gauss's law for the magnetic fields is a statement that there are no magnetic monopoles, and can be expressed as [**12**,**38**,**39**]:

$$\nabla \cdot \boldsymbol{B} = 0 \qquad (22)$$

2.3.2 Lorentz Forces

During the electromagnetic forming process, a strong transient electromagnetic field is generated in the gap between the coil and the workpiece. The transient nature of the electromagnetic current induces Eddy currents in the workpiece, which flow in opposite direction to the initial current discharge in the coil. The interaction of these currents is an intense repulsive force between the coil and the workpiece. Lorentz's law governs the generation of these forces [**12**,**38**]:

$$\boldsymbol{F} = \boldsymbol{J} \times \boldsymbol{B} \qquad (23)$$

where $\boldsymbol{F}$ is the Lorentz force.

2.4 Electromagnetic Pulse System Components

A magnetic pulse system has five main components: a *power supply*, a *bank of capacitors* to store the energy, a control unit to operate the machine, a *high current switch* and a *coil*.

Figure 13: Electromagnetic pulse machine [40].

2.4.1 Capacitor Bank

In order to supply the high amount of energy required by this process, the energy is stored (over a period of time) and then discharged quickly thought the coil. For such purpose, a capacitor bank is used. This component is one of the most important and expensive parts of the electromagnetic pulse machine. In terms of requirements, three can be highlighted: low self-inductance; minimum weight and dimensions; should withstand a high number of pulse discharges.

Inside the bank, the capacitors are connected in parallel to increase the total capacitance of the discharge circuit [**13**,**27**]. The relation between energy E stored and the charging voltage V_0 is given by:

$$E = \frac{CV_0^2}{2} \qquad (24)$$

2.4.2 Coil and Fieldshaper

The coil is responsible to convert the electrical current discharge into electromagnetic forming pressure. Therefore, the coil represents the actual tool of the electromagnetic process [**11**,**32**]. The pressure generated, called magnetic pressure, will deform the workpiece. This pressure acts in both workpiece and coil (action-reaction). Consequently the coil must withstand high magnetic forces without mechanical failure as well as high operating voltage, magnetic flux and heating [**27**,**41**]. According to Psyk, et al. [**32**] the coil must provide:

- A high conversion coefficient of the energy supplied by the capacitor bank;
- High mechanical resistance;
- Low inductance and consequently high frequency of the discharging current;
- Resistance to electrical over-voltages;
- A simple design performance.

The coil itself shall be made from a highly conductive material, usually a copper or aluminium alloy and can be a single-turn or multi-turn coil. The number of turns of the winding is crucial, as it influences the resistance and the inductance of the coil and the coil workpiece unit (lower number of turns, lower inductance) [**32**]. There are mainly three types of coils [**42**]:

- Compression coils - the coil surrounds the tubular workpiece, which generates compressive forces on the tube walls.

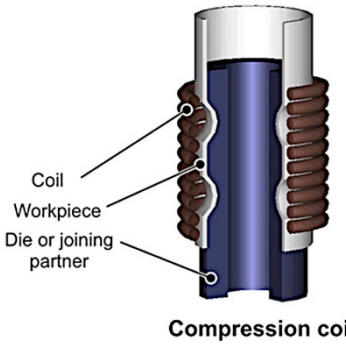

Figure 14: Compression coil [43].

- Expansion coils - the coil is placed inside the workpiece (tube), a die surrounding the tube defines the final shape of the tube.

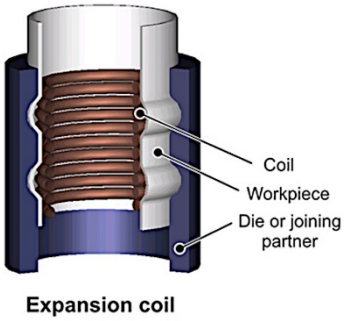

Figure 15: Expansion coil [43].

- Flat spiral coils, the coil has a pancake like form, and the die shape determines the final shape of the metal sheet.

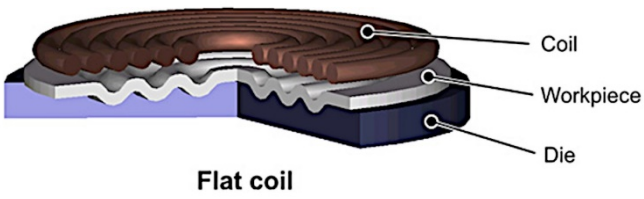

Figure 16: Before and after sheet metal forming [43].

The fieldshaper is commonly used to concentrate the magnetic flux and apply the magnetic pressure over a specific area of the workpiece. When a single turn coil is used, a fieldshaper is not required; the magnetic pressure will be concentrated in the working zone. Such type of coil can be manufactured as a solid

component to resist the acting forces. On the other hand, when using a multi-turn coil, the fieldshaper is important to focus the spread current from the many windings on a small area as well as to concentrate the current generated by the windings. [**13**,**26**,**35**].

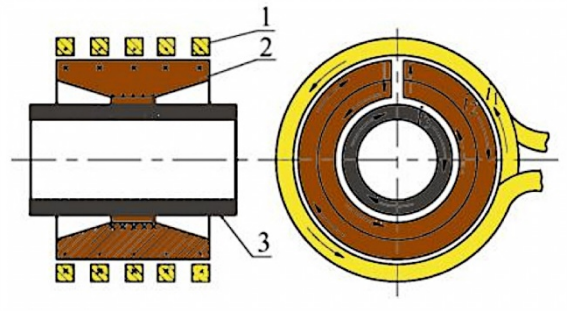

Figure 17: 1- Multi-turn coil, 2- Fieldshaper, 3- Workpiece [26].

When a fieldshaper is used, the magnetic pressure that the coil has to withstand is smaller than the pressure that acts on the workpiece, increasing the service life of the coil. Besides, the production of a fieldshaper is more economical and quicker than a spiral coil. The flexibility of the tool also improves with the use of a fieldshaper since, the same coil, with different fieldshapers can be used to preform different parts/dimensions. As seen in Figure 17, the fieldshaper is sectioned with at least one radial slot, this is important to promote the current flow, from the surface of the fieldshaper to the workpiece placed inside. Also, the magnetic pressure on the workpiece will be lower in the region adjacent to the cut. Though a small cut is preferable it has to be wide enough to prevent arc generation (in addition insulators of polyamide are added inside the slot) [**13**,**32**,**44**]. Decreasing the radial gap between the fieldshaper and workpiece increases the magnetic pressure [**11**]. Figure 18 shows the current flow on the cross-section of a fieldshaper with and without a radial cut.

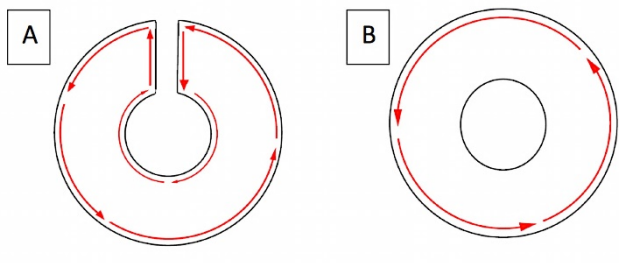

Figure 18: Cross-section of a fieldshaper with (A) and without (B) radial cut [11].

Additionally, regarding the geometry of the fieldshaper, Psyk, et al. [**32**] states that the overall length of the fieldshaper should be adjusted to the coil length. If the fieldshaper is shorter than the tool coil an inhomogeneous loading of the coil occurs which will result in a reduced lifetime of the coil. If the fieldshaper is longer than the tool coil the energy transfer has low efficiency.

Concerning the efficiency of the energy transfer, the material of the fieldshaper should have high electrical conductivity. Therefore, a compromise

between the requirements considering strength and the conductivity has to be found. Frequently used materials are copper and copper-alloys, aluminium and aluminium-alloys as well as brass and bronze [**32**].

2.4.3 Workpiece

The EMF process is more suitable for materials with a high electrical conductivity. The process is more efficient with materials such as aluminium and copper alloys. According to Psyk, et al. [**32**], the maximum amplitude of the magnetic pressure is nearly proportional to the square root of the electrical conductivity. The authors also state that, the smaller the electrical conductivity of the workpiece, the more energy will be transferred into Joule losses. When the electrical conductivity of the workpiece is comparably smaller, the magnetic field penetrates in the workpiece easily, which causes smaller magnetic pressure [**32**], consequently the process' efficiency will decrease.

The shielding behaviour of the magnetic field improves with a lower value of the skin depth [Equation (16)]. In this case the induced current will flow closer to the surface of the workpiece and reduces the penetration of the magnetic field into the workpiece. The skin depth can also be presented as:

$$\delta = \sqrt{\frac{\rho}{\pi f \mu_0 \mu_r}} = \frac{1}{\sqrt{\pi f \mu_0 \mu_r \kappa}} \qquad (25)$$

where ρ is the resistivity of the conductor, f is the frequency of the current, μ_0 is the permeability of the free space, μ_r is the relative permeability of the conductor and κ is the electrical conductivity.

As can be seen in the equation above, the shielding behaviour of the magnetic field improves with higher electrical conductivity of the workpiece material, higher frequency of the discharge current and higher relative permeability of the conductor. In addition, this leads to an increase of the magnetic pressure [**13**]. The graph below presents the skin depth function of the frequency for different materials. Figure 19 shows that less conductive materials have a higher skin depth, implying that, for these materials, the frequency needs to be significantly superior in order to obtain lower skin depth and consequently higher magnetic pressure.

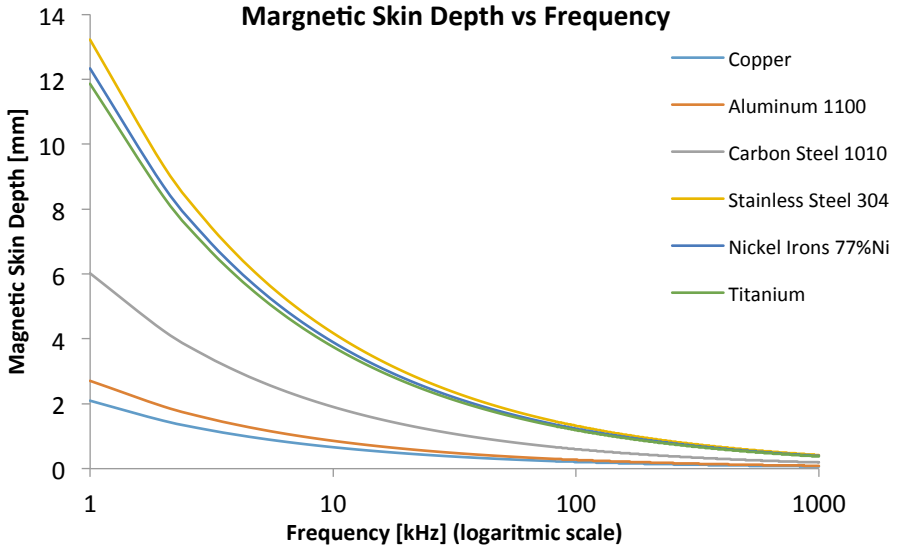

Figure 19: Skin depth as a function of the frequency for different materials.

The values of electrical conductivity used for plotting Figure 19 are presented in the table below.

Table 1: Electrical conductivity.

Material	Electrical Conductivity [S/m]
Copper Pure	5.800×10^7
Aluminium 1100	3.445×10^7
Carbon Steel 1010	6.993×10^6
Stainless Steel 304	1.450×10^6
Nickel Irons 77% Ni	1.667×10^6
Titanium	1.798×10^6

2.5 Advantages and Limitations of Electromagnetic Pulse Technology

EMPT has several advantages that make it an appropriate alternative to conventional mechanical forming processes. The principal advantages of the process are listed below [**26**,**27**,**32**]:

- Due to the high workpiece velocities and high strain rates (in the range of 10^4 s^{-1}) the mechanical properties of the workpiece material can be improved compared to quasistatic ones;
- In the field of forming applications wrinkling is suppressed, as the forming process takes place at high velocity, the change in direction of the compressive stress causing wrinkling is inhibited;
- Concerning the forming applications springback is significantly reduced in comparison to convectional quasistatic forming operations (the die design simplifies);

- High productivity, the production rate is limited by the time required for loading and unloading of the part. According to Psyk, et al. [**32**] production ratios of 350-400 parts per hour can be achieved;
- Due to contact-free force application, the surface finish can be achieved before the operation of electromagnetic forming;
- Since no lubricants are used, the process is environmentally friendly. Also, this results in a simplification of the workpiece processing, as there is no need to clean the workpiece;
- High repeatability can be achieved by adjusting the forming machine once;
- Flexible processing technology, because the same coil can be used for forming workpieces of different configurations;
- Possibility to join dissimilar materials including material combinations of metals and polymers.

Although EMPT has numerous advantages, it has also some limitations and inconveniences as reported below [**26**,**27**,**32**]:

- The process is more suitable for materials with a high electrical conductivity. Only electrically conductive materials can be formed directly. For non-conducting materials is required an intermediate conducting piece;
- Only a small part of the charging energy is used for the plastic deformation resulting in a comparable bad efficiency;
- Significant requirements regarding safety aspects are necessary, because of the high intensity of current and voltage;
- The required equipment is expensive and physically large;
- The technology is not applicable to large dimension workpieces, mainly because of the designing of the induction coils and the requirement of more energy. This would translate into a larger capacitor bank and higher initial spending;
- Materials with low resistivity can be easily formed (copper and aluminum alloys), when using materials of high resistivity the cost of process may be comparatively higher.

2.6 Electromagnetic Pulse Crimping

Electromagnetic Pulse Crimping allows obtaining joints that present characteristics similar to the ones made by conventional processes. In EMPC the energy stored in the capacitor bank is discharged instantly through the coil. The magnetic field produced by the coil induces Eddy currents into the workpiece, which produce its own magnetic field. The forces generated by the two magnetic fields oppose to each other. Therefore, a repelling force between the coil and the workpiece is generated. Consequently, if the forces generated are higher than the yield strength of the workpiece, its dynamic plastic deformation takes place [**22**,**26**,**27**]. Electromagnetically crimping an electrical cable is schematically represented in the figure below.

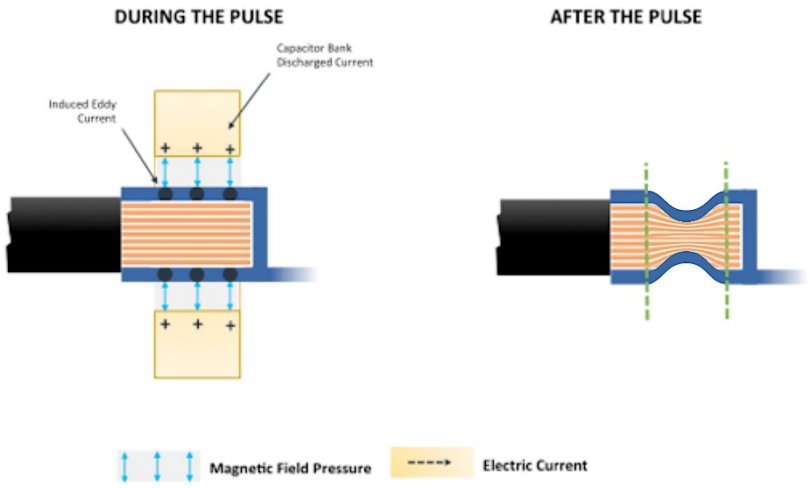

Figure 20: EMPC process (adapted from [25]).

2.6.1 Electromagnetic Pulse Crimping Applications

The first introduction of EMPT equipment in industry was in about 1964 at General Motors and was used to shrink retaining rings onto neoprene boots. Though the machine was technically primitive when compared to today's equipment, it operated reliably producing automotive components during many years. The EMF equipment was particularly vital as a learning tool for manufacturing engineers to learn what can be done with EMPF and for equipment designers to improve the process and equipment [**11**].

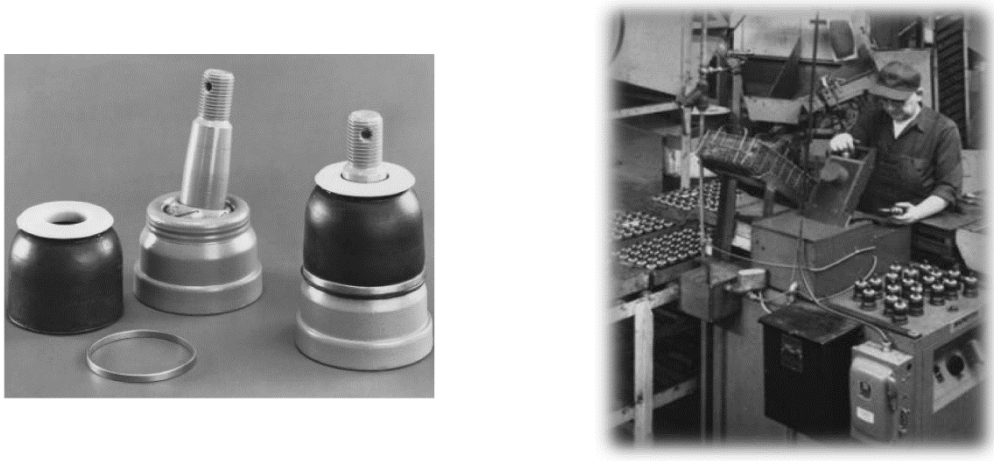

a. b.

Figure 21: a. First industrial application used to shrink retaining rings onto neoprene boots; b. Electromagnetic metal forming machine built by General Atomic in the early 1960's and used by GM as a manually operated single station assembly machine [11].

A study performed by Ralph Shäfer [**29**] intitled "Industrial Application of the Electromagnetic Pulse Technology" states that EMF crimping represents a technical and economic alternative to mechanical crimping processes. The non-contact process that EMF offers, creates a more uniform pressure over the

circumference with none of the variation nor tool marks inherent in mechanical processes.

Ralph Shäfer [29] also reported that EMF crimping of electrical cables and contacts leads to a very high and uniform compression. The electrical resistance of EMPT crimped cable connectors is up to 50% lower than of those produced by mechanical crimping.

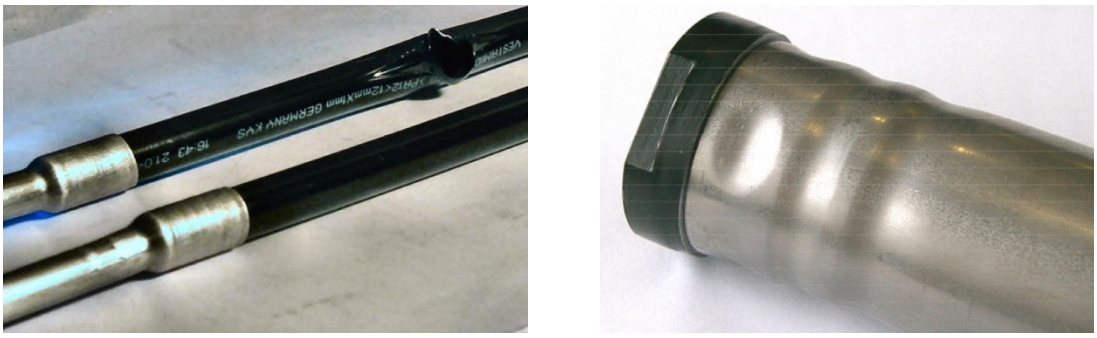

Figure 22: The picture in the left shows crimping of steel fittings onto rubber hoses. The picture in the right shows crimping of a steel truck wing holder [29].

In addition Ralph Shäfer [29] stated that EMPC requires minimal set-up times between different workpiece geometries and offers excellent repeatability. The industrial use of EMPC is widespread with approximately 400-500 EMPT machines installed worldwide. EMPT is often used for joining dissimilar materials such as aluminium or magnesium tubes to steel or plastic inserts. EMPT is used for making very lightweight structures in the transport industry, e.g. for seats of cars and aircrafts - Figure 23.

Figure 23: EMPT crimping of dissimilar materials for lightweight seat structures of cars and aircraft [29].

A study presented by Eguia et al [30], entitled "Improved Crimp-Joining of Aluminium Tubes onto Mandrels with Undulating Surfaces", in which the authors tried to produce high strength structural joints that were cost effectively fabricated by EMC instead of EMPW. The authors reported that there are two key factors in the design and performance of a crimped electromagnetic tube joint. First, is the state of residual stress that exists after the crimped joint is created. The second key issue is the configuration of the joint. The study also includes crimping onto "textured" surfaces such as screw threads and knurls.

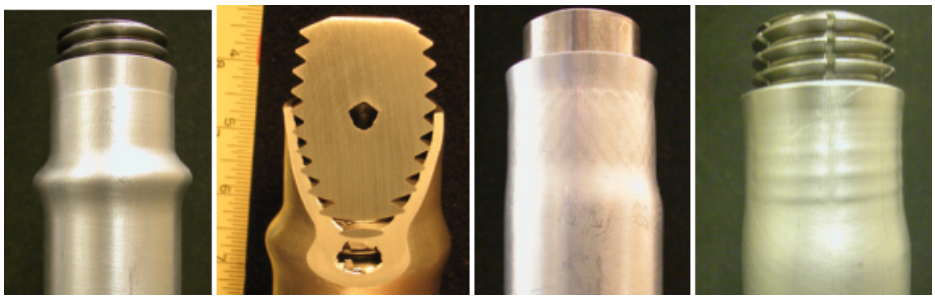

Figure 24:Examples of crimp joints based on surface impression [30].

Eguia et al [30], concluded that crimp joining offers a particularly effective, low-cost and efficient way of joining tubes to mandrels. They stated that there are two especially appealing aspects. First, high velocity forming typically develops a natural interference fit that resists motion. Second, by forming onto undulating surface joints that have the strength of the parent tube in torsion and tension can be created at modest impact velocities.

2.6.2 Related Patents

A brief research concerning the existence of patents related to EMPC was made in order to better understand the state of the art of the technology. Almost all the items listed are US Patents. In between them, there are two patents issued in the 60's devoted to the concept of an electromagnetic system for general forming, while the most recent ones (2006-2009) are focused on the concept of a proper crimping setup to be applied in the automotive (CSA, Hyundai) and aeronautic sectors (Boeing). All patents listed can be found on www.google.com/patents.

Table 2: Patents list.

Publication	Title	Publication Date	Inventor	Abstract
WO 2006101914 A1	Electromagnetic forming crimp	28Sep2006 **Company:**	Dennis Kreft Cooper Standard Automotive Inc	A vehicle cooling system includes a plurality of lines that connect a radiator to a vehicle transmission and an engine. A tube extends from each of the components, and the tubes are each connected to an end of a hose at an interface. The hose is made of a different material than the tubes. A crimp ferrule is located around each of the interfaces. An electromagnetic source applies an electromagnetic field to the

				interfaces to compress the crimp ferrule around the interfaces, creating a secure mechanical joint between the tubes and the hose.
US 6990840 B2	Conjoining apparatus using electromagnetic forming	31Jan2006 **Company:**	Shin Hee Park Hyundai Motor Company	A conjoining apparatus using electromagnetic forming includes a fieldshaper for concentrating a magnetic field to a conjoining working object, a coil for generating and applying the magnetic field to the fieldshaper such that the fieldshaper can form a reactive force, and a charging circuit for supplying electricity to the coil. An auxiliary ring having higher conductivity than steel is disposed between the fieldshaper and the working object for generating an induced magnetic field.
US 3108325 A	Forming device	29Oct1963 **Company:**	George W Harvey Gerald L Allen Gen Dynamics Corp	The present invention relates generally to forming devices and, more particularly, to a device in which metallic material may be formed by the energy acquired from a magnetic field. Accordingly, it is an object of the present invention to provide a magnetic forming device which includes means for increasing the force applied to the metallic material being formed. A further object of the present invention is the provision of means for concentrating the force in a magnetic forming device. Still another object is the provision of a force-concentrating means in a magnetic forming device, which means is durable and efficient in operation and economical to manufacture.
US 2976907 A	Metal forming device and method	28Mar1961 **Company:**	George W Harvey David F Brower Gen Dynamics Corp	An object of the present invention is to provide a method and a device for forming metal in which the energy necessary for forming the metal work piece to a desired shape is acquired from a varying magnetic field. A further object of the present invention is to provide a metal forming device in which the metal work piece is formed in a desired manner by one or more force impulses set up by a varying magnetic field. Still another object of the present invention is to provide a metal forming device which is economical to manufacture, and rugged, durable and efficient in operation.

US 7513025 B2	Magnetic field concentrator for electromagnetic forming	7Apr2009 **Company:**	Allen Fischer The Boeing Company	A magnetic forming system for creating a fluid circuit joint between a tube and a fitting includes an induction coil. The induction coil may form a first stage electromagnetic current. A field concentrator may focus the first stage electromagnetic current to form a second stage electromagnetic current. An insert may focus the second stage electromagnetic current to form an electromagnetic field. The electromagnetic field forms the fluid circuit joint. The induction coil may be insertable within the tube, generate an electromagnetic field, and impose the electromagnetic field on and to expand a portion of the tube within the fitting to form the fluid circuit joint. The system may include a receptacle that is external to the tube and the fitting. An insert may be mechanically coupled within the receptacle and limit the outward expansion of the tube and the fitting.

2.7 Numerical Modelling

Beading the development of an EMPT process into a profitable industrial application requires numerous studies to efficiently model the process. Although the physics of the interaction phenomena's are well understood, accurate simulation of the highly dynamic process still represents a challenge for the scientific community. This is due to the fact that it is required to numerically account for electromagnetic, mechanical and thermal phenomena along with their effect in material's behavior. Since the process is considered to be adiabatic, in the current models, the thermal-conduction effects were neglected. Therefore, the process is often considered as a combination of electromagnetic and mechanical problems [12,27]. The literature presents three different approaches for numerical modeling of EMPT, namely *non-coupled*, *loosely-coupled* and *fully coupled* approach. A brief description of these approaches is presented in the following paragraphs.

In the **Non-Coupled Approach,** the Lorentz forces are calculated without taking into account the workpiece deformation and velocity. These forces are input loads for the mechanical simulation, which is performed in one step only. This approach neglects the forces evolution during the process caused by geometry changes. As a result of this simplification, the process is considered the most efficient since it takes less computation time. The non-coupled approach can be schematically represented as seen in Figure 25 [12,27].

Figure 25: Non-coupled approach (adapted from [12]).

In the **Loosely-coupled Approach**, at each step of time increment, the induced Lorentz forces in the workpiece are calculated with the electromagnetic model. These forces are automatically transferred as input loads into the mechanical model. In this approach, the workpiece deformation is calculated and the geometry updated in order to transfer it to the electromagnetic model for the next time increments. This procedure is repeated iteratively until the Lorentz's forces are insignificant. Researchers have gradually adopted the *loosely-coupled* approach since it returns accurate results with low computational time (when compared to the *fully coupled* approach). Although this methodology is more accurate than the *non-coupled* approach it still neglects the thermal effects, since the process was assumed to be adiabatic [**12**,**27**,**45**]. Figure 26 presents a schematic representation of the *loosely-coupled* approach.

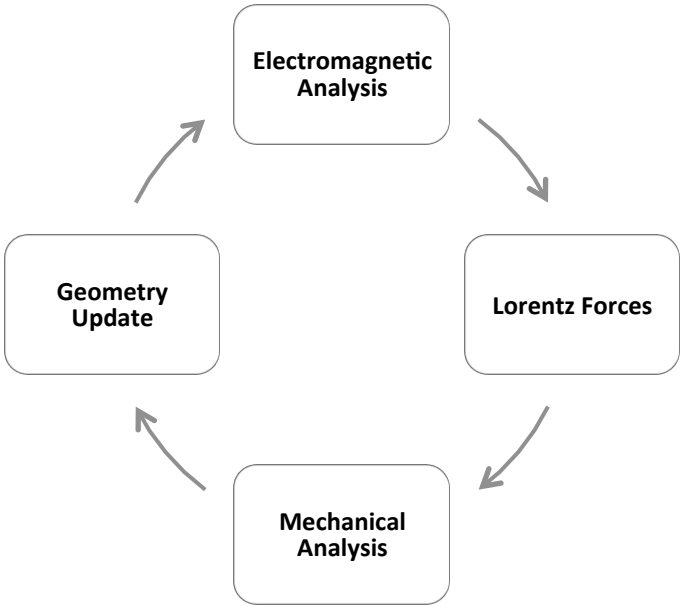

Figure 26: Loosely-coupled approach (adapted from [27]).

Both *non-coupled* and *loosely-coupled* approaches have been extensively used and cited by many authors, as e.g., Ulacia et al. [**46**] and Pérez, Aranguren, et al. [**45**] presented studies in which, the *non-coupled* approach and the *loosely-coupled* approach are compared for sheet metal forming, concluding that both approaches

present results in agreement with the experimental data. However the *loosely-coupled* approach presents more accurate results, on the back to more computational time.

In **Fully-Coupled Approach**, the electromagnetic, mechanical and thermal effects are computed simultaneously for each time step. This is the most accurate method to model the EMPC process. However, this is a highly complex procedure to obtain a converging solution, due to the high computational cost for solving inter-related equations. In addition, the complexity of the solution makes it the less efficient method. Figure 27 is a schematic representation of the *fully-coupled* approach [**12**,**27**,**47**].

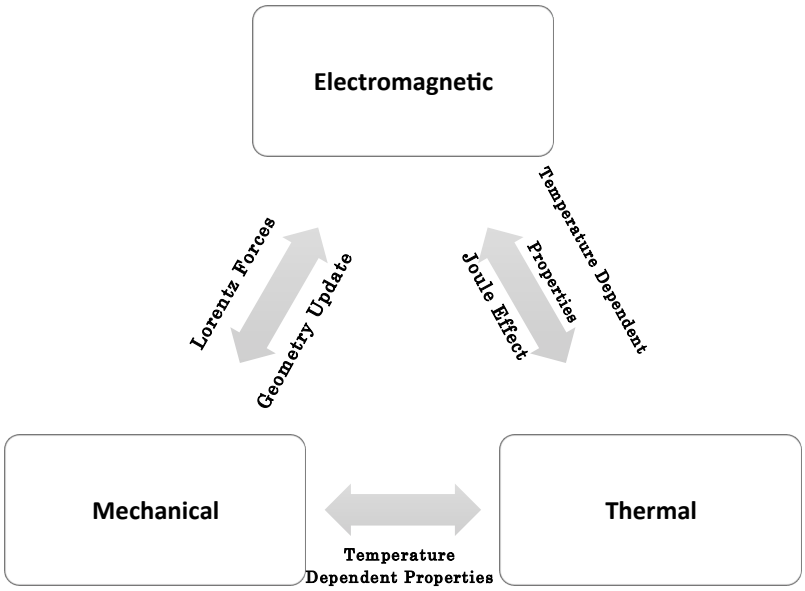

Figure 27: Fully-coupled approach (adapted from [12]).

Fully-coupled 3D simulation towards the study of EMPF has been presented by Stiemer, et al. [**48**]. This method has also been used by Doley et al. [**49**] to predict the interaction of the electromagnetic field and the structural deformation in order to determine the effect of the first current peak during the EMPF.

3 DEVELOPMENT OF THE ELECTROMAGNETIC PULSE CRIMP TOOL

The present chapter is related to the development of a customized electromagnetic crimp tool for YSE products. In first place, the different case studies are identified. Their mechanical properties and technical requirements are presented and, in order to assess the applicability of the EMPC technology for this product, a preliminary exploratory set of experiments was conducted. The results of these experiments allow assessing the potential applicability of EMPT for crimping electrical cables. Furthermore, the preliminary experiments have particular importance to understand the terminal-cable bonding principles as well as the behaviour of the different components during the EMPC process. These are key in development of a customized tool, along with the materials selection for its manufacturing.

Lastly, the numerical simulation of the EMPC process is introduced. The aim is to evaluate the performance of the tool concept previously developed as well as to estimate the discharge voltage required to crimp the electrical cables. Numerical analysis encompassed numerous steps such as the 3D modelling, meshing and keyword files creation. The results returned by numerical simulation were considered to be promising, allowing to validate the concept developed.

3.1 Case Studies: Materials and Technical Requirements

YSE has selected three different combinations of terminals and cables. This selection enabled the pre-assessment of the joint quality, mechanical resistance and failure mode, as well as the range of main process parameters to be used. YSE provided a wide set of information including 2D and 3D drawings, dimensions and materials of the terminals and electrical wires to be combined, as well as the mechanical properties of the joints. The different combinations of terminals/cables provided by are shown in Table 3.

Table 3: Terminal/Wire combinations provided by YSE.

# Combination	Terminal				Wire	
	Ref.	Diameter [mm]	Length [mm]	Thickness [mm]	Ref.	Cross-Section Area (T) [mm²]
A	7009-2054	8.00	32.00	1.20	T2IRSP	16.00
B	7009-2055	9.50	36.00	1.25	PT3DSP	25.00
C	7004-1327-02					

Figure 28: 3D drawing of the electrical terminals.

Regarding the EMPC process, it is important to refer that the terminal is called the "process workpiece", since this is the part that will be deformed by electromagnetic forces. Therefore, it is of paramount importance to have knowledge of the geometric characteristics, as well as the material properties of each terminal (Figure 28). The terminal's material is copper (Cu/b_1 – AFNOR or DHP - ISO), with a thin external tin (Sn) coating layer of 3 µm, which is critical to avoid corrosion of the terminal. DHP is a non-alloyed copper (99.90% of copper Cu) with a residual deoxidizer, phosphorus (P) in about 0.013% to 0.050% [**50**]. According to the information provided by YSE, the terminals present hardness values between 50 HV and 75 HV.

Moreover, YSE, provided requirements for critical functional properties, such as the compression ratio, electrical resistivity and tensile strength. The values presented in Table 4 should be considered as the minimum force under tensile conditions, the maximum electrical resistivity and the minimum compression ratio values accepted.

Table 4: Requirements for the critical functional properties of YSE crimp joints.

# Combination	Force [N]	Electrical Resistivity [mv/A]	Crimping Ratio (C) [%]
A	1750.0	-	15-50
B	784.0	0.120	
C	2940.0		

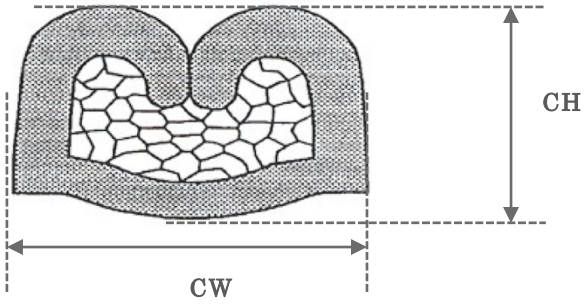

Figure 29: Crimp cross-section [51].

The parameters defined as minimum in Table 4 are determined by the crimping ratio, defined as follows [52]:

$$C = \left(1 - \frac{T}{A}\right) 100\% \qquad (26)$$

where C is the crimping ratio, T is the area contained by the crimp tools and A the sum of the cross sectional areas of the terminal and the conductor.

A typical mechanical/electrical resistance curve provided by YSE, as a function of the crimping height (CH), is presented in Figure 30. It is possible to observe, both over and under compression can result in poor electrical and/or mechanical performance. It must be noted that the CH values associated with the optimal mechanical or electrical performance do not match, meaning that a compromise is required, i.e. it is often necessary to sacrifice the mechanical resistance in favour of the electrical resistance ("Validated Crimp Height" zone).

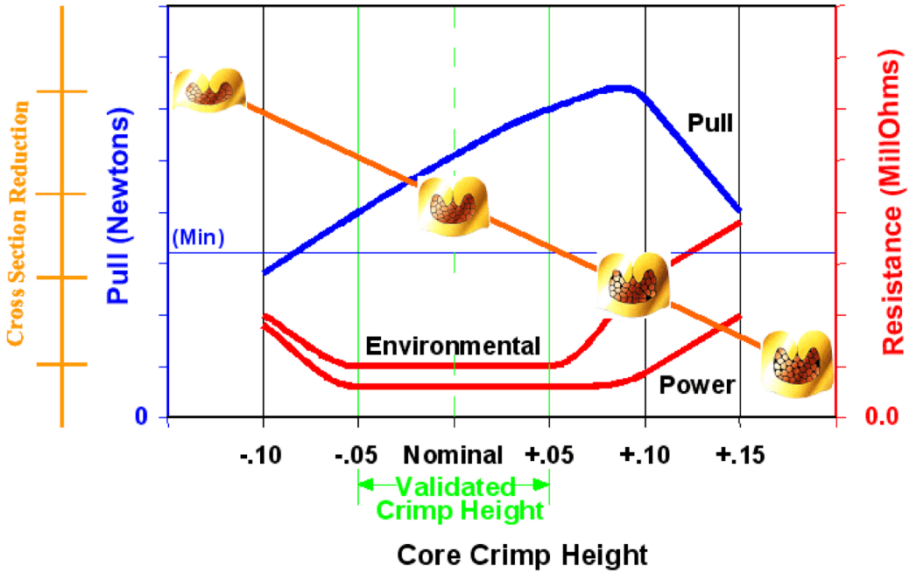

Figure 30: Typical mechanical/electrical vs. crimp height curve [51].

3.2 Preliminary Experiments

In order to verify the applicability of the process for crimping electrical cables, exploratory experiments were performed. All tests were executed in a magnetic pulse system 25 kJ/ 25 kV available at INEGI facilities. The system is equipped with two capacitor modules, each one with a capacitance of 40 μF, having the machine a total capacitance of 80 μF. The maximum energy storage is 25 kJ, being the maximum charge voltage and output current of 25 kV and 400 kA, respectively. Additionally, magnetic pulse system characteristics are presented in Table 5.

Figure 31: EMP machine.

Table 5: Magnetic pulse system specifications.

Specification	Value	Units
Capacitance	80	μF
Resistance	19	mΩ
Inductance	0.1	μH

Using the equation below, was possible to determine the relation between the input voltage and output energy as shown in Figure 32.

$$E = \frac{1}{2}CV^2 \qquad (27)$$

where E is the equivalent energy, C is the capacitance of the machine and V the discharge voltage.

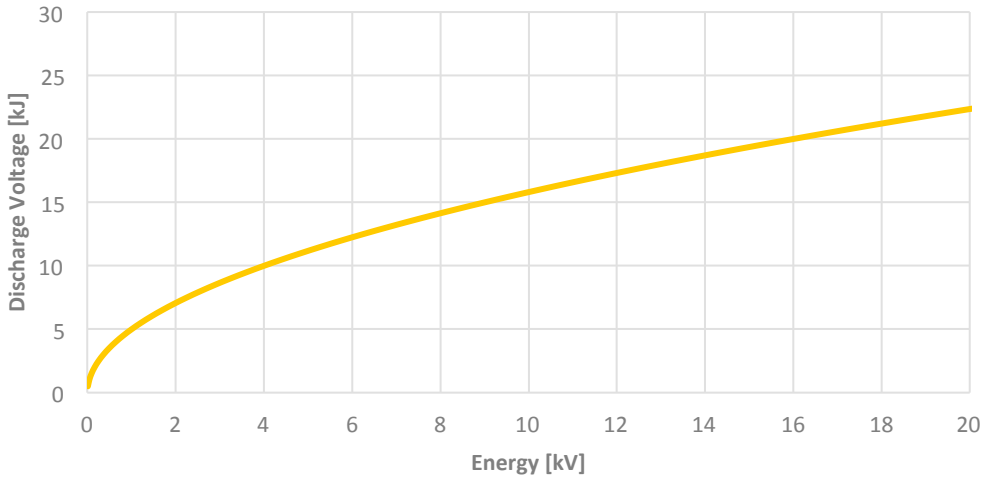

Figure 32: Discharge Voltage vs. Energy.

In order to induce the required magnetic pressure to collapse the terminal into the conductor, a copper wire, with 3 mm of cross-section, was winded around the terminal – Figure 33. It is important to mention that the copper wire has a special insulation to prevent arc generation during the pulse. After the coil was winded, the terminal was removed and its ends were scraped in a lathe, aiming to remove the insulation, this is imperative to promote the current flow since the coil ends will carry the pulsed current – Figure 34. The machine setup for the experiments was prepared by firstly placing insulator sheets above the machine coupling devices. On top of the insulators, a wood board and a rubber layer was placed. Using two bolts, this configuration was fixed along with the coil, as shown in Figure 35. In the same image, the terminal is wrapped in a special insulator, Kapton, with the purpose to insulate the terminal from the current, preventing arc generation. The tests were performed using a single pulse. The three different terminal/wire combinations were tested (Table 3). The energy values used in these preliminary experiments were in the range from 1.5 kJ to 5 kJ.

It is also relevant to mention that handmade coil*s* are destroyed and partially vaporized during the energy discharge - Figure 36. This is a consequence of the intense magnetic forces created by the energy discharge that will result in the plastic deformation of the terminal, which will, with the same intensity, affect the coil. Although copper has high electrical conductivity (required for the process), it also has poor mechanical properties that are not capable to withstand the high magnetic forces during the pulse.

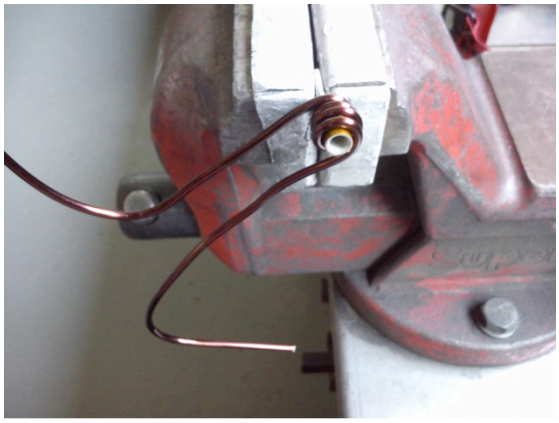

Figure 33: Handmade winding.

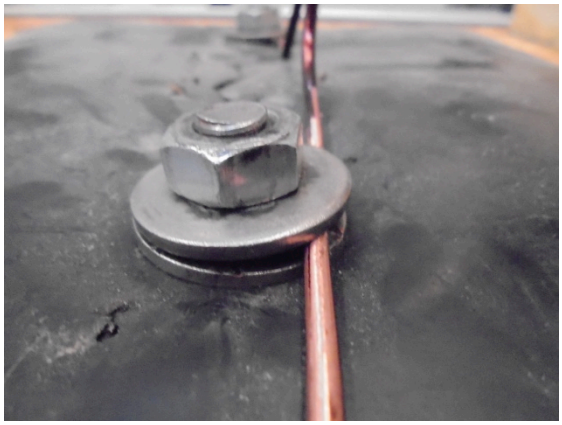

Figure 34: Scrapped ends detail.

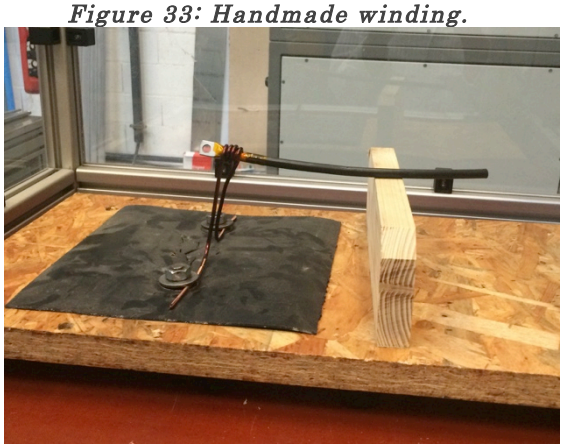

Figure 35: Setup prepared for the preliminary experiments.

Figure 36: Destroyed coil after the pulse.

In order to pre-assess the strength of the joints a set of tensile tests were conducted. Due to machinery limitations related to the slip between the free end of the cable and the machine claws, the cables were crimped on both sides. It is important to mention that the tensile test performed by YSE has a different setup from the one performed in INEGI. However, the performance of the tensile tests allowed having an indication of the tensile values that a crimp joint by EMPC can achieve. An example of the force-displacement curve obtained is shown in Figure 38 (speed: 5 mm/min; at room temperature: 23°C). Some aspects should be highlighted such as: till a displacement of 10 mm, the force is constant, and suddenly drops; the failure mode of the joints was the copper wire rupture, and no slip between the terminal and the wire was verified; the maximum force measured for the different combinations is presented in Table 6.

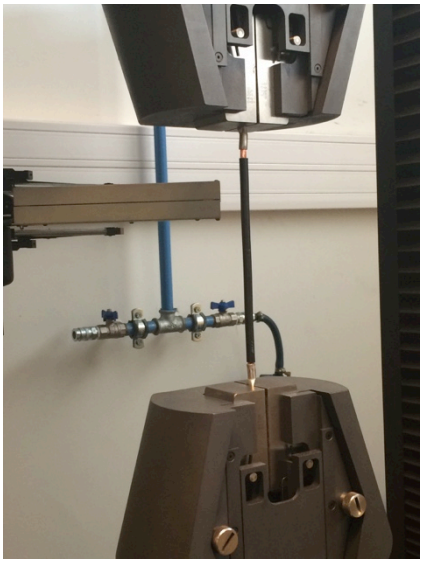

Figure 37: Preliminary tensile test.

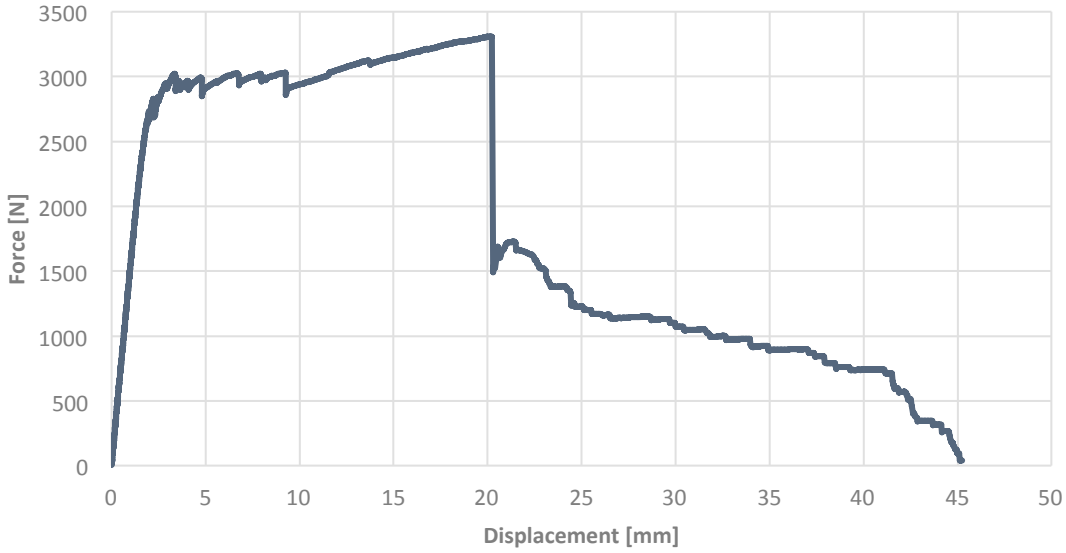

Figure 38: Force vs. Displacement curve achieved during the preliminary tensile test of combination #C by EMPC.

Table 6: Comparison between the force of the tensile test by preliminary EMPC and set by YSE.

# Combination	Reference Values [N]	Maximum Force [N]
A	1750.0	1500.0
B	784.0	2600.0
C	2940.0	3310.0

The results of the tensile tests presented in Table 6 were considered promising; at the exception of #A, combinations #B and #C presented maximum tensile values higher than the ones set by YSE crimping capability tests. Nevertheless, higher values of energy can be used, meaning that the value of the tensile strength in combination #A can be increased. However, in order to compare

the strength of the EMPC connections with the reference ones, the same standardized procedure should be used.

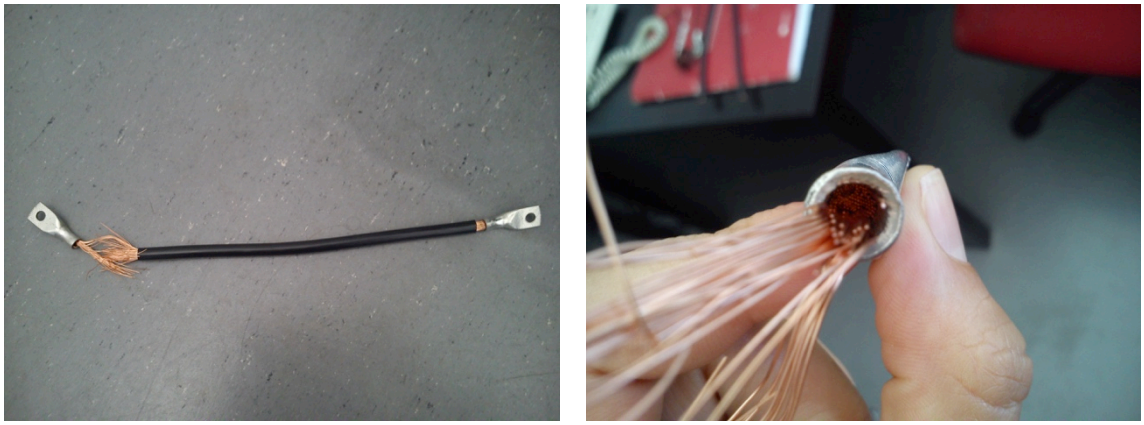

Figure 39: Failure mode details.

At the moment when the crimped wire was taken off from the EMP machine, the visual aspect of the terminal revealed a change in its brightness. One of the reasons pointed out is that higher brightness level can be caused by the vaporization of the coating during the EMPC process. In order to investigate this phenomenon, samples were cut and prepared for SEM/EDS[1] analysis as shown in Figure 40.

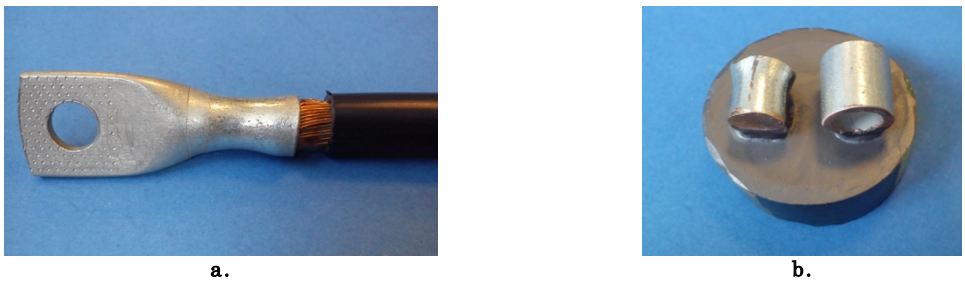

a. **b.**

Figure 40: a. Detail of the modification of surface finish after compression b. Samples prepared for SEM observation.

The results of the SEM/EDS analysis are presented in Figure 41. As can be observed both the non-deformed terminal (green line) and the EMPC sample (red line) present the same amount of tin (Sn), meaning that the coating was not vaporized during the process. However, a higher value of copper (Cu) is seen in the EMPC sample, which probably results from the vaporization of the coil during the pulse. This leads to the possibility that the modification of the surface aspect can be related with two mechanisms: copper deposition on the surface and the significant deformation. Furthermore, literature refers that texture changes due to the high strain rate can also be affecting the surface finish [**53**].

[1] SEM/EDS analysis makes use of the X-RAY spectrum emitted by a solid sample when bombarded with a focused beam of electrons to obtain a localized chemical analysis. Sample preparation is achieved by embed the samples in epoxy resin blocks [91].

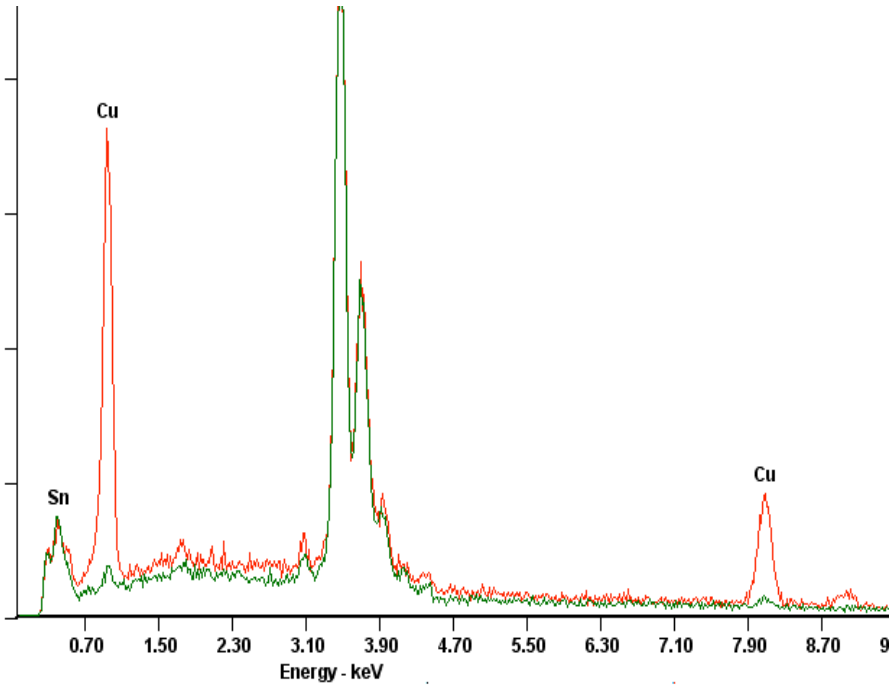

Figure 41: Results of the EDS analysis. Comparison between a non-deformed terminal (green line) and one crimped by magnetic pulse technology (red line).

3.3 Customized Tool Design

A customized tool set was developed to crimp the electrical cables. The tool includes three main components, which have been described more widely in Section 2.4, namely:

Primary Coil – the coil is the key tool of EMPC process, and it should be designed taking into account the components to be joined.

Fieldshaper – this component is used to concentrate the magnetic flux and produce even magnetic pressure over the desired area. Despite the unavoidable losses associated with energy dissipation, the electromagnetic field produced by the fieldshaper in the work zone is stronger than that produced by the primary coil. Using a fieldshaper also improves the EMPC flexibility, since a single coil, with a reduced number of fieldshapers, can be applied to a wide range of workpiece dimensions – different terminals.

Two Electrical Insulators – placed between the main coil and the fieldshaper and between the fieldshaper and the workpiece. The insulators purpose is to prevent the presence of electrical arcs between the different components.

The drawing of the EMPC tool set, developed specifically for crimping the electrical cables for YSE, is presented in Figure 42. The design chosen is a single-layer with 5.5-turn solenoid coil (component #1) inductively coupled to the conical fieldshaper (component #2). It is important to mention, that the tool final design is constrained by the ability of the milling experts to produce the exact shapes of the components of the EMPC tool defined in the 3D drawing.

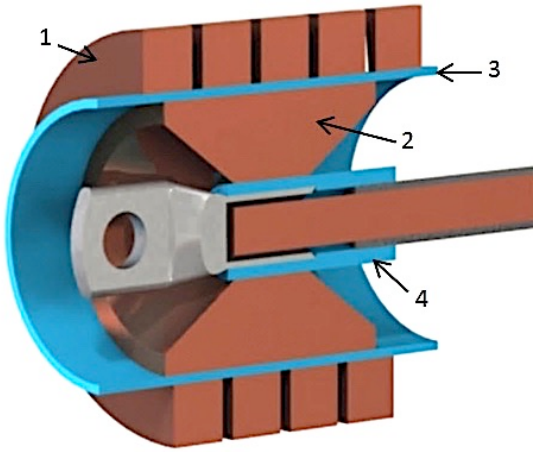

Figure 42: 3D model of the EMPC tool and its main components: 1. Primary coil; 2. Fieldshaper; 3. Electrical insulator; 4. Electrical insulator.

Regarding the insulators (component #4) besides their function of preventing electric arc, they are also used to correctly place the terminal. In this project, additional devices were designed for coupling the main tool to the magnetic pulse workstation - Figure 44. In terms of the design of the main individual components, the following can be summarized:

Primary Coil: The inner diameter and axial length of the multi-turn coil were defined based on dimensions of the fieldshaper. The optimum number of turns per unit of length depends on the generator capacity and magnetic pressure required to deform the terminal. Increasing the number of turns per unit of length, for the same discharge current, increases the magnetic field intensity. On the other hand, the reduction of the coil pitch will increase the total inductance of the system, resulting in the decrease of peak discharge current. This results in leak of magnetic flux through the workpiece, and loss in process efficiency. For this case, 5.5 turns have been selected – preliminary electromagnetic simulations support this design and are shown in the following section.

Fieldshaper: The geometric aspects mainly define the fieldshaper design i.e. by the desired shape of the work zone, by the diameter of the terminal as well as by the width of the compression zone. A conical shape was selected, since the decrease on the radial length will favour the increase of the current density, allowing not only the homogenization of the magnetic field, but also, a significant increase of the magnetic pressure on the workpiece area.

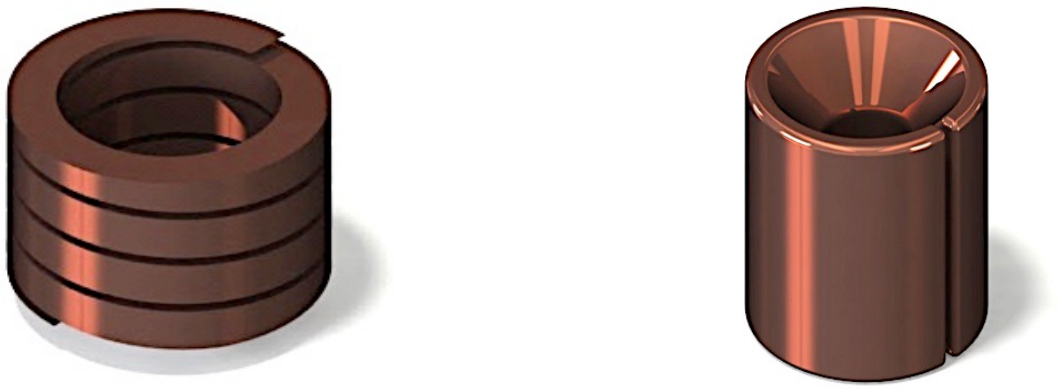

a. b.

Figure 43: a. Primary coil; b. Fieldshaper (w/radial slit detail) developed.

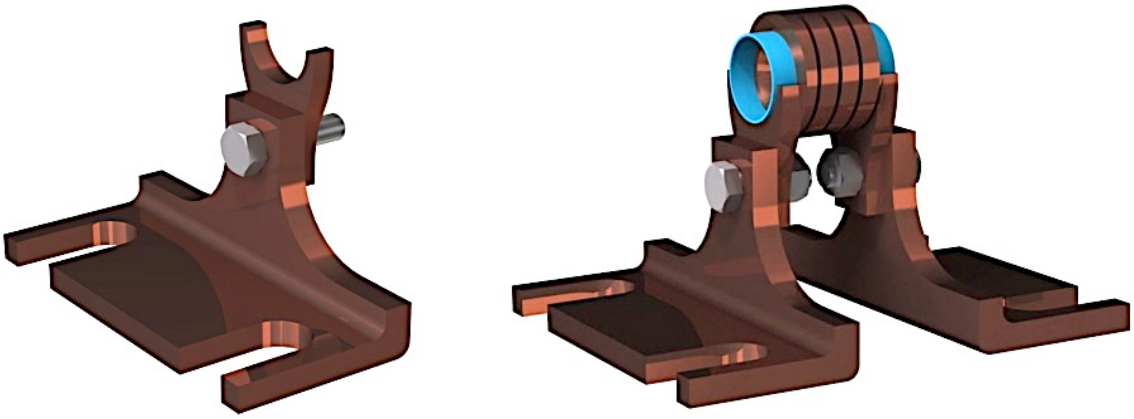

a. b.

Figure 44: a. Detail of the coupling device; b. 3D Model of the EMPC setup.

Concerning the tooling materials, it is important to remember that the coil and the fieldshaper material should combine good electrical conductivity with strong mechanical endurance against the pulse loads and thermal shocks. The alloy suggested to YSE (responsible for tool manufacturing) for the coil, fieldshaper as well as for the coupling device is Cu 18150. This is a Chromium (Cr) Zirconium (Zn) Copper (Cu) alloy that presents high electrical conductivity, hardness and ductility as well as excellent resistance to softening at elevated temperatures (little effects by Joule effect). This alloy presents chromium (Cr) between 0.50 % to 1.50 % and zirconium (Zr) between 0.05 % and 0.25 % [**54**].

Table 7: Comparison between pure copper and chromium zirconium copper alloy [55].

Properties	Pure Copper (Cu)	Chromium Zirconium Copper (Cu 18150)
Yield Strength [MPa]	33.30	370.00
Modulus of Elasticity [GPa]	117.00	123.00
Thermal Conductivity [W/mK]	399.00	325.00
Electrical Conductivity [MS/m]	59.27	46.49

Table 7 shows that all properties of pure copper and the chromium zirconium copper are comparable with the exception of the Yield Strength. This property has special relevance, since, as explained before, the tool will have to withstand the same forces as the ones applied to the workpiece. Higher yield strength, results in a more durable coil and fieldshaper that will, most likely, not collapse with few

shots. In addition, the Cu 18150 alloy has lower thermal conductivity, which is favourable since the tool will have to endurance numerous cycles of discharge current that cause heating on the workpiece by Joule effect. As for the insulators, G-10 laminated phenolic composite is typically used. This is a glass-epoxy laminate composite and is specified for its extremely high strength and high dimensional stability with temperature.

3.4 Numerical Modelling

The main purpose of using numerical tools in the simulation of EMPC process is not only to observe the magnetic flux distribution through the coil, and thus accurately predict the terminal behaviour during deformation, but also to provide an early estimation regarding the order of magnitude of corresponding process parameters. However, due to high complexity and combination of electromagnetic, mechanical and thermal problems, the numerical simulation of EMPC process is still a challenge. Numerous models were developed in the last decades, and some of them were discussed in the previous section. Still, their complexity and time required to present a convergent solution motivates the need for improvement. The numerical simulation was performed using the software LS-DYNA® (available in the 980 version).

LS-DYNA® is a highly advanced general-purpose, non-linear, finite element program, capable to simulate complex problems. This software is especially appropriate to investigate phenomena that involve large deformations, sophisticated material models and complex contact conditions [**39**]. The Electromagnetic solver in LS-DYNA® focuses on the calculation and resolution of the so-called Eddy currents and their effects on conductive pieces. In electro-mechanics, passing an alternating fast rising current in a conductor causes self-induction. The self-induction in conductors is the responsible for a second phenomenon called skin effect. The resolution of these two-coupled phenomena allows calculating the Lorentz force and the Joule heating energy. The Electromagnetic solver works by firstly solving a full Eddy current problem on one full period using a “micro” ElectroMagnetic (EM) time step, during this procedure, an average of the EM fields and Joule heating energy are computed. It is assumed that the properties of the material: heat capacity, thermal conductivity and electrical conductivity do not change over a certain number of oscillation periods defined by a “macro” time step. The “macro” time step can have the same time as the total time of the run, as long as the properties of the material are not temperature dependent. Following this, no further EM calculation is done over the macro time step and the Joule heating is simply added to the thermal solver at each thermal time step. After reaching a “macro” time step, a new cycle is initiated with a full Eddy current resolution. This method can efficiently solve the electromagnetic problems, which involve a big amount of current oscillation periods [**56**].

LS-DYNA® works with keyword files towards problem modulation, one file containing the mesh information, one for the structural problem and other covering the electromagnetic problem. These files are coupled between them, in a way that, during the simulation the solver will compute the different problems using the information contained in each file. In the following sections, a description of each one of the keyword files is presented.

- **MESH FILE**

The mesh file was obtained by firstly creating the 3DCAD model in *SolidWorks*®, this was then exported to ABAQUS®. Though LS-DYNA® possesses CAD manipulation/meshing tools these are not as user friendly as the ones presented by ABAQUS® software, and, thus making it the chosen to mesh generation. The different components of the tool and the terminal itself were meshed with C3D8R elements – continuum, 3D, 8-node with reduced integration [**57**]. As for the cable, it was meshed with S4R elements – shell, 4-node with reduced integration [**57**]. Following the mesh creation, the model was exported to LS-DYNA®. With the model exported and saved as a keyword file, the step that follows is the creation of SETs, which are a group of nodes or elements that will, in the electromagnetic file, carry the information related to the place where the current enters and exits in the coil - Figure 46. Additionally, a SET containing the inside of the terminal is added; this represents the place where magnetic shielding occurs - Figure 47. The SET's created, have their own ID making them unique to the program, this is important once they will be called for their ID's in the electromagnetic file.

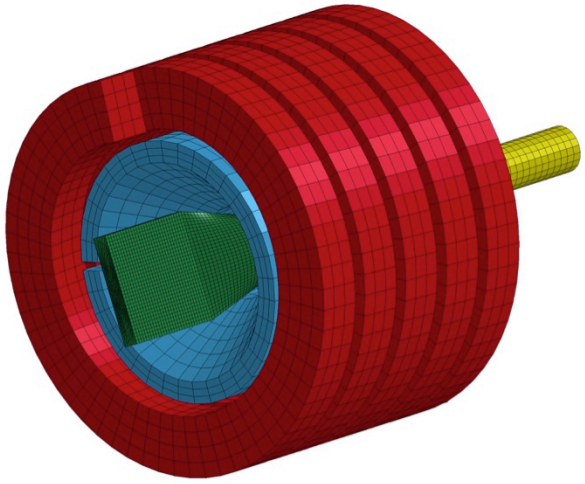

Figure 45: 3D finite element model of the EMPC simulation.

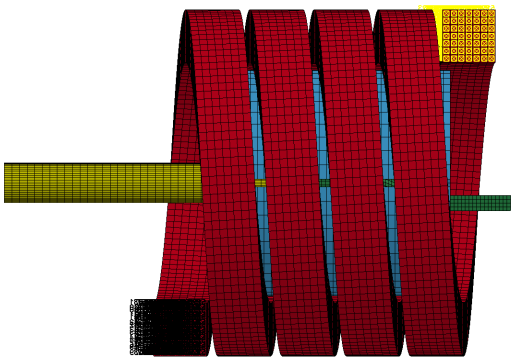

Figure 46: Coil In and Out SET's.

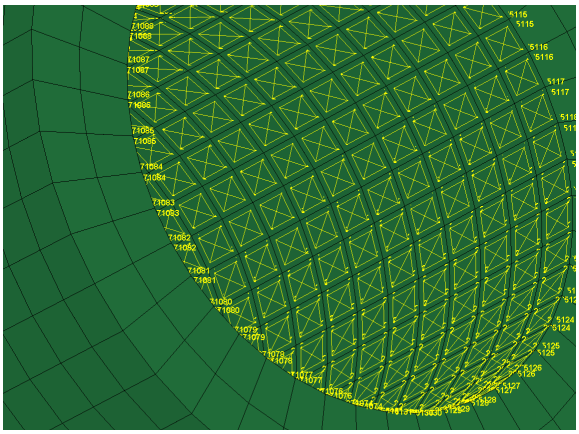

Figure 47: Terminal interior SET.

Summing up the keywords present in the mesh file created for problem modulation:

***BOUNDARY_SPC_SET** – keyword that is related to the boundary conditions. The terminal was fixed in its axial direction;

***SET_NODE_LIST_TITLE** – containing the group of nodes that are part of the boundary condition previously defined;

***SET_SEGMENT_TITLE** – containing the elements that in which different electrical/magnetic conditions will be applied.

#sid: 1 – COIL_IN #sid: 2 – COIL_OUT #sid: 3 – TERMINAL_IN

***ELEMENT_SOLID** – containing the mesh information of each one of the solid parts existent in the model;

#pid: 1 – COIL #pid: 2 – FIELDSHAPER #pid: 3 – TERMINAL

***ELEMENT_SHELL** – containing the mesh information of each one of the shell parts existent in the model.

#pid: 4 – CABLE

- **STRUCTURAL FILE**

The structural file contains information regarding the mechanical problem. Firstly, the information related to the time control parameters were set. Termination time was specified into the keyword card, stating that, as the time chosen is achieved, the calculation stops. Following, the time-step size to be used in the calculation, as well as the plotting output were defined. Also, in this file, the materials for each one of the parts were set. This involved the knowledge of material parameters such as density, Young's modulus, and Poisson ratio. Furthermore, the material used for the terminal had also to be characterized, taking into account the type of solicitation that will occur during the crimping

process (e.g. high values of deformation and high values of strain rate). Among the numerous material laws capable of describing the material behaviour, as described in Section 3.4.1, Johnson-Cook law was the one used. Is important to refer that the coil and the fieldshaper were defined as elastic parts and the cable was set as a rigid part. Information regarding the contact surface-to-surface that will occur once the terminal collapses into the cable is also present. In the end of the file, is included the mesh file previously created. The units used are in agreement with the S.I. system.

Summing up the keywords present in the structural file created for problem modulation (widespread information about the keywords can be found on [**58**]):

***CONTROL_TERMINATION** – stops the job. The endtime variable, was defined according to the time that the current discharge takes to reach the peak and diffuse through the different components, as well as the time the workpiece takes to be completely deformed;

Card	1	2	3	4	5	6	7	8
Variable	endtim	endcyc						
	5.50E-5	0						

***CONTROL_TIMESTEP** – controls the time-step and its evolution. The dtinit variable goal is to define the increments, in which the computation is made;

Card	1	2	3	4	5	6	7	8
Variable	dtinit	tssfac	Isdo	tslimit	dt2ms	lctm	erode	ms1st
	1.50E-6	0	0	0	0	5	0	0

***DATABASE_BINARY_D3PLOT** – controls the output file. The dtinit variable defines the time instants that will be written in the output file;

Card	1	2	3	4	5	6	7	8
Variable	dtinit	tssfac	Isdo	tslimit	dt2ms	lctm	erode	ms1st
	1.50E-6	0	0	0	0	5	0	0

***MAT_ELASTIC** – defines an isotropic elastic material, parameters in use were provided by the material suppliers [**59**];

Card	1	2	3	4	5	6	7	8
Variable	mid	ro	e	pr	da	db	not	used
	1	8.49e-3	12.30e10	0.31	0	0	0	0

***MAT_SIMPLIFIED_JOHNSON_COOK**– defines the material using a simplified version of the Johnson-Cook law, the parameters in use were found on literature [**60**];

Card1	1	2	3	4	5			
Variable	mid	ro	e	pr	vp			
	2	8.49e-3	12.30e10	0.31	0			
Card2	**1**	**2**	**3**	**4**	**5**	**6**	**7**	**8**
Variable	a	b	n	c	psfail	sigmax	sigsat	epso

	74.00	375.00	0.398	0.0208	1.0e1	1.0e1	81.0e28	1.00

***MAT_RIGID**– define parts that will be considered by the software as belonging to a rigid body, the parameters in use were provided by YSE;

Card	**1**	**2**	**3**	**4**	**5**	**6**	**7**	**8**
Variable	mid	ro	e	pr	n	couple	m	alias
	3	8.49e-3	12.30e10	0.31	0	0	0	0

***SECTION_SOLID**– defines section properties for solid continuum elements;

Card	**1**	**2**	**3**	**4**	**5**	**6**	**7**	**8**
Variable	secid	elform	aet					
	1	1	0					

***SECTION_SHELL** – section properties for shell elements;

Card1	**1**	**2**	**3**	**4**	**5**	**6**	**7**	**8**
Variable	secid	elform	shrf	nip	propt	qr/irid	icomp	setyp
	2	2	1.00	2	1	0	0	1
Card2	1	2	3	4	5	6	7	8
Variable	t1	t2	t3	t4	nloc	marea	idof	edgset
	0.05	0.05	0.05	0.05	0	0	0	0

***PART**– relates the part ID to *SECTION and *MATERIAL;

Card	1	2	3	4	5	6	7	8
Variable	pid	secid	mid	eosid	hgid	grav	adpopt	Tmid
$COIL	1	1	1	0	0	0	0	0
Card	1	2	3	4	5	6	7	8
Variable	pid	secid	mid	eosid	hgid	grav	adpopt	tmid
$FiELDS	2	1	1	0	0	0	0	0
Card	1	2	3	4	5	6	7	8
Variable	pid	secid	mid	eosid	hgid	grav	adpopt	tmid
$TERM	3	1	2	0	0	0	0	0
Card	1	2	3	4	5	6	7	8
Variable	pid	secid	mid	eosid	hgid	grav	adpopt	tmid
$CABLE	4	2	3	0	0	0	0	0

***CONTACT_AUTOMATIC_SURFACE_TO_SURFACE**– the main purpose is to set the parts between which contact will occur during problem computation.

Card	**1**	**2**	**3**	**4**	**5**	**6**	**7**	**8**
Variable	ssid	msid	sstyp	mstyp	sboxid	mboxid	spr	mpr
	4	3	3	3	0	0	0	0

- **ELECTROMAGNETIC FILE**

The third file required for the EMPC process modulation is the electromagnetic one. This file contains information regarding the circuit type and its characteristics, which are obtained as shown in Section 3.4.2. Furthermore,

using the SET's previously created in the mesh file, the current flow through the coil is assigned, as well as, the magnetic shielding inside the terminal. The electromagnetic file also contains the definition of the material type, for each one of the materials created in the structural file – insulator, conductor carrying a source and conductor not connected (where the Eddy current problem is solved). Finally, this file has included the structural file previously created.

Summing up the keywords present in the electromagnetic file created for problem modulation:

***EM_CONTROL** – enables the EM solver and set its options. The time increments and instants were defined according to the methodology explained in the keyword of the structural problem;

Card	1	2	3	4	5	6	7	8
Variable	emsol	numls	dtinit	dtmax	t_init	t_end	ncyclfem	ncyclbem
	1	0	1.00e-6	1-00e-6	0	0	20	20

***EM_CIRCUIT** – defines the electrical circuit properties. The resistance, inductance and capacitance are defined according to the values obtained in section 3.4.2;

Card1	1	2	3	4	5	6	7	8
Variable	circid	circtyp	lcid	r/f	l/a	c/t0	v0	
	1	3	0	12.96	2.50e-4	8.00e-8	9.00e9	
Card2	1	2	3	4	5	6	7	8
Variable	sidcurr	sidvin	sidvout	partid				
	1	2	1	0				

***EM_BOUNDARY** – defines boundary conditions for the electromagnetism problems. The btype variable is referent to the magnetic field shielding of the terminal interior – SET 3;

Card	1	2	3	4	5	6	7	8
Variable	ssid	btype						
	3	9						

***EM_MAT_001**- defines the electromagnetic material type and properties.

Card	1	2	3	4	5	6	7	8
Variable	em_mid	mtype	sigma	eos				
	1	3	43.50	0				
Card	1	2	3	4	5	6	7	8
Variable	em_mid	mtype	sigma	eos				
	2	4	43.50	0				
Card	1	2	3	4	5	6	7	8
Variable	em_mid	mtype	sigma	eos				
	3	4	25.00	0				
Card	1	2	3	4	5	6	7	8
Variable	em_mid	mtype	sigma	eos				
	4	1	0	0				

3.4.1 Material Definition

To simulate the materials behaviour is necessary to have knowledge of their mechanical characteristics. Knowing these characteristics is possible using the stress-strain curve, which is obtained by performing a tensile test. This test is one of the most common methodologies to measure material strength. It involves the material linear stretching up to failure and can be used on most types of materials. Tensile tests give information about yield strength, ultimate tensile strength, modulus of elasticity, and elongation at fracture among other important properties [61]. To perform this test, samples of the material are prepared taking into account the international standard ISO 6892-1:2009. In Figure 48 is shown the sample shape and dimensions.

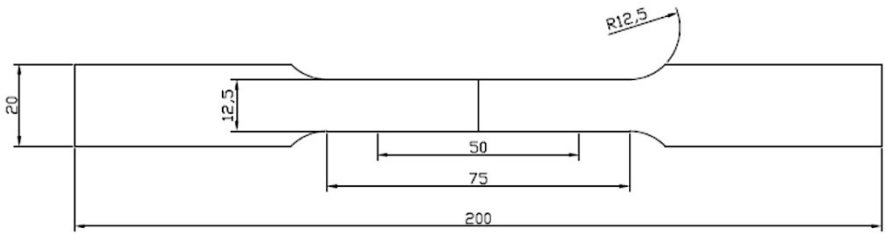

Figure 48: Tensile test sample shape and dimensions [12].

The force and displacement resulting from the tensile test are converted to engineering stress-strain using the relation [50]:

$$\sigma_{eng} = \frac{F}{A_0} \quad (28)$$

where F is the applied force and A_0 is the initial area.

The deformation is expressed in terms of strain, ε_{eng}, given by the relation [50]:

$$\varepsilon_{eng} = \frac{L - L_0}{L_0} \quad (29)$$

where $L_0$is the initial length of the sample and L the final length.

The true stress-strain curve is then calculated using the engineering one, using the following relations [50]:

$$\sigma = \sigma_{eng}\left(1 + \varepsilon_{eng}\right) \quad (30)$$

$$\varepsilon = ln\left(1 + \varepsilon_{eng}\right) \quad (31)$$

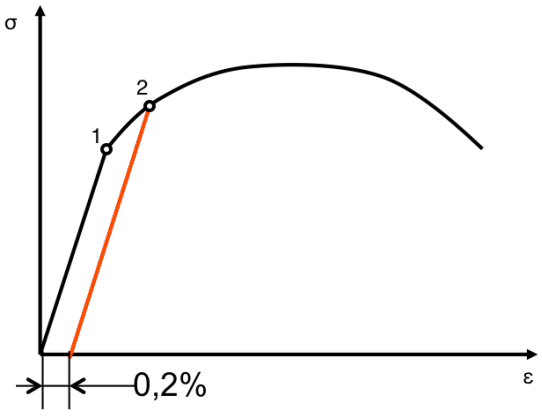

Figure 49: Stress-Strain curve.

Hooke's Law, Equation (32), describes the true stress-strain curve in the elastic part. The point 1 in the figure above corresponds to the Elastic Limit, and point 2 to the Yield Strength. As for the plastic part, there are several studies that present formulations capable to describe the material's behaviour during plastic deformation such as: **Hollomon** [62] - Equation (33), **Swift** [62] - Equation (34), **Voce** [63]- Equation (35) and **Johnson-Cook** [64] - Equation (36).

$$\sigma = E\varepsilon \qquad (32)$$

$$\sigma = K\varepsilon^{n} \qquad (33)$$

$$\sigma = K(\varepsilon_0 + \varepsilon)^{n} \qquad (34)$$

$$\sigma = S\left[1 - Ae^{-B(\varepsilon_0+\varepsilon)}\right] \qquad (35)$$

$$\sigma = (A + B\varepsilon^{n})(1 + Cln\dot{\varepsilon}^{*})(1 - T^{*m}) \qquad (36)$$

Concerning the laws above, the one used in the material definition for modeling the tooling and EMPC process is the Johnson-Cook law, and regarding the law chosen the parameters are as follow: A is yield stress of the material under reference deformation conditions, B is strain hardening constant, n is strain hardening coefficient, C is strain rate strengthening coefficient and m is thermal softening coefficient. In the expression corresponding to the Johnson-Cook model the strain rate, $\dot{\varepsilon}^{*}$, and the homologous temperature are calculated using the relations [64]:

$$\dot{\varepsilon}^{*} = \frac{\dot{\varepsilon}}{\dot{\varepsilon}_{ref}} \qquad (37)$$

$$T^{*} = \frac{T - T_{ref}}{T_m - T_{ref}} \qquad (38)$$

where $\dot{\varepsilon}_{ref}$ and T_{ref} are the reference strain rate and deformation temperature respectively, T_m is the melting temperature of the material and T the deformation temperature. Since the materials provided to perform the tests were in product form, produce tensile testing samples was not possible. However, the parameters for the Johnson-Cook law, as well as other electrical, mechanical and

magnetic properties have been discussed in literature and the simulation was created based in these values.

3.4.2 Resistance-Inductance-Capacity

The Resistance-Inductance-Capacity (RLC) characteristics of the magnetic pulse system present in INEGI facilities were measured using a Rogowski coil, so as to be introduced into the electromagnetic file of the LS-DYNA® model. Rogowski coils consist of a wire wound on a non-magnetic core - Figure 50. This coil is placed around the conductor with toroidal shape and the magnetic field produced by the current induces a voltage in the coil. The voltage output produced by the coil is proportional to the rate of changing current. Afterwards, this voltage is integrated, consequently producing and output proportional to the current [65,66].

The voltage, *v(t)*, is a function of winding factor, *Kr*, and the frequency, *Fr*, of the sinusoidal current, *i(t)*.

$$v(t) = Kr.Fr.i(t) \qquad (39)$$

where *Kr* is function of the winding characteristics such as cross-sectional area, *s*, the number of turn per unit length, *n*, and the symmetry of the coil. An integration of voltage gives a measure, proportional to *Kr*, of the instantaneous *RMS*[2] current in the conductor [67].

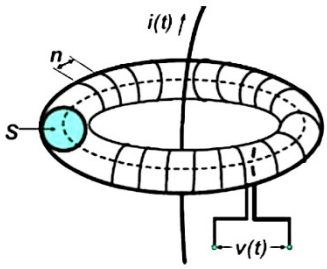

Figure 50: Rogowski coil [67].

The machine available in INEGI's facilities has a built in Rogowski, so, in order to obtain the system parameters the machine was connected to a computer that reads the voltage discharge and returns a curve like the ones presented in the graphic below with the dashed line. Is important to mention, that the curves returned are corrected with parameters that the machine developers have previously selected. To obtain the calculated curves, represented with solid lines, a curve-fitting algorithm was used to compute the resistance and the inductance of the machine. The Levenberg-Marquardt algorithm, available in the MATLAB® toolbox, was used. The approximation mechanism consists of an iterative improvement of the parameter values in order to reduce the sum of the squares of the errors between the function and the measured data points [68,69]. In short, Levenberg-Marquardt combines the advantages of the steepest descent method, which gives the minimization along the direction of the gradient, with the Newton

[2] The RMS – Root-Mean-Square is the equivalent direct current value of an alternating current signal [94].

method that, using a quadratic model allows to speed up the process of finding the minimum of a function [70]. Due to the advantages inherent to its approach, it has become a standard technique for nonlinear least-squares problems, widely adopted for dealing with data-fitting applications.

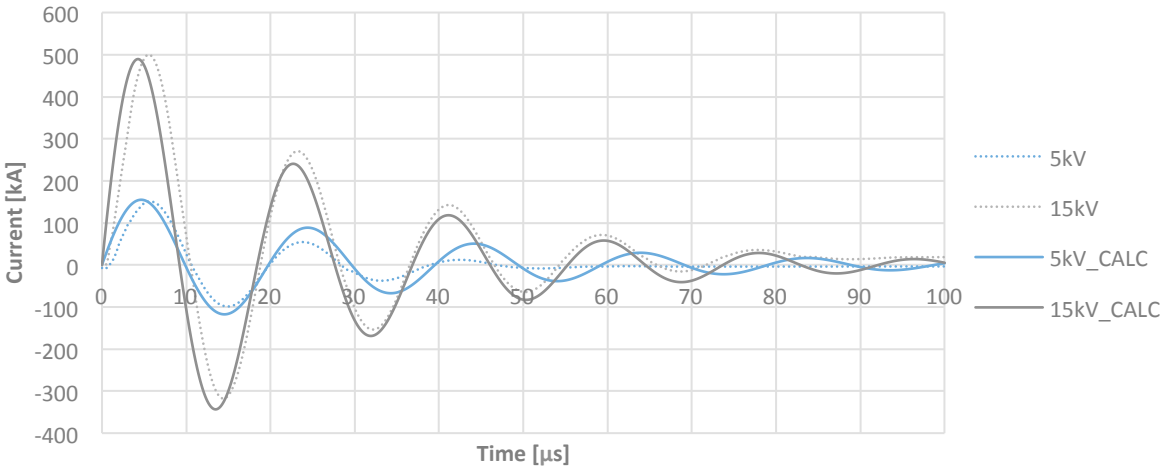

Figure 51: Curve current vs. time.

3.4.3 Pressure Magnitude

In addition, to have a preliminary indication about the pressure magnitude that has to be applied to deform the terminal, a brief estimative was performed using the Thin-Walled Pressure Vessel theory. Towards applying this formulation, it is necessary to assume that the terminal is a tube and is a container subjected to an external pressure, p, as shown in Figure 52, made of an isotropic material and, additionally, it is assumed that the wall thickness is very thin when compared to its radius [71].

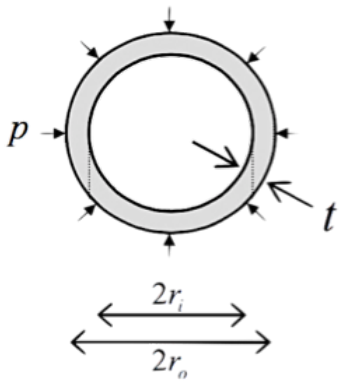

Figure 52: Cylindrical pressure vessel with external pressure (adapted from [72]).

Following the hypothesis of this theory, the pressure required can be calculated using the following equation [73,74]:

$$\sigma = \frac{F}{A} = \frac{p\pi r_i^2}{2\pi r t} \Leftrightarrow p = \frac{2\sigma t}{r_i} \qquad (40)$$

where σ is the stress, F the force, A the cross sectional area, p the external pressure and r and t are the radius and the thickness, respectively. Assuming that σ is equal to $2\sigma_u$, being σ_u the ultimate tensile strength of the material, and taking into account the problem data, the minimum required pressure to deform the is given by:

$$p > \frac{2\sigma_u t}{r_i} \Leftrightarrow p > \frac{2\times138\times10^{6}\times1.25\times10^{-3}}{2.80\times10^{-3}} = 1.23\times10^{8}[N/m^2] \quad (41)$$

Following the calculation of the minimum value of pressure needed, it is necessary to find the value of current that allows achieving the calculated magnetic pressure. Therefore, taking into account the definition of magnetic pressure and its dependence, it is possible to determine the consequent magnetic field by using the following relation:

$$p = \frac{B^2}{2\mu_0} \Leftrightarrow B = \sqrt{2\mu_0 p} = \sqrt{2\times4\pi\times10^{-7}\times1.23\times10^{8}} = 17.60\ [T] \quad (42)$$

Considering the coil's geometry and properties presented above, the required discharge current to achieve the computed magnetic pressure can be determined by:

$$I = \frac{Bh}{\mu_0 N} = \frac{17.60\times31.3\times10^{-3}}{4\pi\times10^{-7}\times5.5} = 79.97\ [kA] \quad (43)$$

where N is the number of coil windings and h the coil's height.

As stated in previous sections, in the electromagnetic pulse crimping process is highly important to assure that the skin depth is lower than the terminal thickness. As the terminal thickness and electrical conductivity are already known, the minimum frequency that allows that, at least, the skin depth is equal to the thickness, ensuring the magnetic field shielding, and can be calculated as follows:

$$f = \frac{\rho}{\pi\mu_0 t^2} = \frac{1.68\times10^{-8}}{\pi\times4\pi\times10^{-7}\times(1.25\times10^{-3})^2} = 2.72\ [kHz] \quad (44)$$

where ρ is the electrical conductivity, t is the thickness and μ_0 is the magnetic permeability.

3.5 Numerical Simulation

Numerical simulation can be summed up into two different scenarios, corresponding to the two terminal diameters to be crimped – #A and #B + #C. The FEM analysis was performed for combinations #A and #B, #C was left apart since the terminal's diameter of combination #C is approximately the same as #B. Moreover, due to geometry simplifications the only apparent difference between combination #B and #C was eliminated.

In order to have an indication about the terminal behavior with different values of energy, a batch of numerical simulations was performed and the final compression level of the terminal was analyzed. The goal is to observe in what ranges of energy is expected to perform the experiments.

Towards having a better perception of the compression that the terminal is subjected as well as its final diameter, a LS-DYNA® tool was applied. This particular tool allows evaluating the terminal's diameter throughout every instants of the crimping process. It is important to refer that the present simulation is not capable to predict if the crimp was successfully attained or not. The geometric properties of an electrical cable, composed by a significant number of thin copper wires is challenging to model, and, on the other hand, the cable's properties were not provided by YSE, being the most feasible solution consider the cable as a rigid part. Therefore, it is only possible to observe if the energy applied will be enough to reach the cable's diameter. Besides, it is noteworthy to refer that, as the EMPT is a dynamic process, the high velocity impact of the terminal against to the wire can cause the so called rebound effect[3], meaning that an extremely high value of discharge voltage (energy) can result not only in the collapse of the terminal but also in a lower value of compression [**75**].

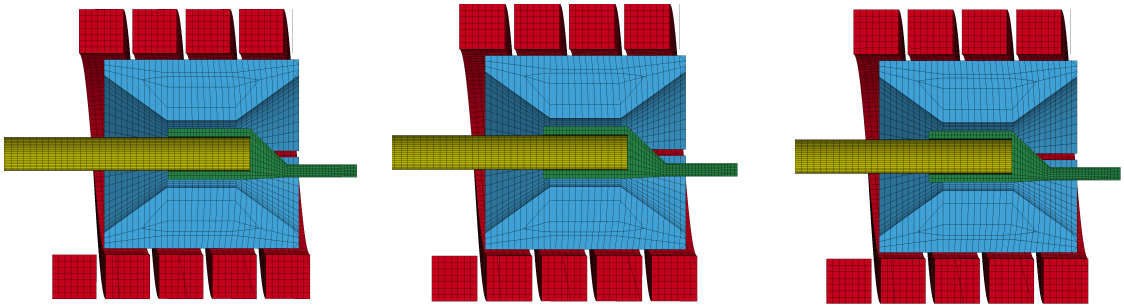

Figure 53: Different positions of the terminal inside the fieldshaper.

Previously to testing different values of energy, the influence of the LWZ parameter was analyzed. This allows having the perception of what position promotes a more uniform crimp. LWZ, is a parameter that relates the axial position between the "coil + fieldshaper" and the terminal. The tests were performed for three different positions and relating to the position of the terminal inside the "coil + fieldshaper". The figures above illustrate this condition (a. terminal outside the fieldshaper; b. terminal midway the fieldshaper; c. terminal inside the fieldshaper). Taking into account the results, the position chosen to perform the numerical simulations is b.

[3] Rebound effect is a result of the high velocity impact between the workpiece and die. This phenomenon occurs when the workpiece contacts with the die. A part of the kinetic energy, obtained by the fast acceleration, is converted into plastic deformation work, and the other part that is not capable to dissipate in a short time results in rebound effect [74].

The FEM analysis presented results that are considered to be promising. The magnetic field contour during the first current peak is shown in Figure 54. It can be seen that the magnetic field flows correctly through the fieldshaper. It is possible to observe the induction of the magnetic field in the coil that, in its turn, induces Eddy currents in the fieldshaper, which will induce Eddy currents and consequently a magnetic field in the terminal.

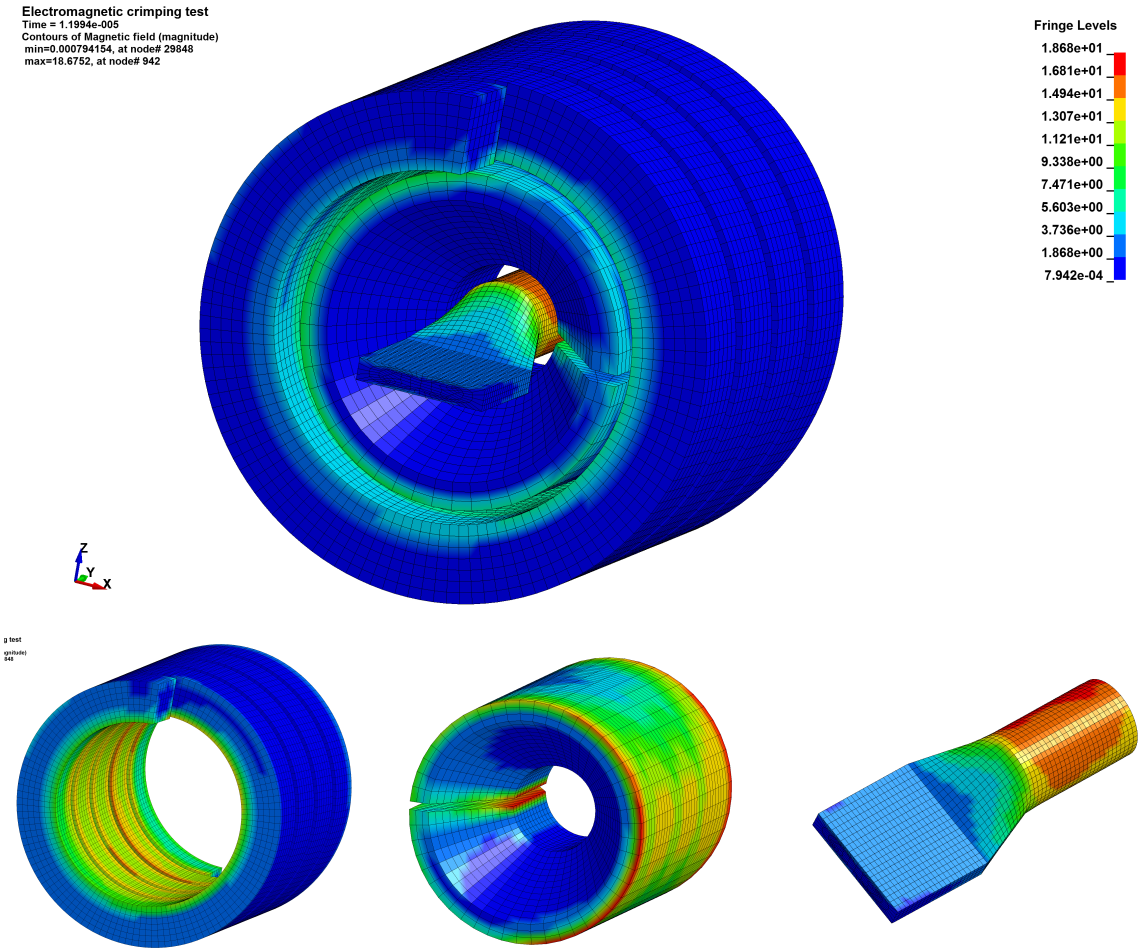

Figure 54: Induced magnetic field during the 1st peak of current [T].

The projected concept coil seems to generate an appropriate force distribution pattern distribution pattern over the terminal. Note that the magnetic field distribution over over the terminal allows verifying the validity of the numerical simulation. The results show lower magnitude in the place corresponding to the fieldshaper slot - Figure 55. Besides, the results permit to observe that the frequency values are high enough to ensure that the skin depth is lower than the terminal thickness -

Figure 56. This is a key condition to guarantee the process' efficiency. Most likely, this is a consequence of the combination of high electrical conductivity and considerable thickness of the terminal, requiring relatively low frequency values to guarantee magnetic field shield.

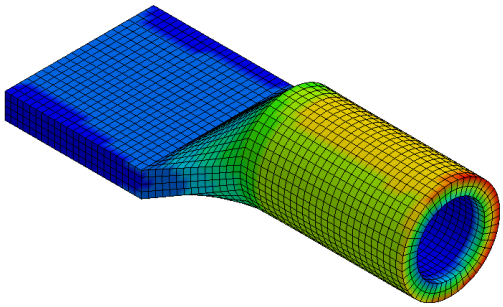

Figure 55: Detail of the magnetic field in the slot zone.

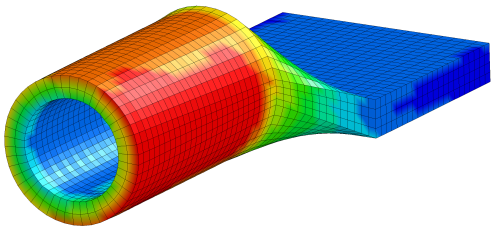

Figure 56: Magnetic field shielding inside the terminal.

For this approach the cable was, as stated previously, considered to be a rigid element. The results obtained for the different levels of energy are presented in Figure 57. The compression ratio was determined using a relation of areas, as detailed more thoroughly in Chapter 4, section 4.2.1.

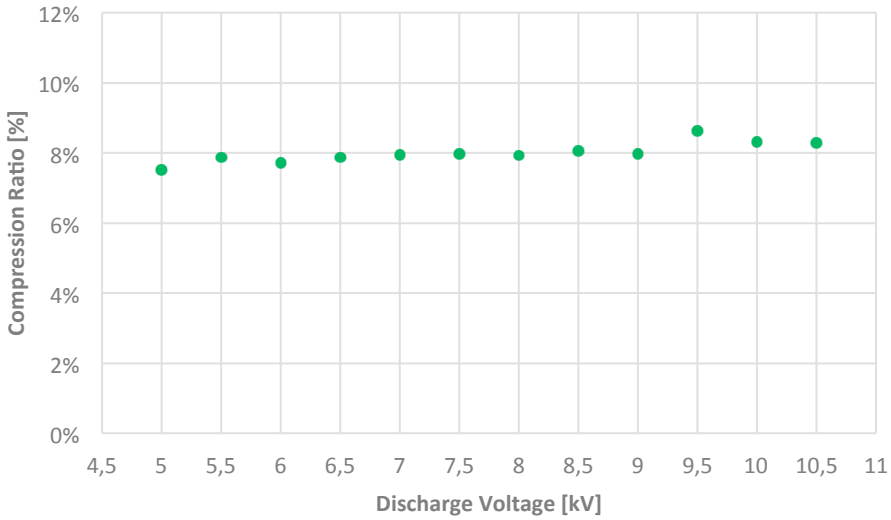

Figure 57: Simulation results plot - Terminal's Final Diameter vs Discharge Voltage for 16 mm².

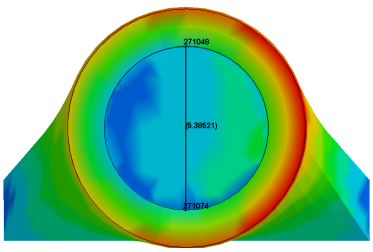

Figure 58: Final diameter - 5 kV.

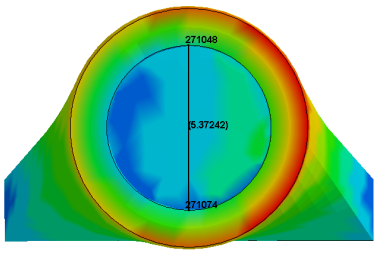

Figure 59: Final diameter - 7.5 kV.

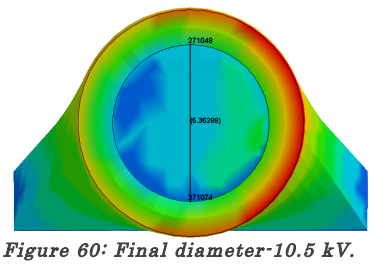

Figure 60: Final diameter-10.5 kV.

The measurement of the terminal's final diameter and the observation of the simulation's evolution, revealed some concerns related to rebound effect. The terminal reached the surface of the cable and, in the following step time, it returned back. In short, the impact energy was not dissipated towards the

deformation of the cable, resulting in a higher final diameter than what was expected for values of energy that, according to the preliminary experimental tests produced a crimped joint. As a consequence of these drawbacks, a new approach was developed, in which the cable was considered as a solid part with plastic properties, as will be explained in the following section.

3.5.1 Alternative Approach

In order to solve problems related to the rebound effect previously detected, a new approach was followed. Consequently, some changes were applied to the numerical model. The cable was considered to be a solid part, with plastic behavior, enabling the cable to dissipate part of the energy applied to the terminal, causing the cable deformation. As data about cable's properties was, as stated previously, not provided by YSE, cable's properties were considered to be the same as the terminal. The modifications applied into the different files of the numerical model are presented in the marks below, is important to refer that no changes were applied in the electromagnetic file.

- **MESH FILE**

In this file, the keyword - ***ELEMENT_SHELL –** was deleted, and a solid element was generated.

***ELEMENT_SOLID**

#pid: 4 – CABLE

- **STRUCTURAL FILE**

In the structural file, all keywords that had some relation with the cable had to be rectified, since the cable is now a solid with different number of elements. The keywords - ***MAT_RIGID** - ***SECTION_SHELL** - ***CONTACT_AUTOMATIC_SURFACE_TO_SURFACE** – were deleted. The rectified and added keywords are presented below.

***PART**– relates the part ID to *SECTION and *MATERIAL;

Card	**1**	**2**	**3**	**4**	**5**	**6**	**7**	**8**
Variable	pid	secid	mid	eosid	hgid	grav	adpopt	tmid
$CABLE	4	1	2	0	0	0	0	0

***CONTACT_SURFACE_TO_SURFACE** – the main purpose is to set the parts between, which, contact will occur during problem computation.

Card1	**1**	**2**	**3**	**4**	**5**	**6**	**7**	**8**
Variable	ssid	msid	sstyp	mstyp	sboxid	mboxid	spr	mpr
	4	3	3	3	0	0	0	0
Card2	**1**	**2**	**3**	**4**	**5**	**6**	**7**	**8**
Variable	fs	fd	dc	vc	vdc	penchk	bt	dt
	0	0	0	0	0	0	0	1.00e20
Card3	**1**	**2**	**3**	**4**	**5**	**6**	**7**	**8**

Variable	sfs	sfm	sst	mst	sfst	sfmt	fsf	vsf
	1.00	1.00	0	1.00	1.00	1.00	1.00	1.00

***CONTROL_CONTACT** – changes defaults for computation with contact surfaces.

Card1	1	2	3	4	5	6	7	8
Variable	slsfac	rwpnal	islchk	shlthk	penopt	thkchg	orient	enmass
	0.10	0	1	2	1	0	1	0
Card2	1	2	3	4	5	6	7	8
Variable	usrstr	usrfrc	nsbsc	interm	xpene	ssthk	ecdt	tiedprj
	0	0	0	0	4	0	0	0
Card3	1	2	3	4	5	6	7	8
Variable	sfric	dfric	edc	vfc	th	th_sf	pen_sf	
	0	0	0	0	0	0	0	
Card4	1	2	3	4	5	6	7	8
Variable	ignore	frceng	skiprwg	outseg	spotstp	spotdel	spothin	
	0	0	0	0	0	0	0	
Card5	1	2	3	4	5	6	7	8
Variable	isym	nserod	rwgaps	rwgdth	rwksf	icov	swradf	ithoff
	0	0	1	0	1	0	0	0
Card6	1	2	3	4	5	6	7	8
Variable	sheldg	pstiff	itchcnt	tdcnof	ftall	unused	shltrw	
	0	0	0	0	0		0	

The simulation results, shown in terms of compression ratio, are presented in the following figures. It is important to refer that, in this approach, the cable presents some deformation, in agreement with the terminal's compression. According to the results of the compression levels, shown in the plot of the Figure 61, and in agreement with YSE specifications presented in Table 4, it is considered expectable to achieve an effective joint between the components for discharge energy above 8.5 kV. Meaning that at least 15% of compression ratio (minimum indicated by YSE) is achieved. At this level, the compression of the outer workpiece, and the consequent deformation of the inner part, are considered to be significant, and high enough to achieve a successful union.

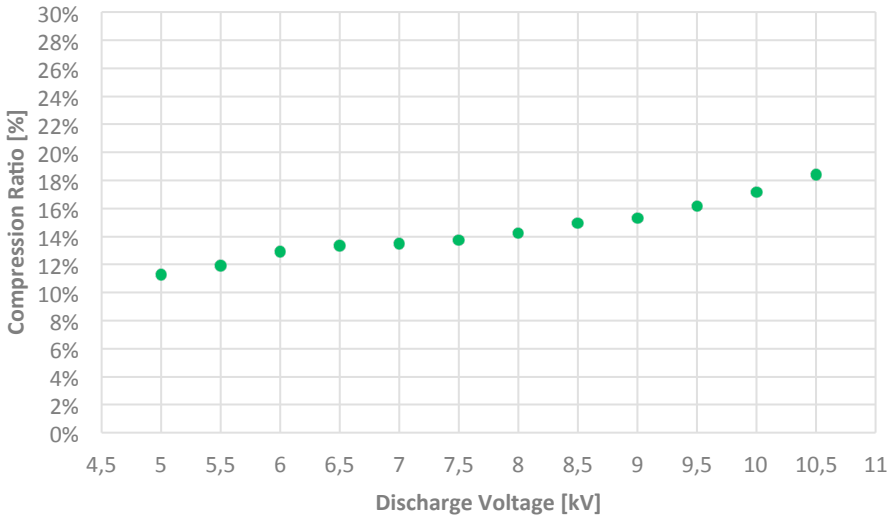

Figure 61: Simulation results plot - Terminal's Compression Ratio vs Discharge Voltage for 16 mm².

The numerical simulation was also performed for the 25 mm² terminal, the results obtained are presented in the Figure 62. According to the compression ratio of the parts, and the minimum value identified by YSE, it is expectable to achieve a connection with a discharge voltage above 8.5 kV. Intuitively, was predicted that the combination #A would be critical to EMPC, due to higher gap distance between the fieldshaper and the terminal [**76**]. Since, higher gap results in lower efficiency of the process and, therefore, higher energy has to be applied to cause deformation of the terminal. However, when the results of both simulations (combination #A and #B) are compared, the energy required to deform combination #B in such way that the connection takes place, is similar to the required to crimp combination #A. Two main factors may be causing this result. Firstly, the thickness of the terminal from combination #B is slightly higher than the thickness of the combination #A, which, among the higher value of diameter, results in a higher value of mass to accelerate against the cable. On the other hand, the distance between the terminal and the cable of the combination #B is higher than #A, meaning that the terminal needs to travel a higher distance, requiring more energy.

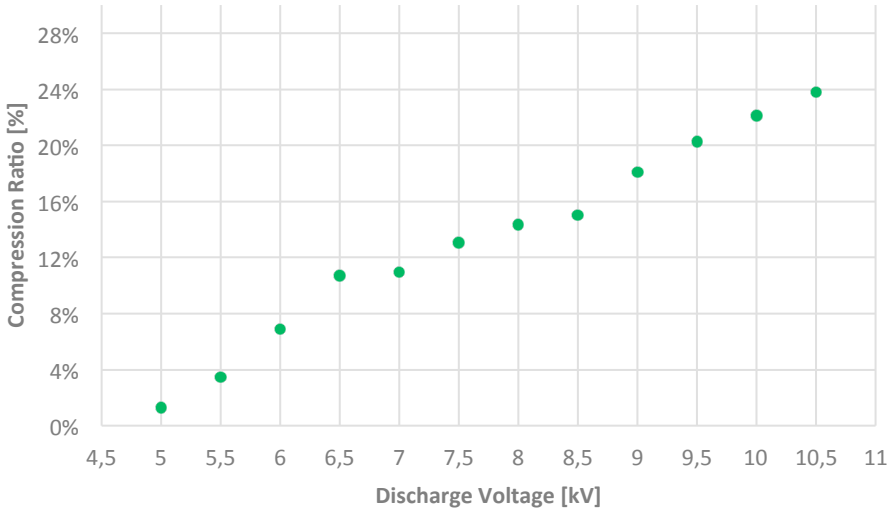

Figure 62: Simulation results plot - Terminal's Compression Ratio vs Discharge Voltage for 25 mm².

3.6 Concluding Remarks

In this chapter, a new type of electromagnetic actuator is presented. It aims to provide an effective electromagnetic crimp of the electrical cables processed by YSE. The development of such actuator, comprised by 4 principal components; namely: a primary coil; a field shaper and two electrical insulator and position parts, was supported by a preliminary set of experiments which allows to conclude that reliable joints can be obtained making use of handmade disposable coils, and relatively low values of charging energy, since suitable compression ratio and joint strength values were obtained. In addition, to support the process of development and design, the numerical analysis of the coil is presented. The electromagnetism module, developed in LS-DYNA® for coupled mechanical/thermal/electromagnetic simulations was used to perform the numerical simulations. The electromagnetic fields are solved using a Finite Element Method for the conductors coupled with a Boundary Element Method for the surrounding air/insulators. These preliminary simulations have allowed not only the validation of the tooling developed but also to perceive the terminal's behavior during the process.

However, and despite the promising results, the amount of simplifications required to multidisciplinary numerical modeling, and the lack of knowledge regarding the materials behavior under high strain rates as well as the approximations related to the cable geometry and the tool total inductance, can compromise the accuracy of simulation results. The results presented in this section will be compared with the experimental ones, and the viability of the implemented model discussed. Summing up the predicted discharge energy required to crimp the different joints: combination #A at least 8 kV, combination #B and #C at least 8.5 kV.

The performance of the developed tool requires experimental validation.

4 EXPERIMENTAL VALIDATION

The work presented in this chapter is related to the execution of the EMPC experimental runs and required iterations, responding to one of the major goals of this thesis: the characterization of the electromagnetically crimped joints, achieved by a customized tool, developed for YSE's electrical terminals.

In the first section of this chapter, tool manufacturing process and assembly steps are presented. Follows a brief description of the setup preparation and tool acceptance procedure. The tool performance validation, the core of this chapter, was divided in different steps. In a first stage, the terminals were subjected to free compression tests (i.e. without wire), aiming to assess its sensitivity to the magnetic field generated by different discharge levels. Based on the behaviour and compression level revealed by the components, a matrix of experiments was selected for the following crimping tests. In order to assess the strength of the EMPC joints, uniaxial tensile tests were conducted. Additionally, aiming at a more detailed evaluation, the samples were prepared and subjected to metallographic analysis. The crimping ratio, an important measure of tool performance, was also determined by using calliper measurements. The experimental results are exhaustively analysed and compared to the ones achieved by numerical simulation, performed in the last chapter.

Finally, several considerations related to the tools performance and other experimental issues are presented.

4.1 Tool Manufacturing and Assembly

The manufacturing of the developed electromagnetic actuator involved a procurement of workshops capable to produce, with the required precision, the different components of the crimping tooling system. Due to the complex geometry of the coil winding, the machining process is a complex task. Therefore, and in context of the straight collaboration between the Professors' Glenn Daehn group of the Ohio State University and INEGI, the tool's manufacturing was ordered to them. This group has over 20 years of experience with EMF processes, which made them the selected for tool manufacturing. In the following figures it is possible to observe the different components, during the manufacture and the assembly stage.

Figure 63 and Figure 64 shows the end plates and the coil yokes, respectively, Figure 65 shows the fieldshaper and Figure 66 presents the coil.

Figure 63: Coil yokes.

Figure 64: Coil endplates.

Figure 65: Fieldshaper.

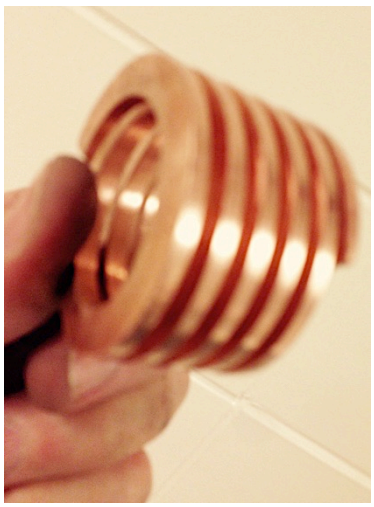

Figure 66: Coil.

The assembly of the different components was achieved by firstly brazing the coil to the yokes and, afterwards, the end plates were screwed to the yokes - Figure 67. Then, as shown in Figure 68, the coil was externally reinforced with glass fibre-epoxy resin composite, in order to enhance its mechanical resistance during the EMPC processing. As mentioned, the coil and the terminal are subjected to the same pressure (action-reaction), which can cause the expansion of the coil, leading to its rupture. This reinforcement prevents this expansion, increasing the coil's lifetime.

Figure 67: Brazed yokes.

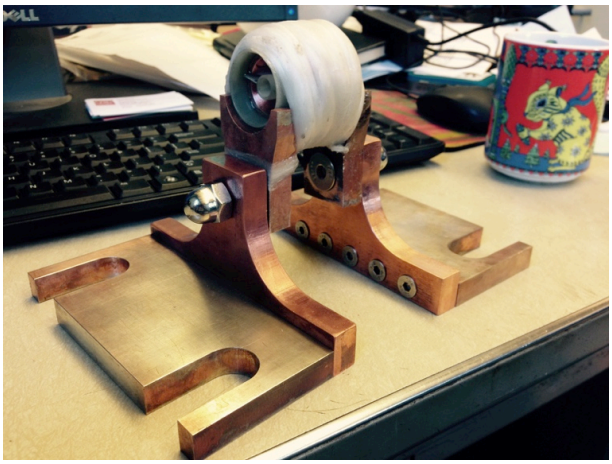

Figure 68: Tool assembly.

During the manufacturing process, the OSU team identified some potential improvement on the design developed by INEGI. Therefore, additionally to the ordered tool, the manufacturer delivered an alternative design with a smaller number of windings (3 instead of 5.5 turns as depicted in Figure 69) and, with a slightly different fieldshaper with two slots (the ordered fieldshaper has one slot). As a result, there are two different tools for testing with different characteristics to be analysed in the final crimped products. In order to validate both coils, and assess the difference between them, several rounds experiments were performed, as will be presented in section 4.2.

Figure 69: Manufactured coils. Left: Original design with 5.5 turns. Right: Alternative design with 3 turns.

4.2 Tools' Experimental Assessment

This section is dedicated not only to the validation of the designed concept but also, to the comparison between the original and alternative design. From now on, the original design will be referred as Design #1 (or #1) and the alternative one as Design #2 (or #2). Along with the tool, YSE has provided the raw material required to perform tool's validation. Terminals for the three different combinations and cables cut in samples with 200 mm of length, with a welding

bath in one of the edges. The welding bath prevents the terminal from slipping through the grips during the mechanical characterization tests.

Once the tools arrived to INEGI's facilities, they were assembled on the magnetic pulse system and some early tests ought to be performed. Firstly, the coil was screwed to the workstation and initial tests, at 5 kV, were conducted with nothing inside the coil. This allowed observing if the coil was properly connected to the machine and if the different components were properly coupled between them. As stated before, this is of paramount importance to prevent electrical arcs remember that if any electrical arc occurs during the crimping process it will most likely result in the coil destruction.

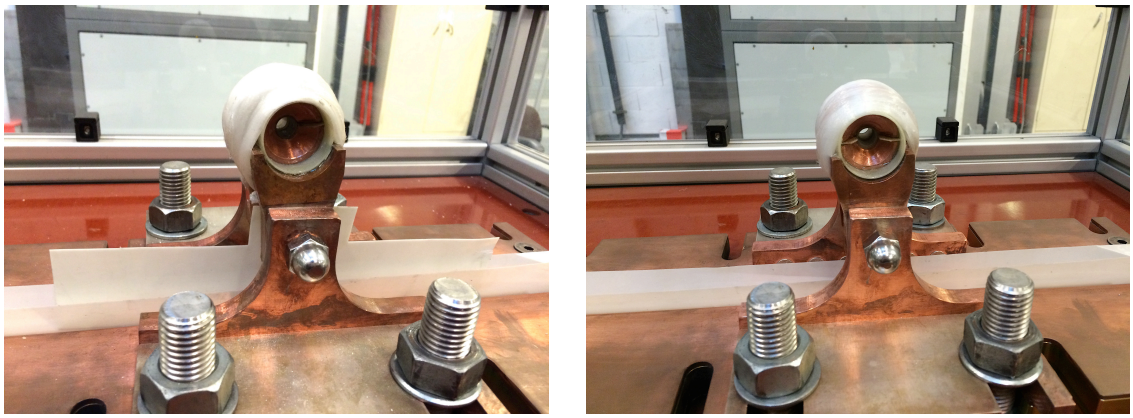

Figure 70: Assembly of Design #1 –left; Assembly of Design #2 – right.

4.2.1 Experimental Procedure

As mentioned in several parts of this document, there are three different combinations under study (#A, #B and #C). The steps described below were repeated for all the cases, aiming not only the evaluation of the tooling system performance/behaviour but also the assessment of the joints characteristics achieved by the electromagnetic crimping process. The overall procedure follows:

1. Free electromagnetic compression of the terminals – The three different terminals were compressed by using 4 different values of discharge voltage. The idea of using of an empty terminal is to observe the behaviour when subjected to different levels of magnetic field.
2. Preliminary crimping tests - According to the compression levels obtained in the 1st stage, a preliminary set of experiments was conducted. The goal is, together with the simulation, having a preliminary input regarding the optimal crimping parameters to achieve the required joint strength. Tensile testing have supported this step.

3. Definition of the matrix of experiments – A matrix 4x4 was designed, meaning that a total of 16 tests were performed for each terminal-wire combination. Four different discharge energy levels were selected, based on the 2nd stage results, and, for each level 4 samples were produced.
4. Characterization of the electromagnetically crimped joints - Both mechanical and metallographic analysis was performed. Besides, the compression ratio of the terminal was evaluated. The experimental results were exhaustively analysed and compared to the simulation.

Note that all the mechanical characterization tests were performed using an Intron model 4507 servo-electric universal testing machine at 200 mm/min and at room temperature (23°C). Regarding the visual analysis of the crimping joint, all samples were cut along the radial direction, cleaned, embedded in epoxy resin and polished, revealing the cross-section. Concerning the microscopic observation, the equipment available in INEGI facilities did not possess a magnification factor suitable to observe the entire cross-section. Therefore, the section was dived into slices, which were posteriorly combined.

Furthermore, the external diameters measurement was performed at 4 mm of the base using a calliper. As observed in numerical simulations, the slot zone of the fieldshaper causes an area where the magnetic field is approximately zero resulting in a final cross-section that is not perfectly circular. As a result of the approximately elliptical section, two diameters were measured (smallest and widest). Finally, in order to calculate the compression ratio, a relation of areas was applied. The approximation of the initial area, *Ai*, was obtained using equation (45) and for the crimped area, *Af*, equation (46). Final crimping ratio was computed using equation (47).

$$Ai = \frac{\pi di^2}{4} \qquad (45)$$

$$Af = \frac{\pi . da . db}{4} \qquad (46)$$

$$cr = \left(1 - \frac{Af}{Ai}\right) \times 100\% \qquad (47)$$

with *di* being the initial diameter of the terminal, 8 mm for combination #A and 9.5 mm for combination #B and #C; *da* and *db*, the smallest and widest diameters of the terminal respectively.

Recalling the requirements of YSE, Table 8 presents the critical functional properties of YSE joints: minimum force under tensile conditions and minimum compression ratio.

Table 8: Requirements for the minimal tensile strength and compression ratio.

# Combination	Force [N]	Compression ratio [%]
A	1750	15-50
B	784	
C	2940	

4.2.2 Combination #A

The tests started by crimping the smaller cross-section, combination #A. The free-form compression of this terminal was performed using both tool designs, with discharge voltage between 6-9 kV. The influence of the discharge level on the compression ratio achieved in the free-form of combination #A for both designs can be observed in Figure 71.

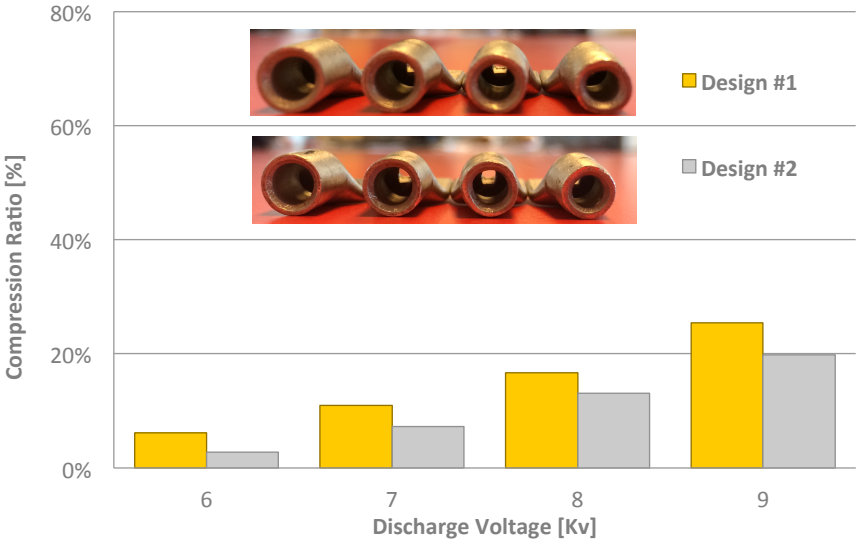

Figure 71: Free-form terminal compression of combination #A for design #1 and #2.

As anticipated, the compression ratio increases with the increase of the discharge energy. However, the crimping ratio required, 15%, is only attained when using discharge voltage values over 8 kV. Taking this into account, and the crimping compression requirements (Table 8), it was settled that for tool's validation stage the discharge energy was in a range between 7.5 kV and 9 kV. The matrixes of experiments executed are presented below.

Table 9: DoE matrix for combination #A, Design #1.

DoE	7.5 kV	8 kV	8.5 kV	9 kV
Samples	**J**	**K**	**L**	**M**
1	J1	K1	L1	M1
2	J2	K2	L2	M2
3	J3	K3	L3	M3
4	J4	K4	L4	M4

Table 10: DoE matrix for combination A, Design #2.

DoE	7.5 kV	8 kV	8.5 kV	9 kV
Samples	**A**	**B**	**C**	**D**
1	A1	B1	C1	D1
2	A2	B2	C2	D2
3	A3	B3	C3	D3

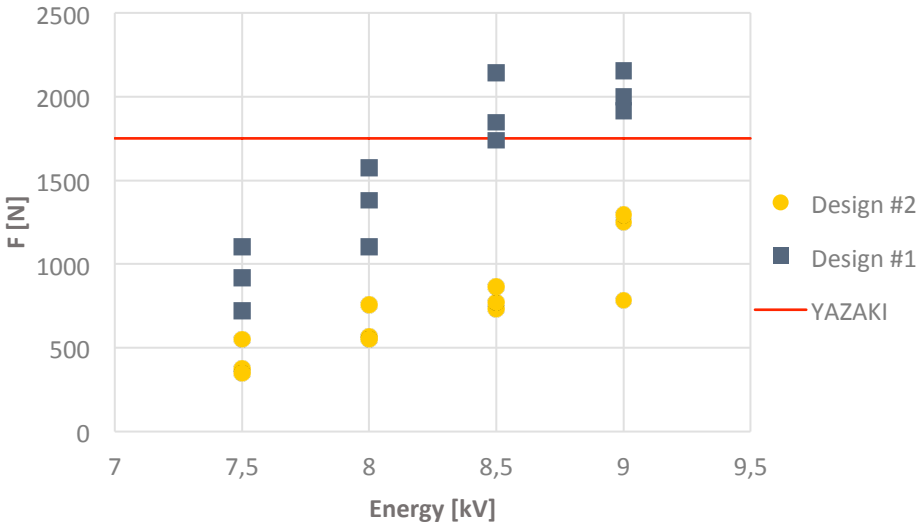

Figure 72: Tensile tests results for combination #A using Design #1 and Design #2.

From the tensile tests results obtained with combination #A it is possible to observe that, for the same energy level, stronger joints can be obtained using design #1. Moreover, design #1 is capable to produce reliable crimp joints, complying with YSE requirements, using energy values equal or superior to 8.5 kV. These results are in line with the results obtained for the free-form terminal's compression since, a similar tendency was observed, i.e., higher terminal compression was obtained at similar conditions.

The apparent higher performance of the original tool design is most likely related to the geometric specifications of both fieldshaper and coil. As stated previously, the slot zone of the fieldshaper is essential to promote the current flow towards the inside of the fieldshaper. However this is an area where the magnetic field is approximately zero, consequently, the fieldshaper with two slots has a superior area where the magnetic pressure is lower. Additionally, it is widely reported in literature (e.g. [**32**]) that the intensity of the magnetic field, and consequently of the magnetic pressure, increases with the increasing number of coil's turns. However, a slight heating of design #1's tool was noticed during tests execution, perhaps due to higher energy density, as the coil turn's cross-section is smaller than design #2. This is a critical issue, as the thermo-mechanical fatigue can be unfavorable to coil's lifetime. Consequently, considering the potential higher robustness of design #2's tool, and despite its lower efficiency, it was decided to use

only this tool for the further tests with larger cross-section materials (combination #B and #C).

The strength of the joints crimped is referenced to the compression ratios presented in the figure below. Once again, it can be observed that the values of crimping ratio obtained for design #1 are superior to those obtained for design #2, which is in line with the results obtained for the free-form compression tests.

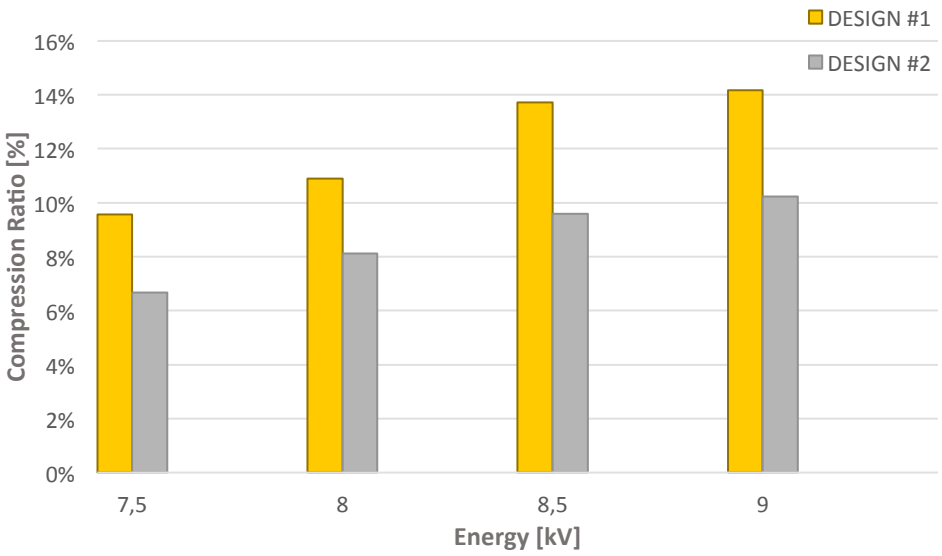

Figure 73: Compression ratio for combination #A, using design #1 and design #2.

Besides mechanical characterization, a visual analysis of the crimping joint was obtained by metallographic preparation and analysis. A sample from each of the levels was analyzed, crimped using design #1, was cut along the radial direction, cleaned, embedded in epoxy resin and polished, revealing the cross-section images shown in Figure 74. These allow observing an increase of the compaction level, and resulting voids reduction, with the increase of the discharge energy.

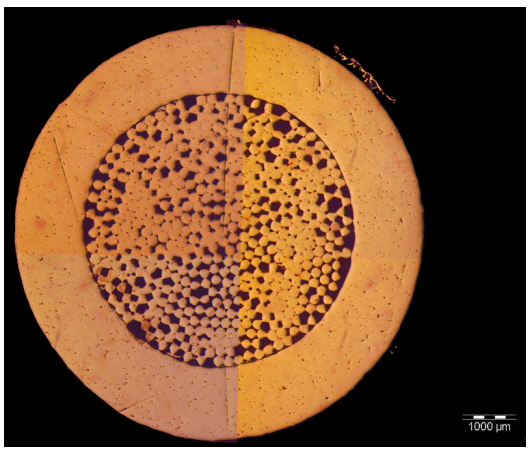

a.

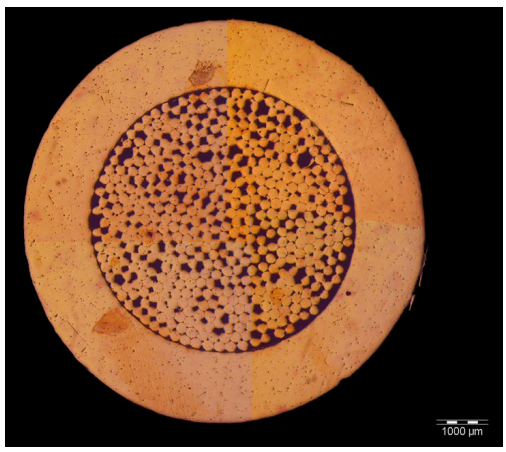

b.

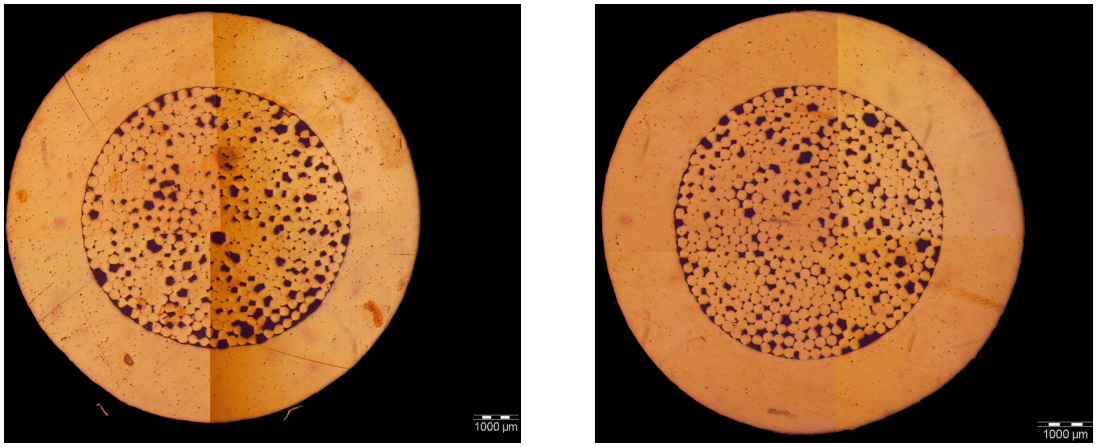

c. *d.*

Figure 74: X-section images of the EMPC joints of Combination #A, using design #1 at: a. 7.5 kV, b. 8.0 kV, c. 8.5 kV and d. 9.0 kV.

4.2.3 Combination #B and #C

Using the same methodology adopted for combination #A, but using exclusively design #2's tool, combinations #B and #C were electromagnetically crimped. Figure 75 presents the results of the free-form terminal's compression, using a discharge voltage range between 6 kV and 9 kV. When compared with the results obtained for combination #A (higher gap between the tool and workpiece), using the same tool (#2), these show that the processing of larger terminal material section resulted in lower compression ratio values, at equal discharge energy level. Moreover, terminal's compression could only be considered promising using the maximum energy level tested (9 kV). Initially, combination #A was identified as the critical case due to higher gap between the terminal and fieldshaper. However, following a more detailed analysis, another parameter, extremely critical for the process was identified. The thickness of terminals #B and #C is higher than the thickness of terminal #A. In some critical cases, the difference is up to 0.20 mm. As stated in literature [**27**] and observed during simulation, the effect of the thickness has more influence in the process than the gap. Meaning that the difference between gaps (approximately equal to 0.75 mm) was somehow overcome by the difference in terminals' thicknesses. This can be more accurately observed in Figure 76 and Figure 77, accessible in a study presented by Siddiqui (2009). [**27**]. In this study, the author investigated the effects of both thickness and gap distance of the workpiece, in the Lorentz force distribution. As can be seen in Figure 76, an increase of 0.25 mm in the workpiece thickness causes a decrease, approximately in double of the force distribution inside the workpieces wall. On the other hand, the doubling of the gap distance between the workpiece and the coil wall does not present such significant influence. However, gap distance still influences the force distribution and should be minimized the maximum possible.

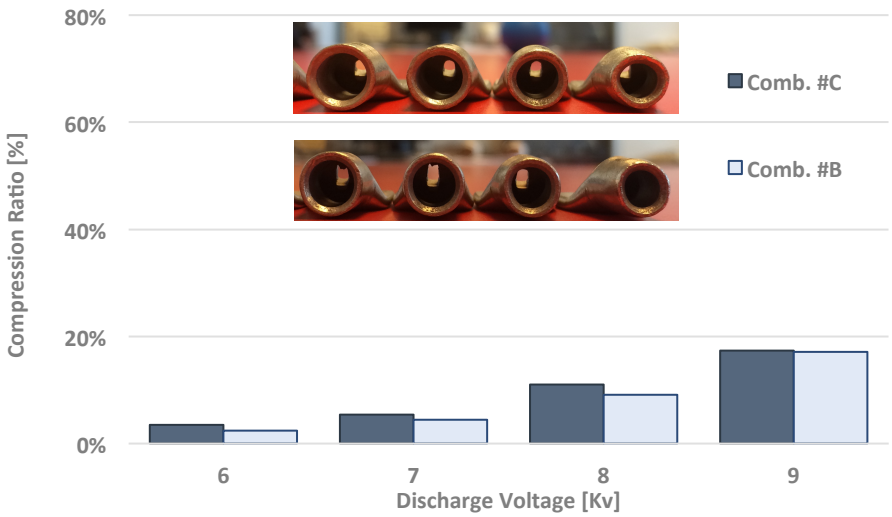

Figure 75: Free-form terminal compression of combination #B and #C using design #2.

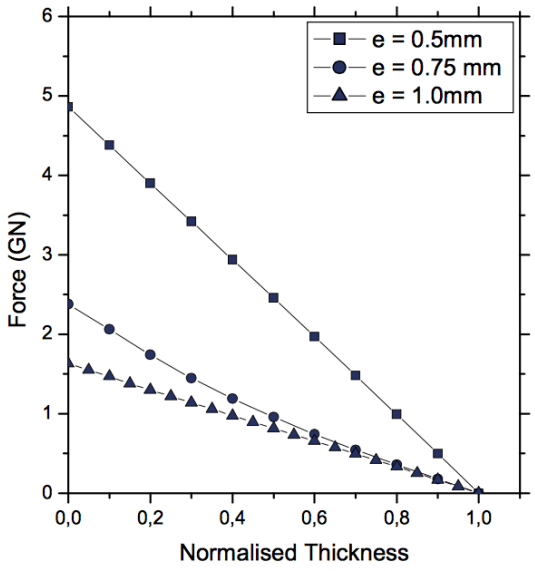

Figure 76: Lorentz force distribution through thickness at peak value of discharge current for different values of sheet thicknesses [27].

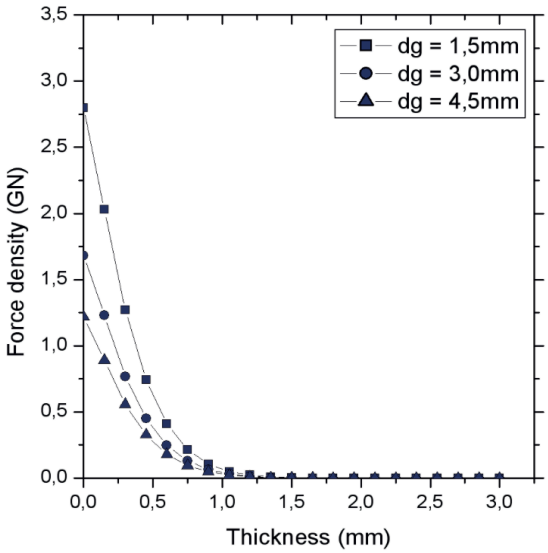

Figure 77: Lorentz force distribution through thickness at peak value for different values of gap distance [27].

Using the information acquired in the terminal's free-from compression, and in order to assess a proper energy range for the larger case studies, some single-shot crimping experiments, using higher energy levels, were anticipated with combination #B and #C. The tensile test results are presented in Table 11.

Table 11: Maximum force value registered during tensile test of EMPC single-shots of combinations #B and #C, using design #2.

Energy	9 kV	9.5 kV	10 kV	10.5 kV
Combination #B Tensile Strength [N] (Required = 784 N)	309	776	1396	1992
Combination #C Tensile Strength [N] (Required = 2940 N)	413	1087	1954	2389

The results obtained are apparently in line with the main conclusions of the free-form terminal compression recalling that, the discharge level necessary to achieve the required joint strength is, in reality, higher than what is needed for the thinner combination #A and that, combination #B systematically presents lower strength values than combination #C, for the same energy level. Which can explained by non-identified differences between the terminals (e.g. surface finish, electrical conductivity, differences in terms of thicknesses etc.). However, though the differences were in a range between 300 N and 450 N, the required tensile strength differs more significantly, $F_{Required}$_#C is about three times that of $F_{Required}$_#B, which prompted to select a lower energy range in tool validation with combination #B, 9 kV to 10.5 kV, in opposite to the range of 10.5 kV to 12 kV selected for the processing with combination #C. The matrixes of experiments executed are presented below.

Table 12: DoE matrix for combination #B.

DoE	9 kV	9.5 kV	10 kV	10.5 kV
Samples	**R**	**S**	**T**	**U**
1	R1	S1	T1	U1
2	R2	S2	T2	U2
3	R3	S3	T3	U3
4	R4	S4	T4	U4

Table 13: DoE matrix for combination #C.

DoE	10.5 kV	11 kV	11.5 kV	12 kV
Samples	**A**	**B**	**C**	**D**
1	A1	B1	C1	D1
2	A2	B2	C2	D2
3	A3	B3	C3	D3
4	A4	B4	C4	D4

In Figure 78 and Figure 79 are presented the tensile test results related to design #2 tool's validation for the development of the EMPC process for combinations #B and #C. These show that energy ranges between 9.5-10.5 kV and 11-12 kV are the suggested for EMPC combinations #B and #C, respectively.

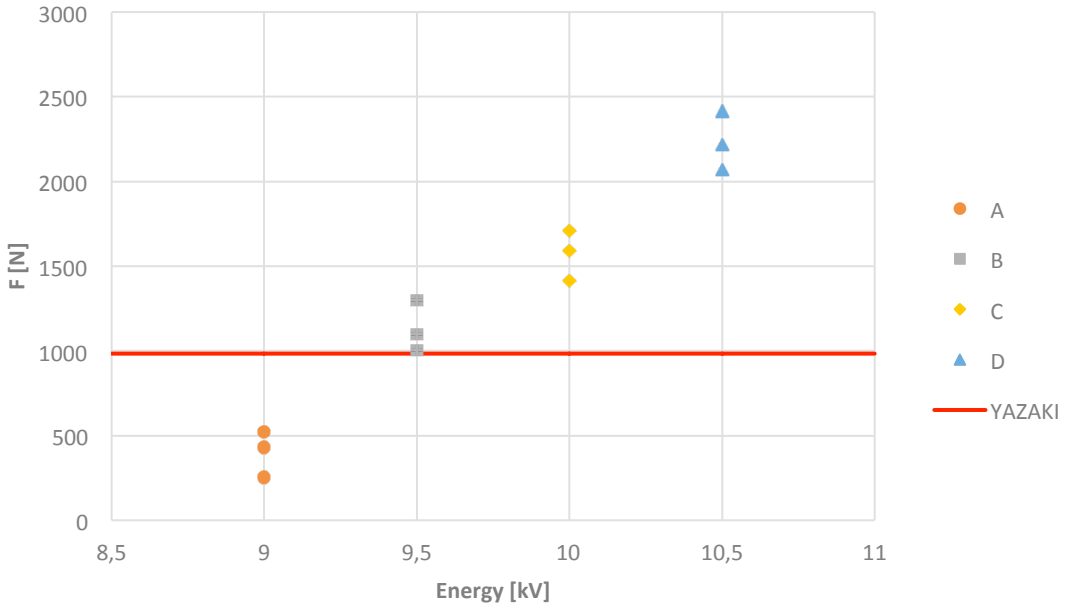

Figure 78: Tensile tests results for combination #B using Design #2.

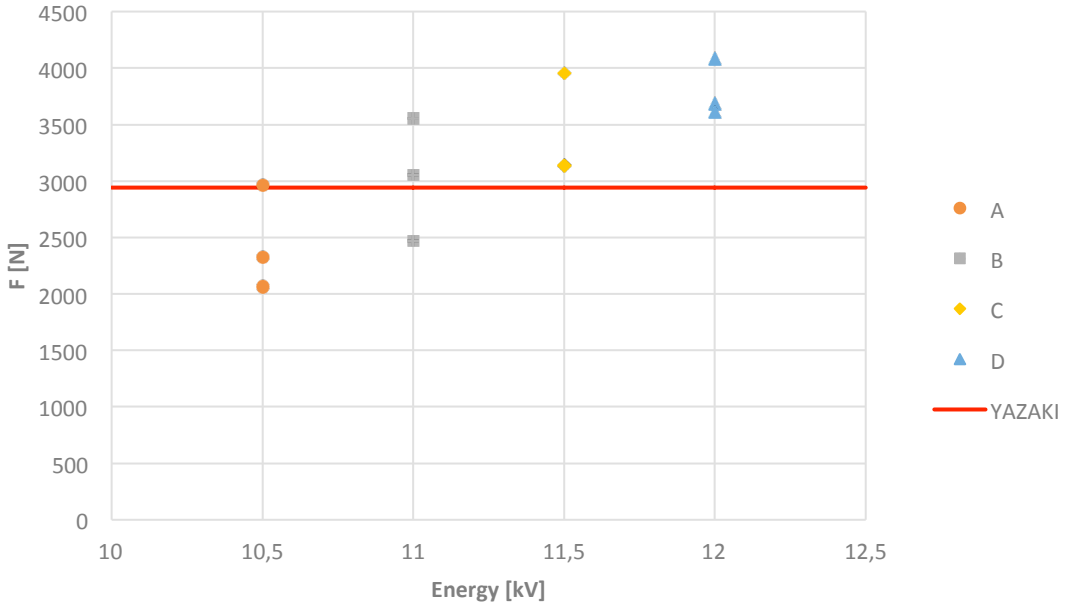

Figure 79: Tensile tests results for combination #C using Design #2.

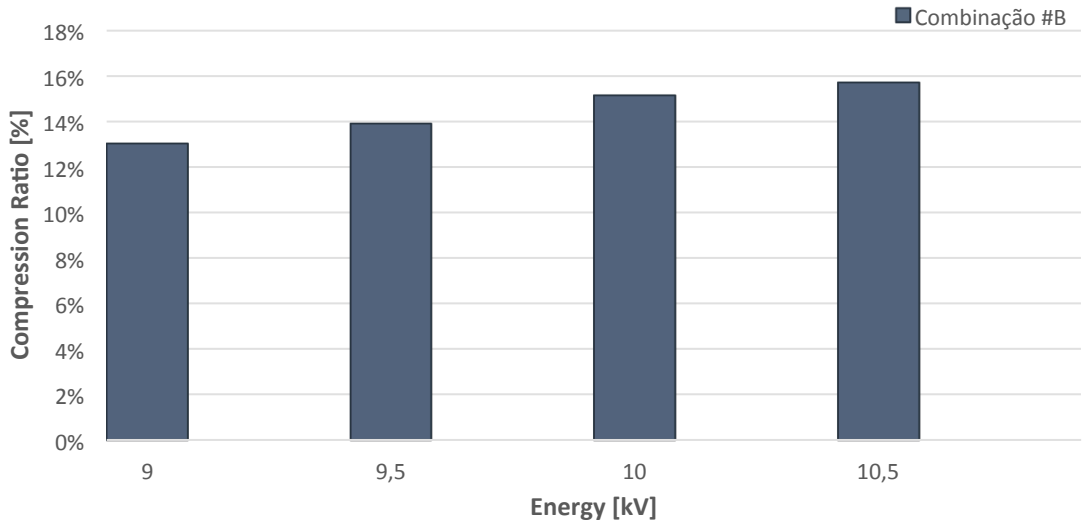

Figure 80: Compression ratio results for combination #B, using design #2.

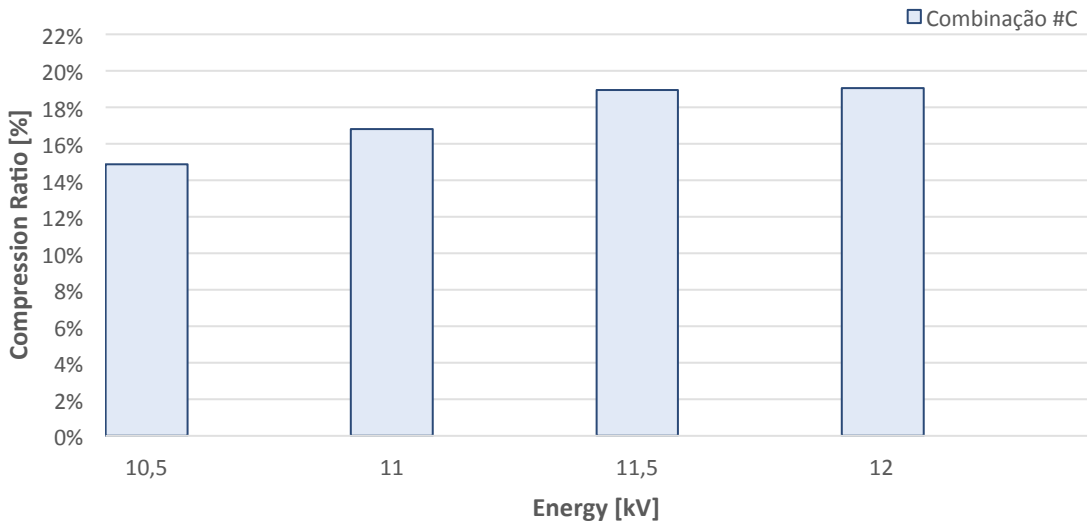

Figure 81: Compression ratio results for combination #C, using design #2.

The results of the metallographic analysis obtained for the larger section's materials are presented in the following figures. As observed in combination #A, the evolution in terms of free-spaces with the incremental increase of 0.5 kV in discharge voltage, is apparently not producing significant visual changes. These results are in with the compression ratio results obtained for the DoE executed. In fact, both results (metallographic and compression ratio) are quite low. Therefore, for combination #B and #C are only presented the extreme cross-sections in terms of discharge voltage. Note that, in Figure 83, d. sample, referent to combination #C crimped at 12.0 kV, a dark zone appeared. Most likely, this was not an effect of EMPC but, probably a consequence of the method used for cutting the sample. This specific samples, has been subjected to several polish steps, however this darker zone did not disappear, meaning that perhaps the material was dragged in sample's preparation.

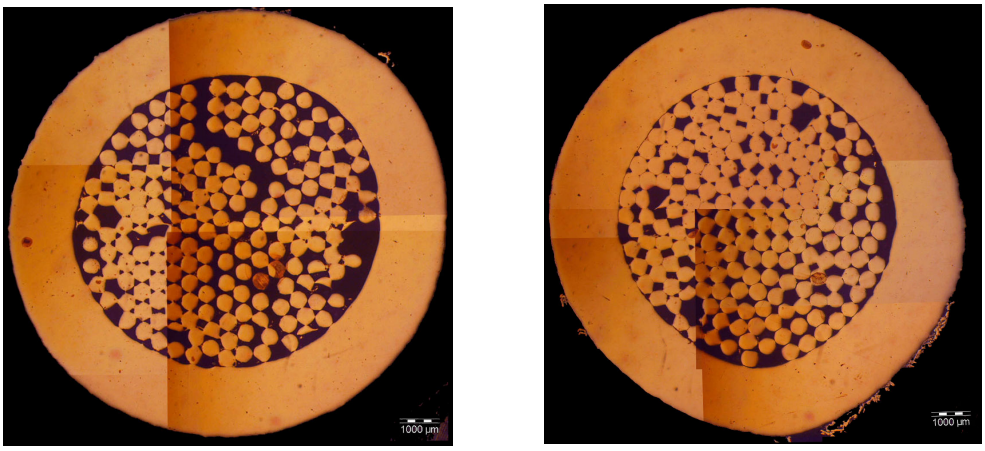

a. *b.*

Figure 82: X-section images of the EMPC joints of Combination #B, using design #2 at: a. 9.0 kV and b. 10.5 kV.

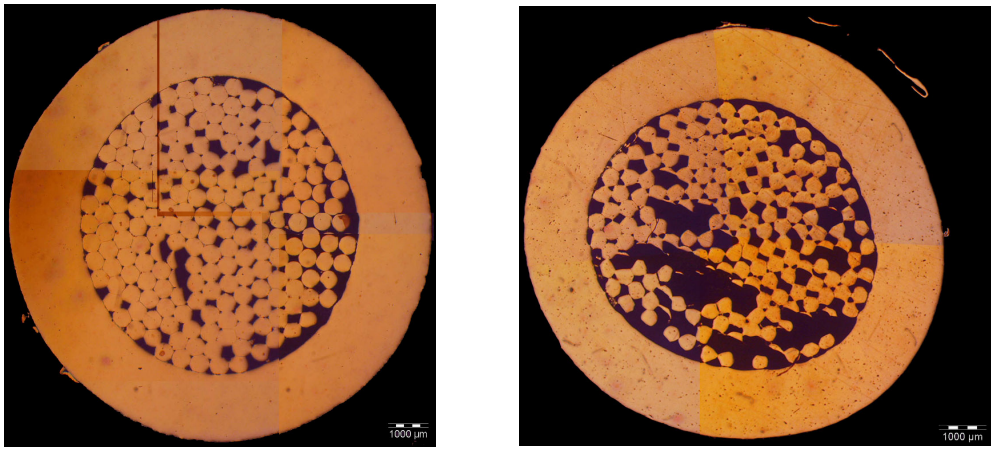

a. *b.*

Figure 83: X-section images of the EMPC joints of Combination #C, using design #2 at: a. 10.5 kV and b. 12.0 kV.

4.3 Experimental Testing vs Numerical Simulation

When comparing the experimental crimping ratio obtained by numerical simulation and experimental testing for combination #A, it can be concluded that for numerical simulation the values obtained are slightly superior to the ones obtained by experimental testing. For example, using discharge voltage of 8 kV, crimping ratios were of 14.28 % and 10.88 % for numerical simulation and experimental testing, respectively and for discharge voltage of 9 kV, these were of 15.30 % and 14.17% for numerical simulation and experimental testing, respectively. Note that, combinations #B and #C cannot be compared, as numerical simulations were performed using the original design and the experimental tests were carried out using the alternative design tool.

The disparity between the numerical and simulation crimping ratios, may have multiple causes. First of all, it is worth mentioning that although the numerical model developed follows the experimental trends, some physical

phenomena were neglected, for instance the temperature effects during the EMPC process. Note that temperature influences both workpiece deformation and electrical resistivity. For example, the increase of the temperature leads to an increase of the electrical resistivity [**32**].

Another field that requires further attention is the material modelling. A more suitable model, tanking into account the high-strain rate and temperature can contribute, significantly, to numerical simulation accuracy. Moreover, the effects of some other geometrical and process parameters can probably be causing the disparities obtained. These may include the geometrical simplifications made for both the terminal and cable but also, made to the coil geometry (end plates, were also not considered). All of these will influence, negatively, the total inductance of the system by increasing this value. Higher inductance of the system, decreases the efficiency of the process since, higher values of discharge energy need to be applied in order to cause the workpiece deformation (this is related to topics presented in Chapter 2 section 2.2). Taking into account the considerations stated, the numerical simulation results are considered to be valid as they predict the tool's behaviour in terms of current flow.

4.4 Concluding Remarks

Taking into account the experimental work presented in this chapter, some remarks concerning the methodology followed can be made. A brief description of the most important observations is presented in the following paragraphs.

During the experiments referent to combination #C some issues related to dimensions/tolerances have emerged. The correct position of the terminal inside the fieldshaper revealed to be a difficult task. The diameter defined for the positioning system (component #4) was not high enough to contemplate the terminal's manufacturing tolerances. Besides, a decrease of the effective diameter of the coil could have occurred during its production. As is known, the fieldshaper has one or two slots, depending on the design, at the moment that the fieldshaper was placed inside the insulator, component #3, it was most likely squeezed, and, as a consequence, the internal diameter of the fieldshaper may become slightly reduced. In addition, the placing/insulator part, place where the terminal will be positioned, has a thin wall made of compressible material, which can effectively cause the diameter's reduction. In line with this, the diameter of the positioning system (component #4) was modified using a drill tool.

In what concerns the performance evaluation of both designs some advantages and limitations can be highlighted. As mentioned, design #2 leads to lower current density, resulting in lower compression levels, but, on the other hand, presents a higher performance in terms of thermal-mechanical fatigue. The apparent robustness of design #2 promoted its selecting for the more extended sets of experiments. However, during the last round of experiments, an unexpected "failure" of the fieldshaper was noticed. The upper half of the fieldshaper slipped though the inferior part. Probably, the glue that bonds the fieldshaper and

isolating plates together failed due to both impact and temperature rise. The fieldshaper was repaired; all parts were glued together and correctly placed. Note that the concept developed allows the ease the replacement and repair of the different components.

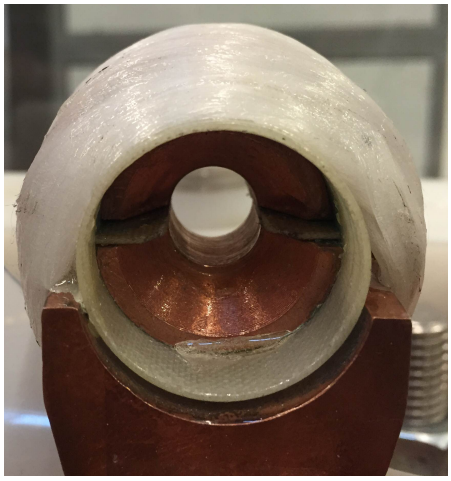

Figure 84: Detail of fieldshaper's positioning.

Regarding to the tensile tests performed for combinations #B and #C, some topics need special consideration. For these combinations it is not possible to present the tensile curves due to machinery failure since, this did not save the data related to the strain of the samples in test, only the maximum values were recorded.

From the results presented in this chapter, the following can be concluded:

• The EMPC with the magnetic pulse system 25 kV/ 25 kJ, making use of the developed customized tool, have resulted in effective joints for the three different combinations of terminals/wires under study.

• The combinations with higher cross-section (25 mm2) require higher values of energy than the combination with lower cross-section (16 mm2) to achieve the same levels in terms of compression ratio.

• The uniaxial tensile tests revealed that the tensile strength of the EMPC joints is in conformity with YSE strength criteria for all the combinations.

• The visual observation of the crimping joint, obtained by metallographic analysis, together with the compression ration measurements, give the indication that, in the future rounds of experiments, higher values of energy should be used in order to minimize the void percentage as well as to increase the compression levels.

5 CONCLUSIONS

In order to increase the applicability of the EMPC process, further theoretical and application-oriented research is required, particularly in the field of the development of the electromagnetic actuators. This work has emerged in the context of a partnership set between INEGI and YASAKI Saltano Europe, aiming to verify the applicability of Electromagnetic Pulse Crimping Technology to YSE products. The present dissertation intends to contribute with a new coil design, customized for YSE electrical cables. For such purpose, the basic concepts and a state of art regarding EMPT processes were firstly introduced, aiming to establish the necessary comprehension and familiarity with high-speed forming techniques.

In line with the objective of this work, the development of a customized electromagnetic crimping tool is presented. This process has initiated with a preliminary set of experiments, which were carried out by using handmade disposable coils. Despite the exploratory nature of this early approach, the results obtained allowed assessing the feasibility of EMPT for this specific application, providing the essential inputs for the development process. The actuator projected has four main components: primary coil, fieldshaper, two electrical insulators and two positioning systems. Towards the validation of the tool concept, and in order to understand the terminal's behaviour, the numerical simulation of the EMPC process was performed. For the numerical modelling and simulation LS-DYNA® software was used. The mesh creation, boundary conditions definition and circuit and material properties were part of the modelling process. Numerical analysis involved a couple of iterations, in which two different hypothesis were analysed namely, the cable was considered as a rigid part and considered as a solid element that suffers plastic deformation. The numerical predictions were lately compared with experimental ones.

Tool manufacturing was consigned to a group with several years of experience, and, having this present, the group has proposed an alternative design, which was delivered along with the original one. Therefore, there are two different tool designs to be tested during the validation phase.

Based on the knowledge acquired during the preliminary experimental tests and numerical results, tool manufacturing and validation process was carried out. To assess the viability of the projected concept to crimp YSE products, a

methodology was set and performed for the different combinations in study. The applied procedure involves multiple steps, which include the free-form compression of the terminal, a crimping DoE, tensile testing and, for some of the samples, metallographic analyses. The crimping ratio (C.R) levels, for the samples tested, were also taken into consideration and compared with the obtained by numerical simulation previously performed. Satisfactory agreement has been obtained, since the simulations have suitably captured the general trends of the experiments. However, in terms of magnitude the C.R revealed to be slightly different. Several reasons may be appointed, namely, the numerical model developed does not take into consideration the temperature effects during the discharge, the lack of information about the behavior of the material in high-strain rate environments as well as geometric and process simplifications applied.

The experimental tests performed in this work provided priceless know-how for further development of the crimping process of YSE products. As main conclusion can be stated that reliable joints have been achieved by using the electromagnetic actuator developed within the framework of this thesis. Regarding the performance evaluation of the designs in study, advantages and limitations can be appointed. The original design has higher efficiency in terms of magnetic pressure produced. However this presents lower mechanical resistance, meaning that a compromise is required. The tensile resistance of the EMPC joints is in conformity with YSE strength criteria for all the combinations tested. However, the voiding level revealed in the metallographic analysis and the results obtained in terms of compression ratio, show that higher values of energy should be tested, as will be advised in the future work section.

In short, the work developed during this thesis has a significant contribute for the further implementation of EMPC process in crimping the electrical products.

6 FUTURE WORK

In future, certain improvements may be conducted. Several considerations concerning to the continuity of the presented work are reported in the following:

- New rounds of experimental tests should be conducted. Higher values of discharge energy should be used aiming to decrease the level of void spaces, noticed during metallographic analysis.
- The electrical properties of the joints achieved by EMPC should be investigated. The relation between compression ratio, tensile strength and electrical conductivity must be characterized.
- More accurate models, able to predict the tooling and workpieces behavior during the current discharge should be implemented.
- The coil's life cycle is very difficult to predict, derived from the multiple phenomenon involved during the process in analyses. Methods to have an indication of the coil's lifetime should be developed.
- If the energy needed to achieve the required compression ratio reveals to be higher than the one that the coil can withstand, a new design should be developed.

7 BIBLIOGRAPHY

[1] PREST, "A Comparative Analysis of Public, Semi-Public and Recently Privatised Research Centres," 2002.

[2] YAZAKI. Yazaki-Europe. [Online]. http://www.yazaki-europe.com/index.php?id=49

[3] Milenko Braunovic, Valery V. Konchits, and Nikolai K. Myshkin, *Electrical Contacts: Fundamentals, Applications and Technology*, LLC Taylor & Francis Group, Ed.: CRC Press, 2006.

[4] Magne Runde, Harald Jensvold, and Mario Jochim, "Compression Connectors for Stranded Aluminum Power Conductors," Norwegian University of Science and Technology, Norway,.

[5] M. Braunovic, *Electrical Contacts: Principles and Applications*, Paul G. Slade, Ed. New York: Slade, 1999.

[6] ANIXTER, *Techinical Information Handbook Wire and Cable*, 5th ed., Anyxter, Ed. Illinois: Anixter, 2013, vol. 1.

[7] K. Elliot Cramer, Daniel F. Perey, and William T. Yost, "Wire crimp connectors verification using ultrasonic inspection," in *IV Conferencia Panamericana de END Buenos Aires*, Buenos Aires, 2007.

[8] Association Connecting Electronics Industries, "Introduction to Wire Crimping," IPC, Illinois, 2013.

[9] Cablecraft, "A Comprehensive Guide To Good Crimping Practice," Bedfordshire,.

[10] George E. Dieter, *Mechanical Metallurgy - SI Metric Edition*, McGraw Hill, Ed. London: McGraw Hill, 2001.

[11] G. Zittel, "A historical review of the high speed metal forming," in *4th International Conference on High Speed Forming*, San Diego, 2010.

[12 Inês Vieira Oliveira, "Eletromagnetic Forming Process: Numerical Modelling

] and Analysis of Process Parameters," FEUP, Porto, 2013.

[13 Michaël De Ketele Filip Broekaert, "An exploratory study into the feasibility of
] magnetic pulse forming," Universiteit Gent, Gent, 2009.

[14 Sabith Umer, "Magnetic Pulse Welding, Forming & Crimping," Government
] Engineering College, Kerala,.

[15 Bmax. Bmax. [Online]. http://www.bmax.com/technology/magnetic-pulse-
] forming/

[16 J. -P. Cuq-Lelandais, S. Ferreira, G. Avrillaud, G. Mazards, and B. Rauffet,
] "Magnetic Pulse Welding: Welding windows and high velocity impact simulations," in *6th International Conference on High Speed Forming*, Daejeon, 2014, pp. 199-206.

[17 Gunther Göbel, Eckard Beyer, Jörg Kaspar, and Berndt Brenner, "Dissimilar
] Metal Joining: Macro-and Microscopic Effects of MPW," in *5th International Conference on High SPeed Forming*, Dortmund, 2012, pp. 179-188.

[18 J. Y. Shim, D.H. Park, I. S. Kim, and B. Y. Kang, "Effect of Process Variables
] on the Al/Cu Weldment Using DOW for Magnetic Pulse Welding Process," in *6th International Conference on High Speed Forming*, Daejeon, 2014, pp. 107-116.

[19 R. N. Raoelison et al., "Study of the Elaboration of a Pratical Weldability
] Window in Magnetic Pulse Welding," *Journal of Materials Processing Technology*, vol. 213, no. 8, pp. 1348-1354, August 2013.

[20 V. Shribman, "Magnetic Pulse Welding of Automotive HVAC Parts," PULSAR
] Ltd. Magnetic Pulse Solutions, Yavne,.

[21 Karl-Heinrich Grote and Erik K, Eds., *Handbook of Mechanical Engineering*.
] New York: Springer, 2009, vol. 10.

[22 Fraunhofer IWU, "Electromagnetic Forming," Fraunhofer Institute for
] Machine Tools and Forming Technology IWU, Chemnitz, 2013.

[23 Magpulse. Magpulse. [Online]. http://www.magpulse.co.in/index.html
]

[24 Coilgun Systems. (2004) Coilgun. [Online].
] http://www.coilgun.eclipse.co.uk/coilgun_basics_1.html

[25 Bmax, "Application Technology: Welding," Bmax, Toulouse,.
]

[26 Pieter Vanhulsel Mattias Van Wonterghem, "Magnetic pulse cimpring of

] mechanical joints," Universiteit Gent, 2011.

[27 Muhammad Ali Siddiqui, "Numerical Modelling and Simulation of
] Eletromagnetic Forming Process," Institut de Mécanique des Fluides et des Solides, Strasbourg,.

[28 Bmax. Bmax. [Online]. http://www.bmax.com/technology/magnetic-pulse-
] crimping-expansion/

[29 Pablo Pasquale, Stephan Kallee Ralph Shäfer, "Industrial Application of the
] Electromagnetic Pulse Technology," PSTproducts, Alzenau,.

[30 Inaki Eguia, Peihui Zhang, and Glenn S. Daehn, "Improved Crimp-Joining of
] Aluminium Tubes onto Mandrels with Undulating Surfaces," Department of Materials Science and Engineering, The Ohio State University Columbus, Ohio, 2014.

[31 J. C. Maxwell, "A treatise on electricity and magnetism," University of Oxford,
] London, 1873.

[32 V. Psyk, D. Risch, B.L. Kinsey, A.E. Tekkaya, and M. Kleiner, "Eletromagnetic
] forming-A review," *Journal of Materials Processing Technology*, December 2010.

[33 C. N. Okoye, J. H. Jiang, and Z. D. Hu, "Application of electromagnetic-assisted
] stamping (EMAS) technique in incremental sheet metal forming," *International Journal of Machine Tools and Manufacture*, vol. 46, no. 11, pp. 1248-1252, September 2006.

[34 Gilles Mazars, Gilles Avrillaud, Anne-Claire Jeanson, and Jean-Paul Cuq-
] Lelandais, "Ultra High Power Applications Designed Using the LS-DYNA EMAG solver," Bmax, 2013.

[35 Ahmad K. Jassim, "Magnetic Pulse Welding Technology," *Iraq J. Electrical and
] *Electronic Engineering*, vol. 7, no. 2, 2011.

[36 M. Geier, E. Paese, J. L. Pacheco, R. P. Homrich, and J. C. S. Ortiz, "Proposal
] for a Test Bench for Electromagnetic Forming of Thin Metal Sheets," in *4th International Conference on High Speed Forming*, 2010.

[37 Cornet European Research Programme. [Online].
] http://cornet.efb.de/index.php?menuid=16

[38 Rutgers School of Engineering. Rutgers School of Engineering. [Online].
] http://www.ece.rutgers.edu/~orfanidi/ewa/ch01.pdf

[39 P. L'Eplattenier, G. Cook, and C. Ashcraft, "Introduction of an Electromagnetism Module in LS-DYNA for Coupled Mechanical Thermal

] Electromagnetic Simulations ," in *3rd International Conference on High Speed Forming*, Livermore, 2008.

[40 Bmax. Bmax. [Online]. http://www.bmax.com/products/auxiliary-equipment/
]

[41 Gary F. Benedict, *Nontradiotional Manufacturing Processes*. New York: Marcel
] Dekker, Inc, 1987, vol. 1.

[42 Hassan A. El-Hofy,Mahmoud H. Ahmed Helmi A. Youssef, *Manufacturing
] Technology: Materials, Processes, and Equipment.*: CRC Press, 2012.

[43 ICHSF. ICHSF014. [Online]. http://ichsf2014.com/topics.php
]

[44 Chunfeng Li, Zhiheng Zhao, Zhong Li Haiping Yu, "Effect of field shaper on
] magnetic pressure in electromagnetic forming," *Journal of Materials Processing Technology*, vol. 168, no. 2, pp. 245-259, September 2005.

[45 Iñaki Pérez, Iñigo Aranguren, Beatriz González, and Iñki Eguia,
] "Electromagnetic Forming: A New Coupling Method," *International Journal Mater Form*, vol. 2, pp. 637-640, 2009.

[46 Iñaki Ulacia, Michael Imbert, and Pierre L'Emplattenier, "Influence of the
] Coupling Strategy in the Numerical Simulation of Electromagnetic Sheet Metal Forming," in *10th International LS-DYNA Users Conference*, pp. 17-26.

[47 J. D. Thomas and N. Triantafyllidis, "On electromagnetic forming processes in
] finitely strained solids: Theory and examples," *Jounal of the Mechanics and Physics of Solids*, vol. 57, pp. 1391-1416, 2009.

[48 M. Stiemer, J. Unger, H. Blum, and B. Svendsen, "Fully-couples 3D Simulation
] of Electromagnetic Forming," German Research Foundation, Dortmund, 2006.

[49 J. K. Doley and S. D. Kore, "Fully Coupled Numerical Simulation of
] Electromagnetic Forming," *Key Engineering Materials*, vol. 504-506, pp. 1201-1206, February 2012, http://www.scientific.net/KEM.504-506.1201.

[50 Jean Barralis and Gérard Maeder, *Prontuário de Metalurgia*, 2nd ed.,
] Fundação Calouste Gulbenkian, Ed. Lisboa, 1997.

[51 SAE/USCAR-21, "Performance Specification for Cable-to-Terminal Electrical
] Crimps ," SAE International, 978-0-7680-2107-3 , 2008.

[52 Report given by YAZAKI, "Performance Specification for Cable-to-Terminal
] Electrical Crimps,".

[53 Lawrence M. Gull, Erik A. Moro, and Matthew E. Briggs, "The Effect of

] Tangential Velocity Components and SUrface Evolution on Photon Doppler Velocimetry Measurements," *Report LA-UR-13-20539*, 2013.

[54 ALB. (2009) ALB-Copperalloys. [Online]. http://www.alb-
] copperalloys.com/high-conductivity-copper/c18150/#physical

[55 MATWEB. Mat Web. [Online]. http://www.matweb.com
]

[56 Livermore Software Technology Corp. (2013, March) Dynamore. [Online].
] http://www.dynamore.de/de/download/presentation/dokumente/2013-multiphysik/em-mp2013.pdf

[57 ABAQUS, Inc, "Abaqus Elements - Lecture 2," 2005. [Online].
] http://imechanica.org/files/l2-elements.pdf

[58 LS-DYNA. LS-DYNA. [Online]. http://lstc.com/pdf/ls-dyna_971_manual_k.pdf
]

[59 ALB Copper Alloys Co.,LtdALB. CuCr1Zr – UNS.C18150 Chromium Zirconium
] Copper Alloys. [Online]. http://www.alb-copperalloys.com/high-conductivity-copper/c18150/#details

[60 Biswjit Banerjee, "An evaluation of plastic flow stress models for the
] simulation of high-temperature and high-strain-rate deformation of metals," Department of Mechanical Engineering, University of Utah, Salt Lake City, 2005.

[61 J. R. Davis, *Tensile Testing*, 2nd ed., Davis & Associates, Ed.: ASM
] International, 2004.

[62 N. S. Mishra, Sanak Mishra, and V. Ramaswamy, "Analysis of the temperature
] dependence of strain-hardening behavior in high- strength steel," *Metallurgical Transactions*, vol. 20, no. 12, pp. 2819-2829, December 1989.

[63 Stijn Hertelé, Wim De Waele, and Rudi Denys, "A generic stress-strain model
] for metallic materials with two-strage strain hardening behaviour," *International Journal of Non-Linear Mechanics*, vol. 46, no. 3, pp. 519-531, April 2011.

[64 An He, Ganlin Xie, Hailong Zhang, and Xitao Wang, "A comparative study on
] Johnson-Cook, modified Johnson-Cook and Arrhenius-type constitutive models to predict the high temperature flow stress in 20CrMo alloy steel," *Materials & Design*, vol. 52, pp. 677-685, December 2013.

[65 D. A. Ward and J. La T. Exon, "Using Rogowski coils for transient current
] measurements," Engineering Science and Education Journal, 1993.

[66] IEEE PSRC, "Practical Aspects of Rogowski Coil Applications to Relaying," IEEE PSRC, 2010.

[67] ST, "Current sensing in metering applications using a pulse current sensor and ST metering devices," ST, 2010.

[68] Donald Marquardt, "An Algorithm for Least Squares Estimation of Non-Linear Parameters," *Journal of the Society for Industrial and Applied Mathmatics*, vol. 11, no. 2, pp. 431-441, June 1963.

[69] Kenneth Levenberg, "A method for the solution of certain non-linear problems in least squares," *Journal Information for "Quarterly of Applied Mathematics"*, no. 2, 1944.

[70] Henri P. Gavin, "The Levenberg-Marquardt method for nonlinear least squares curve-fitting problems," Department of Civil and Environmental Engineering, Duke University, 2013.

[71] Lúcia M. J. S. Dinis, "Teoria da Membrana. Cascas de Revolução," Faculty of Engineering of the University of Porto, Porto, 2004.

[72] P. Kelly, *Solid Mechanics*., 2012.

[73] Mao-Hong Yu, Guo-Wei Ma, Hong-Fu Qiang, and Yong-Qiang Zhang, *Generallized Plasticity*. Berlin: Springer Berlin Heidelberg, 2006.

[74] Mao-Hong Yu, Guo-Wei Ma, and Jian-Chun Li, *Structural Plasticity: Limit, Shakedown and Dynamic Plastic Analyses of Structures*, Illustrated ed.: Springer Science & Business Media, 2009.

[75] Xianlong Liu, Liang Huang, and Jianjun Li, "An experiment and simulation study of the rebound effect in electromagnetic forming process," in *6th International Conference on High Speed Forming*, China , 2014, pp. 131-140.

[76] B.S. Kristin E. Banik, "Factors Effecting Electromagnetic Flat Sheet Forming Using The Uniform Pressure Coil ," The Ohio State University, Ohio, 2008.

[77] Hai-Ping YU, Chun-feng LI, Da-hai LIU, and Xian MEI, "Tendency of homogeneous radial deformation during electromagnetic compression of aluminium tube," *Transactions of Nonferrous Metals Society of China*, vol. 20, no. 1, pp. 7-13, January 2010.

[78] Pieter Vanhulsel Matthias Van Wonterghem, "Magnetic Pulse Crimping of Mechanical Joints," Universiteit Gent, 2011.

[79] P. Vanhulsel, M. Van Wonterghem, W. de Waele, and K. Faes, "Groove Design for Form Fit Joints Made by Electromagnetic Pulse Crimping," in *Sustainable*

] *Construction and Design*, 2011, pp. 432-441.

[80] F. M. Song, X. Zhang, Z. R. Wang, and L. Z. Yu, "A study of tube electromagnetic forming," *Journal of Materials Processing Technology*, vol. 151, no. 1-3, pp. 372-375, September 2004.

[81] Roger Mendez, Oscar Fruitos Ruben Otin, "Electromagnetic Metal Forming," International Center for Numerical Methods in Engineering, Barcelona, 2011.

[82] R. N. Raoelison, N. Buiron, M. Rachik, D. Haye, and G. Franz, "Efficient Welding Conditions in Magnetic Pulse Welding Process," *Journal of Manufacturing Processes*, vol. 14, no. 3, pp. 372-377, August 2012.

[83] Daniel G. Pressl, "Investigations of Electromagnetic Welding," Massachusetts Institute of Technology, Massachussetts, 2009.

[84] Iñaki Pérez, Iñigo Aranguren, Beatriz González, and Eñaki Eguia, "Electromagnetic Forming: A New Coupling Method," Labein-Tecnalia, Derio,.

[85] Madhadevan Padmanbhan, "Wrinkling and Springback in Electromagnetic Sheet Metal Forming and Electromagnetic Ring Compression," Ohio State University, 1997.

[86] Inês Oliveira, Pedro Teixeira, and Ana Reis, "Magnetic Pulse Welding of Dissimilar Metals: Influence of Process Parameters," in *6th International Conference on High Speed Forming*, Daejeon, 2014, pp. 117-126.

[87] L. H. Lyu, "Space Physics Lecture Notes," 2011.

[88] Koen Faes, "Tube Welding," Belgian Welding Institute, Ghent,.

[89] K. Faes, W. de Waele, M. Müller, and H. Cramer, "Design of Electromagnetic Pulse Crimp Torque Joints," in *High Speed Forming*, 2014, pp. 39-50.

[90] Michaël De Ketele Filip Broekaert, "An Exploratory Study Into the Feasibility of Magnetic Forming," Universiteit Gent, 2009.

[91] Maneesha Alterkar, Carol A. Homen, and Mohammed A. Kashem, "A Statistical Design of Experiments Approach," *Clinics in Laboratory Medicine*, vol. 27, no. 1, pp. 139-154, 2007.

[92] NPTEL. NPTEL. [Online]. http://nptel.ac.in/courses/Webcourse-contents/IIT-ROORKEE/MANUFACTURING-PROCESSES/Metal%20Forming%20&%20Powder%20metallurgy/lecture9/lecture9.htm

[93] University of Cailfornia Riverside, "Introduction to Energy Dispersive X-ray Spectrometry (EDS)," Central Facility for Advanced Microscopy and Microanalysis, University of California Riverside, California, 2014.

[94] Basic Electronics Tutorials Site. Electronics Tutorials. [Online]. http://www.electronics-tutorials.ws/accircuits/rms-voltage.html

8 ANNEXS

Annex A: Tensile Curves of DoE from Design #1

a. Samples 7.5 kV – J1, J2 and J3

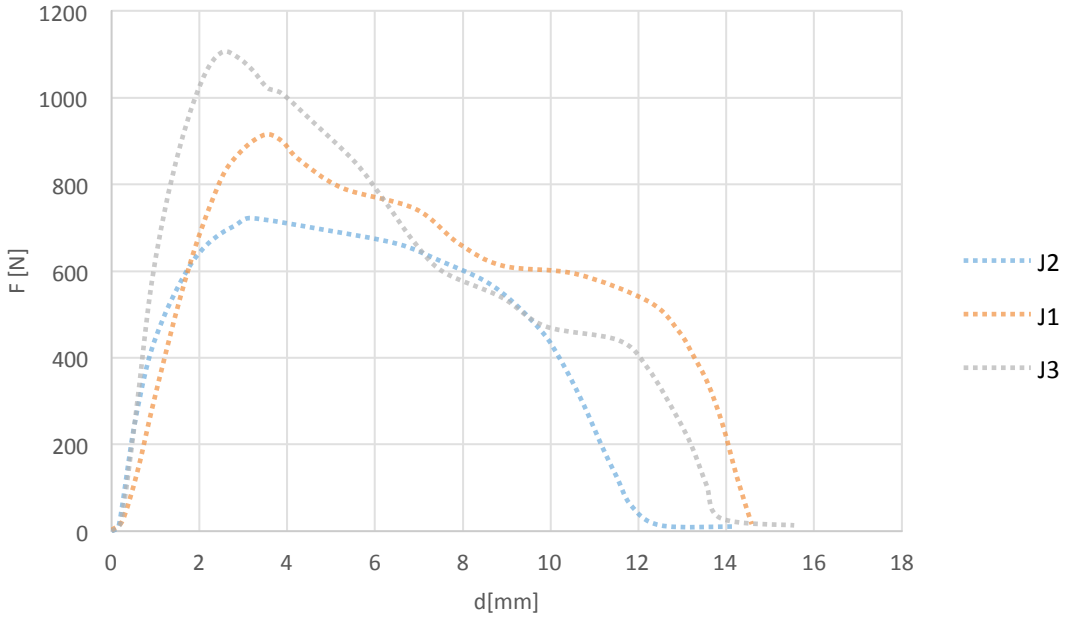

b. Samples 8 kV – K1, K2 and K3

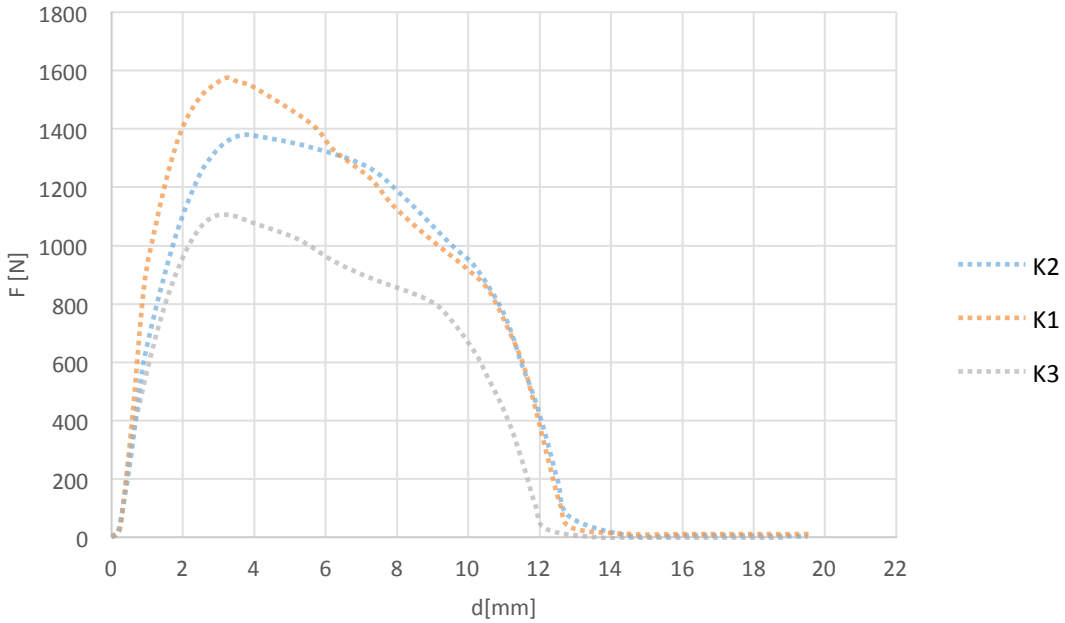

c. Samples 8.5 kV – L1, L2 and L3

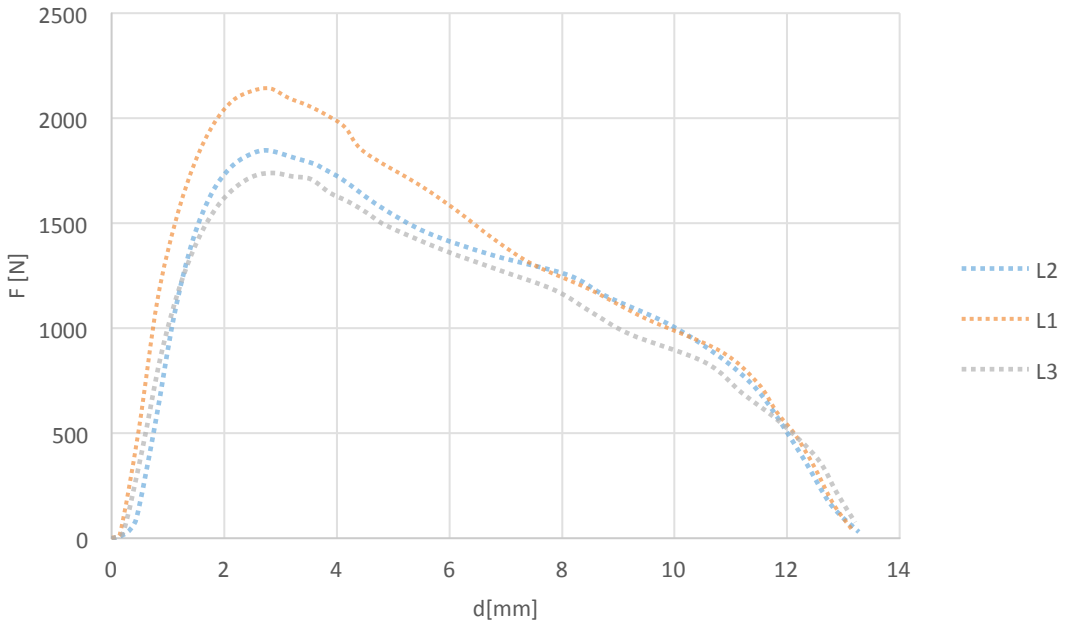

c. Samples 9 kV – M1, M2 and M3

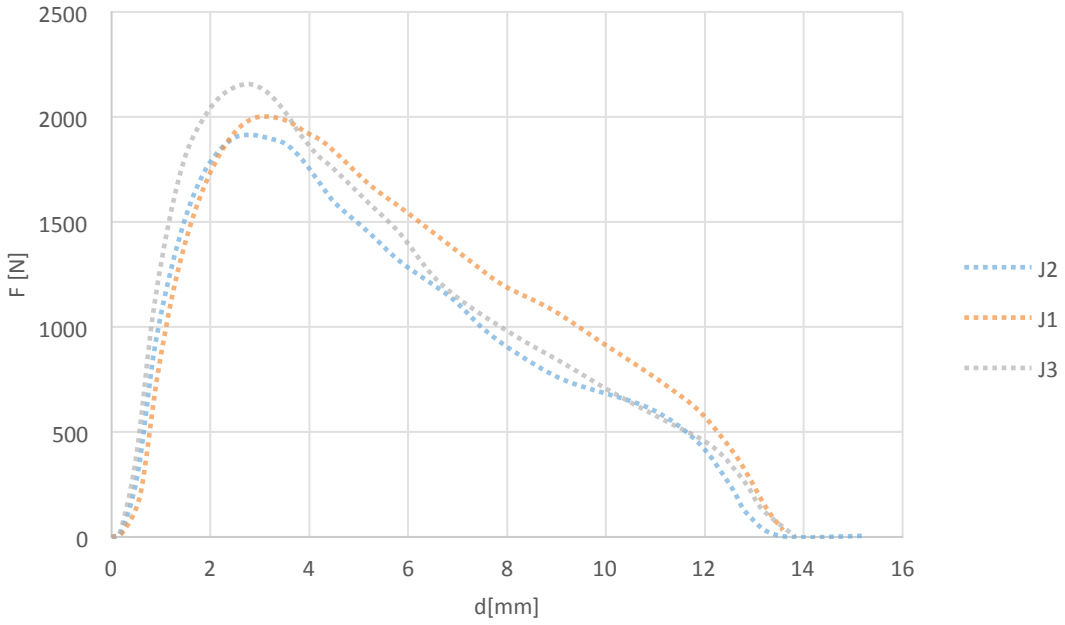

Annex B - Tensile Curves of DoE from Design #2

a. Samples 7.5 kV – A1, A2 and A3

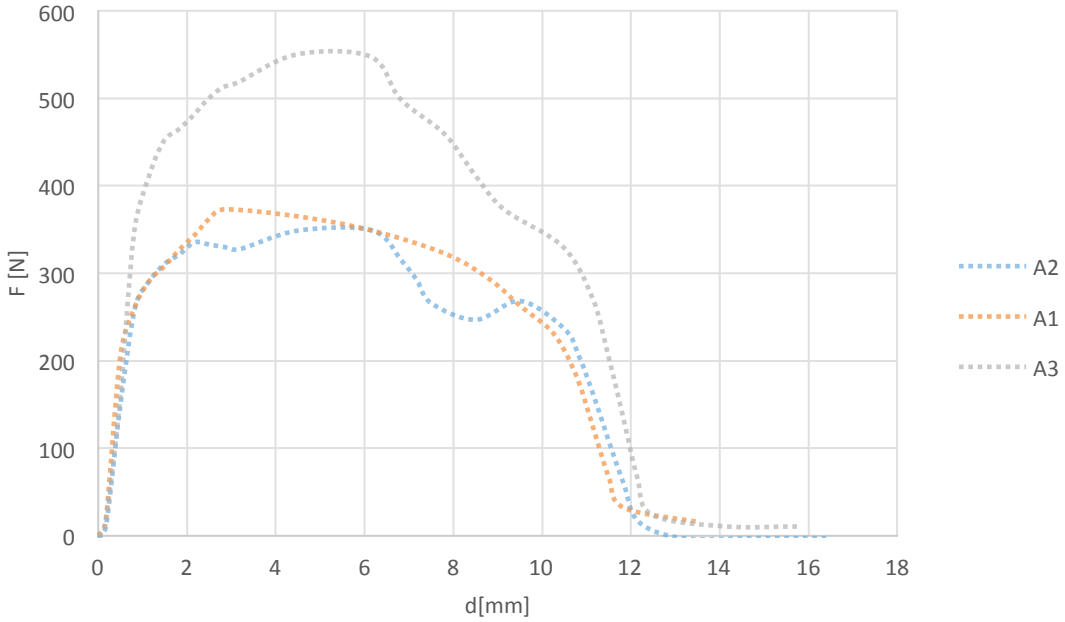

b. Samples 8 kV – B1, B2 and B3

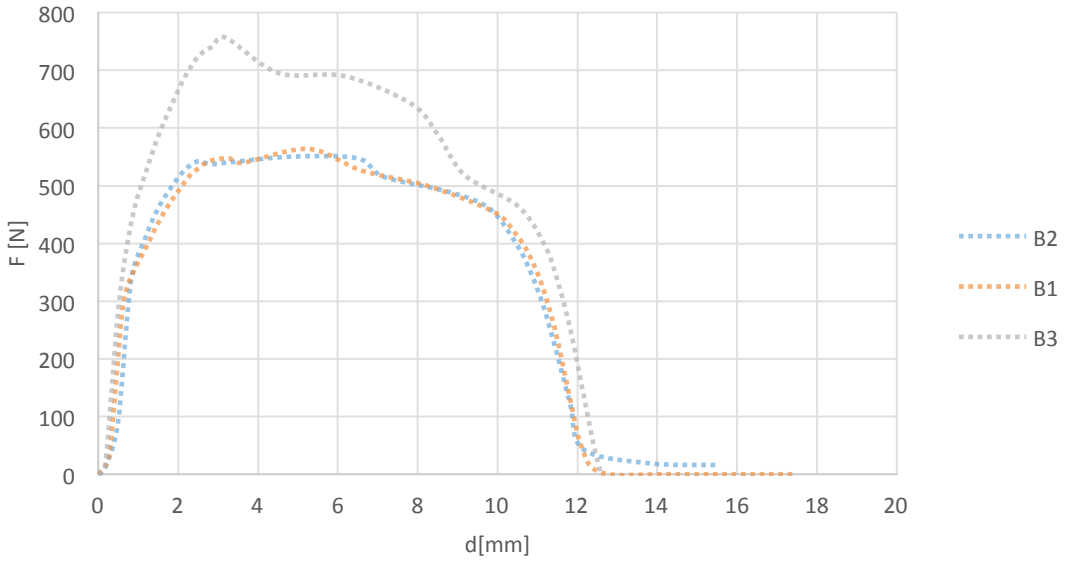

c. Samples 8.5 kV – C1, C2 and C3

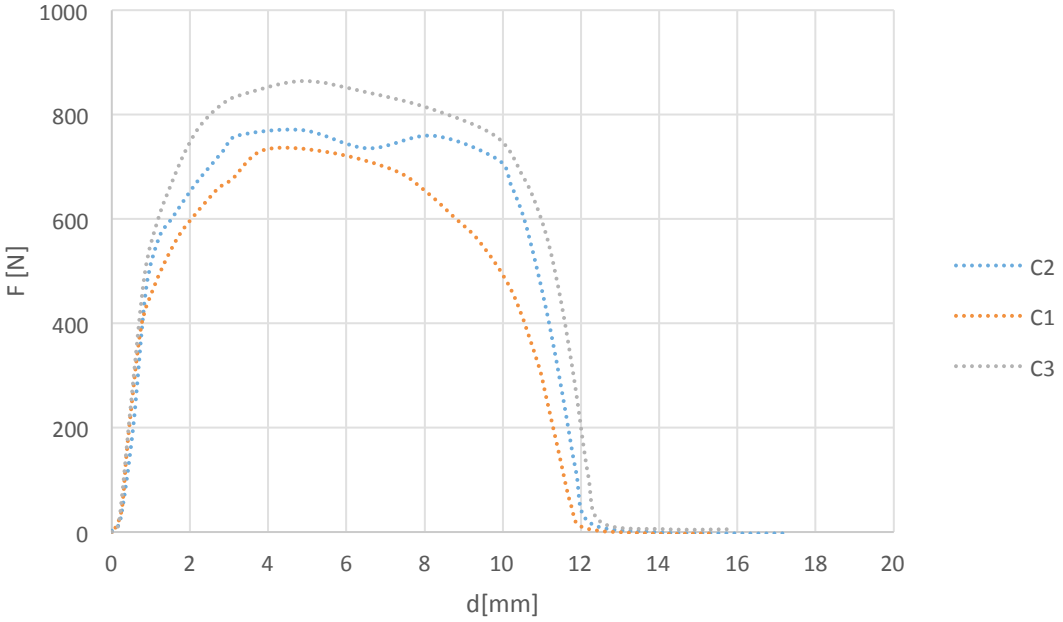

d. Samples 9 kV – D1, D2 and D3